Electron Paramagnetic Resonance Spectroscopy at Zero Magnetic Field

RICHARD BRAMLEY* and STEVEN J. STRACH

Research School of Chemistry, Australian National University, P.O. Box 4, Canberra, A.C.T. 2600 Australia

Received July 26, 1982 (Revised Manuscript Received October 30, 1982)

Contents

I. Introduction

Discovery of the absorption of radio-frequency radiation due to electron paramagnetic resonance (EPR) in bulk matter is generally credited to Zavoiskii,[1,2] who in 1944 showed that some first-row transition-metal complexes had a magnetic field dependent absorption. The low frequencies used (e.g., 12 MHz) meant that 'suppression of absorption' was seen as the magnetic field was increased from low values. A year later,[3] he reported that solid $CuCl_2 \cdot 2H_2O$ had a resonant absorption in a fixed field of 47.6 gauss, which peaked sharply at 133 MHz. Most EPR measurements thereafter were made at frequencies of the order of 10 GHz. Whereas the $CuCl_2 \cdot 2H_2O$ resonance was observed by scanning frequency at a fixed field, this procedure did not prove to be so easy at 10 GHz and virtually all EPR experiments have since been performed by scanning field at fixed frequency. The electron fine structure and nuclear hyperfine structure (hfs) terms in the spin Hamiltonian are often of more interest than the **g** tensor and these interactions generally give rise to observable energy splittings in the absence of an external magnetic field. Historically, EPR spectrometers were developed using swept magnetic fields because of the difficulty of varying the microwave frequency over wide bands and because resonant sample cavities are essentially fixed frequency devices.

It was not until 1961 that the first genuine zero-field (swept frequency) EPR measurements were published by Bogle, Symmons, Burgess, and Sierens.[4] Independently and virtually simultaneously, Kornienko and Prokhorov briefly reported direct zero-field measurements for Fe^{3+} in α-Al_2O_3.[5] The possibility of zero-field resonance (ZFR) was recognized much earlier and the first approximation to such an experiment was performed in 1952 on the peroxylaminedisulfonate radical.[6,7] Sweeping fields of the order of a few tens of gauss displayed the resonances due to the ^{14}N hfs interaction and the zero-field splitting (ZFS) was obtained by extrapolation to zero field. Shortly afterwards approximate values of the zero-field splittings for Fe^{3+} in methylamine–alum were obtained by extrapolation back to zero field of several frequency (near X band)/field measurements[8] and for Gd^{3+} in lanthanum ethyl sulfate by extrapolation from EPR transitions measured at low fields.[9] In 1956, Geusic observed a zero-field transition directly for the first time.[10] Field-swept EPR transitions in ruby (Cr^{3+} in α-Al_2O_3) were made to coalesce at zero field by shifting the microwave frequency around the zero-field resonant value. In 1959 zero-field experiments were performed on $\cdot CH(COOH)_2$ radicals in X-irradiated single crystals of malonic acid.[11] ZFR frequencies were measured by scanning a weak, sine-wave-modulated magnetic field through zero at a series of fixed frequencies. In 1960, low fields were used by Mock in conjunction with millimeter wavelength radiation and the possibilities for ZFR were discussed.[12] Bogle and Symmons' work on Fe^{3+} compounds that began the following year marked the beginning of what can be called true ZFR experiments in which frequency was swept at zero magnetic field.[4,13-15] Since that time, the principal applications have been to rare-earth compounds, mostly Gd^{3+} in various crystalline hosts. Further work with first-row transition ions has been undertaken and several applications to organic radicals have been made.

There has been steady progress in experimental techniques such that sensitivity can now be as good as in EPR experiments. Space and defense science has led to the development of reliable microwave frequency

0009-2665/83/0783-0049$06.50/0

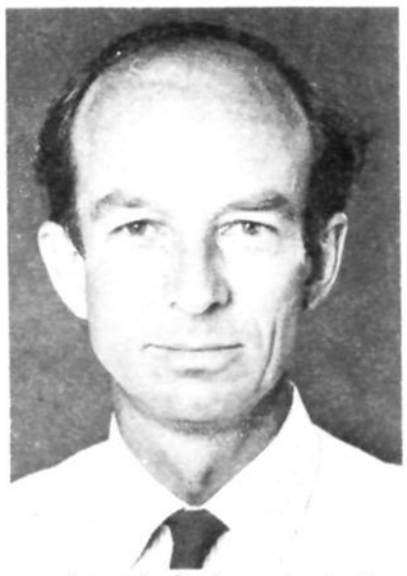

Richard Bramley was born in Sydney, Australia, and was admitted to the degrees of B.Sc. and M.Sc. at the University of Sydney in 1958 and 1959. His Ph.D. degree was obtained at the University of London in 1962 and was based on research undertaken with Professor Sir Ronald Nyholm and Professor B. N. Figgis on NMR chemical shift and relaxation phenomena of heavier nuclei. Following this, he spent 2 years as ICI Postdoctoral Research Fellow at University College London studying exchange interactions between transition-metal ions by EPR spectroscopy; he was appointed to a Lectureship in Chemistry there in 1964. In 1967 he moved to the new Research School of Chemistry at the Australian National University in Canberra, where he is now head of the photophysics group. He began research there with the study of photoexcited states of organic molecular crystals using optically detected EPR methods. The development of frequency-swept techniques for such work in zero magnetic field led to their application to the study of EPR of transition-metal ions in the ground state. His principal research interests are photophysics and magnetic resonance.

Steven Strach was born in Wigan, England, and grew up in Liverpool. In 1970 he obtained a B.Sc. degree at the University of Sheffield and later undertook research there on the application of EPR spectroscopy to the study of surfactant and liquid crystalline systems with Professor N. M. Atherton. He received a Ph.D. degree for a thesis on this work in 1973. After a year's postdoctoral research on the EPR of spin-labelled biological membranes and proteins in Professor D. Chapman's group at Sheffield, he moved to London where he worked for nearly 3 years as a forensic scientist. In 1977 he took a position as Research Associate at the National Research Council of Canada in Ottawa, studying new inorganic radicals by EPR spectroscopy in Dr. J. R. Morton's group. In 1980 he joined Dr. Bramley's group at the Australian National University in Canberra as a Research Fellow and has primarily been involved in the development and application of zero-field EPR techniques, principally to systems containing transition ions. His main interests lie in the application of EPR spectroscopy in the chemical physics area and development of the technique.

sources extending from ~1 GHz to the low frequency infrared region. The microwave components industry has developed and it is now relatively easy to put together a spectrometer which will sweep an octave band anywhere from 1 GHz up to about 40 GHz. Above this frequency, component costs escalate. One should not overlook the fact that many zero-field splittings exceed the normal EPR limit of the order of 1 cm^{-1} and extend beyond the submillimeter region into the far infrared. ZFR measurements have been made in this region (90–3000 GHz, see section III), but techniques for detecting such large zero-field splittings would need developing for routine use. This variable frequency method has been used with and without the magnet. In the same context, zero-field splittings in photoexcited states are often large enough to be resolved optically both for inorganic and organic molecules. In the organic case, a splitting of 20 cm^{-1} has been detected for the lowest triplet state of xanthione[16] and xanthone in alkane matrices is not far behind.[17] In the low frequency region NMR developments are extending slowly towards 1 GHz and a marriage with the microwave region can be expected. The high sensitivity developments in high frequency NMR resonators usefully complement the low ZFR sensitivities as microwave frequencies (and population differences) decrease.

The many complementary advantages of ZFR in EPR studies do not seem to be widely appreciated by EPR spectroscopists. The Zeeman term represented by the **g** tensor is the only term which requires an external magnetic field to be observable. When the principal terms of interest in the spin Hamiltonian are the fine structure and hfs terms, their accurate measurement is hindered by the Zeeman effect in a number of ways. Magnetic inequivalence of otherwise identical paramagnets leads to a corresponding multiplicity of EPR spectra. ZFR line widths can be narrower than their EPR counterparts leading to higher precision in the parameters and better resolution. In EPR, errors of field measurement and of crystal orientation are refined into the zero-field spin Hamiltonian parameters. ZFR can frequently be used with maximum effect in powder samples; single crystals are much less often required. ZFR spectra are generally simpler. Spectra can be simulated theoretically by one diagonalization rather than, as is most often done in EPR, by one diagonalization for every field of interest. These advantages mean that finer effects can be probed and that the validity of particular spin Hamiltonians can be checked. So far, no serious doubts have been cast on the form of the spin Hamiltonian, however there has been an interesting debate in connection with gadolinium ethyl sulfate (see section IVA). In ZFR experiments, resonance frequencies can be considerably lower than in EPR thus reducing dielectric loss problems. This is particularly important for aqueous solutions.

In this review, we endeavor to cover completely what has been done to date using radiation from radio to microwave frequencies on ground-state species. Optically detected ZFR of excited organic triplet states has been reviewed adequately elsewhere.[18–21] Optical detection avoids many of the technical problems associated with microwave detection. Sections on first-row transition ions, lanthanides, organic, and inorganic radicals are included as well as a part dealing with the instrumentation necessary to perform ZFR experiments. We also cover the more general technique of variable frequency EPR and show that this combined with ZFR can provide most of the information about all of the terms in the spin Hamiltonian. Most of the discussion

on the spin Hamiltonian formalism is given in section IIIA.

It is hoped that interest in this area will be stimulated and that the complementary value of ZFR in normal EPR studies will receive due recognition.

II. Instrumentation

A. Introduction

EPR is detected by measuring the net absorption of electromagnetic radiation that results from magnetic dipole allowed transitions in the sample. At zero magnetic field, the polarization of the transitions is determined solely by the magnetic vector of the radiation and the spin system, no external field being involved in determining the eigenfunctions and thus influencing the polarization of the absorption. So, in principle, a matched system consisting of a tunable frequency source, a transmission line containing the spin system in an orientation that suits the polarization of the transition, and a radiation level monitor at the end of the line can detect resonance. As is well known from sensitivity considerations,[22,23] such an arrangement is far from optimum, not least because the transmission line is nonresonant. Also the power detector is likely to have a $1/f$ dependent noise figure which is therefore not suited to the time scale of direct detection.

It is comparatively easy to modulate the resonance process and to use a lock-in amplifier to detect absorption at the modulation frequency f (or at $2f$, vide infra) and thus minimize $1/f$ noise problems. Although zero-field resonance can be detected in a sample with a high concentration of spins placed in a section of transmission line or tunable resonant cavity *without modulation*,[24] such a system would not be generally useful and is not further discussed. Hereafter it will be assumed that modulation is used and further that this is Zeeman modulation of the sample. Frequency modulation of the source, although attractive and simple, in practice causes modulation of the background level of radiation arriving at the detector, and spurious reflections in the transmission line/cavity system are detected along with genuine resonances. It is then necessary to use a Zeeman perturbation to distinguish the spurious from the genuine resonance and this is tedious. Pulsed radiation methods, common for NMR detection, can be applied to detect EPR or ZFR and such techniques will in due course play their part in the study of EPR.

The principles underlying design and performance of a number of representative spectrometers will now be discussed. The field modulation discussion is applicable to all types. Although this review excludes optically detected magnetic resonance (ODMR) in organic molecular crystals, a section is included on the helix, the common resonant or nonresonant device used in such work, since it has occasionally been used in ZFR spectrometers. It is probably used in an unknown mode in ODMR applications or indeed unnecessarily.

B. Field-Modulated, Nonresonant Transmission Spectrometer

Conceptually, a nonresonant transmission spectrometer is the simplest. A block diagram of a sensible minimum configuration is shown in Figure 1. We now discuss each part of such a spectrometer in turn, including the field modulator.

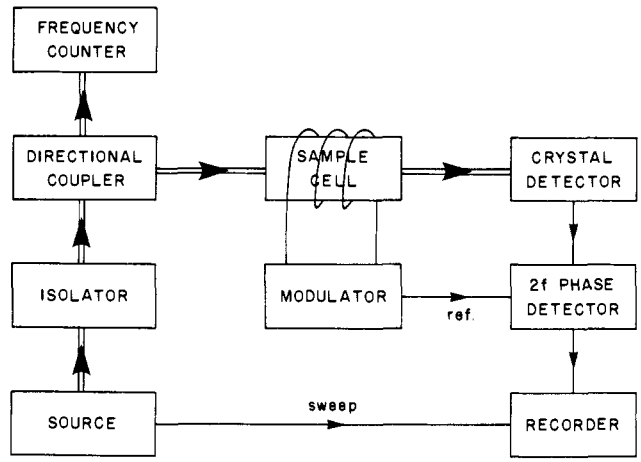

Figure 1. Block diagram of a ZFR spectrometer set up in a nonresonant transmission mode.

By far the most versatile and convenient frequency source is the sweep oscillator, widely available in octave bands up to 8 GHz and thereafter in standard waveguide bands up to 40 GHz and beyond. Less common are oscillators covering even wider bands. Sweep oscillators use backward wave oscillators (BWO) or semiconductor technology, the latter up to about 30 GHz, but this situation is changing rapidly with solid-state devices moving to higher frequencies. Cheaper, but much less convenient, are klystrons and Gunn diode devices. A good reflex klystron has the advantage of low noise and this is important in conventionally (nonoptically) detected EPR and ZFR. In practice, backward wave oscillators and solid state devices perform almost as well, but Gunn devices are somewhat noisier. A sweep oscillator conveniently provides sweep ramp voltages, power supplies, and other features that are expensive to add to simpler oscillators such as a basic cavity-tuned Gunn device. The basic source oscillator itself should provide a few tens of milliwatts if possible.

The isolator is a passive device designed to pass power in one direction and to absorb it in the reverse direction. It protects the generator from reflected power damage and frequency pulling effects, and minimizes reflections and standing waves from mismatches further down the line. The detector is normally matched to the characteristic impedance of the line to absorb all the power. However, accidentally inserting metal, or some dielectrics (the sample itself sometimes), into the line at the sample compartment can reflect all the power and damage an unisolated generator.

Of greatest importance is the sample and its effective compartment. In the case of a waveguide transmission line, which is sensible on filling factor considerations only above about 8 GHz, a hole can be bored through the narrow side(s) of the guide and the sample inserted in a suitable holder. Alternatively, the modulated part of the waveguide can be more or less filled with sample. All samples and their supports present dielectric discontinuities and can cause reflections. At worst, resonant cavities can be created before and after the sample. Depending on the perturbation, spurious sharp dips in detector current can be seen at regular frequency intervals. Without resorting to shaped waveguides and/or samples, it is best to compromise to retain sample

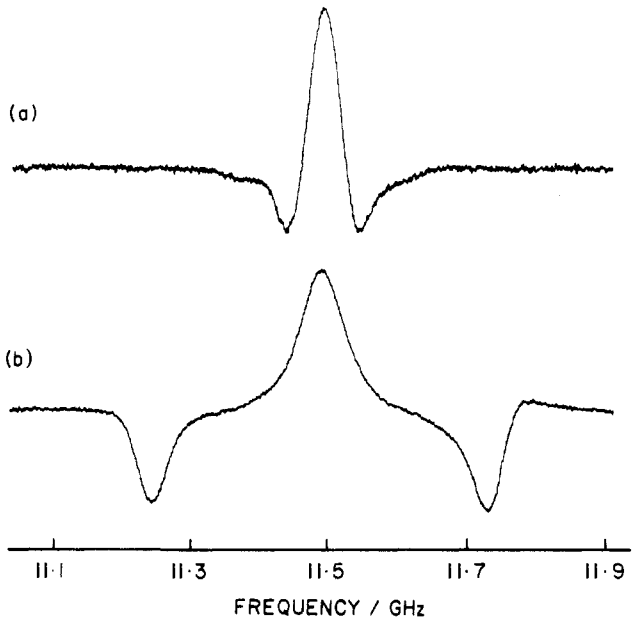

Figure 2. ZFR spectrum of a synthetic ruby (Cr^{3+} in α-Al_2O_3); the transition is centered at 11.493 (±0.005) GHz at 295 K. The microwave polarization was perpendicular to the threefold symmetry (z) axis of the crystal and square-wave bidirectional on–off magnetic field modulation of frequency 700 Hz was parallel to the z axis. The field modulation strength in (a) was ±20 G and in (b) ±90 G. Small distortions of the line shapes in the wings of the spectrum (particularly in (a)) are thought to be due to the magnetic isotope ^{53}Cr (10% abundance, $I = {}^3/_2$). The crystal was supported in a teflon tube which passed through the waveguide and the spectrometer was used in transmission mode.

changing convenience and to use polystyrene, silica, or teflon sample supports with rounded edges. Symmetry can be important in the supporting structures; it is sometimes better to have a tube or support passing right through the waveguide than to have a sample post stopping halfway. These considerations aside, there is still an element of black art left in achieving optimum performance in most systems. Rectangular waveguide has a characteristic impedance which is frequency dependent and a lower frequency cutoff below which radiation will not propagate. At the higher frequency end of a waveguide band, higher modes are transmitted which give rise to uncertainties in optimum sample position and in polarization unless the mode is known. Ridged waveguide[25] has a wider transmission range but is not often used. Zero-field resonance in a sample of ruby (Cr^{3+} in α-Al_2O_3) detected in a waveguide transmission line is shown in Figure 2.

Similar principles apply to coaxial cable cells with the exception that the usual mode is TEM_{01} rather than TE_{01} in waveguide. A consequence is that the line impedance is now independent of frequency. The coaxial line can be homemade with the dielectric replaced by sample. It is possible to tailor the conductor diameters to match the impedance of this cell to that of the remaining transmission line. The filling factor is very good but the homogeneity of the microwave magnetic field is poor, a factor which influences the resonance line shape if the modulating field is also inhomogeneous along the same (radial) gradient. Alternatively, a hole can be bored normal to the line, passing directly to the central conductor or between it and the outer conductor. In these cases, the filling factor is poor. Coaxial line can be used up to about 26 GHz (top end of the common 18–26 GHz band). Its characteristic impedance Z_0 depends only on the radius ratio of the outer and inner conductors and the permeability, μ, and dielectric constant, ϵ, of the dielectric and/or sample:

$$Z_0 = 60(\mu/\epsilon) \ln (r_0/r_i) \text{ ohms}$$

where μ is generally 1 and $\epsilon = 1$ for air.

It is essential that the transmission line, samples, and supports are free from magnetic inclusions or dust as these will move under the influence of magnetic modulation and set up acoustic waves in the transmission line, giving rise to spurious resonances. Modulation-induced eddy currents can also set up acoustic waves. Whether single crystals or powders are used influences the choice of waveguide or coaxial line. Useful polarization information can be obtained if the microwave field direction is constant over the volume of the single crystal. Such a condition is more easily met in a waveguide than in coaxial line.

The detector is a diode or more complex junction device that rectifies the microwaves. It should clearly be efficient, sensitive, have low noise, and be chosen or used so as to have linear current output with respect to incident power (square law behavior).

The field modulation can be provided externally or internally to the transmission line. In the latter case, for example, a wire loop surrounding the sample, care is required to minimize reflections. Since the Zeeman effect is generally nonlinear at low magnetic fields, sine-wave modulation (and detection at twice the modulation frequency) will not faithfully reproduce the lineshape. It should be noted that the observed lineshapes can be distorted by the field modulation waveform at the sample. Care may be needed to recover the intrinsic lineshape. Square-wave modulation of large amplitude compared with the linewidth is almost always used. With half the cycle grounded so that no field is applied, the output signal is the oscillating difference between the spectrum with the field on and off (see Figure 3). For large enough amplitudes, phase detection at the modulation frequency f reproduces the line shape. Oppositely signed satellites generally appear. (See Figures 2 and 3.) In the case of a single crystal of known orientation, either the g value or the modulation amplitude may be determined if one of these is known. For randomly oriented samples, such as powders and glasses, the field-on satellites are the envelopes of the individual satellites for all orientations. With center-zero, bidirectional square-wave modulation, the signal is phase detected at twice the fundamental modulation frequency. (See Figure 3.) Bidirectional modulation is not absolutely necessary. It is either a convenience using a sine-wave input followed by clipping and shaping, or in our case, was available from an NQR frequency modulator. The antisymmetry of this waveform gives no even harmonics in its Fourier synthesis, so there are no pickup problems at $2f$. Without this or elaborate screening, pickup interference can be severe. Amplitudes up to 200 gauss or more (peak-to-peak) are useful although much smaller fields suffice for narrow lines in many cases. Providing such a field at the sample with a good square-wave *field* profile is not trivial. The sharp rise and fall of the driving current is limited by the rise time of the coils which is equal to their inductance divided by the series resistance in the circuit. This limits modulation frequencies to 1 or 2

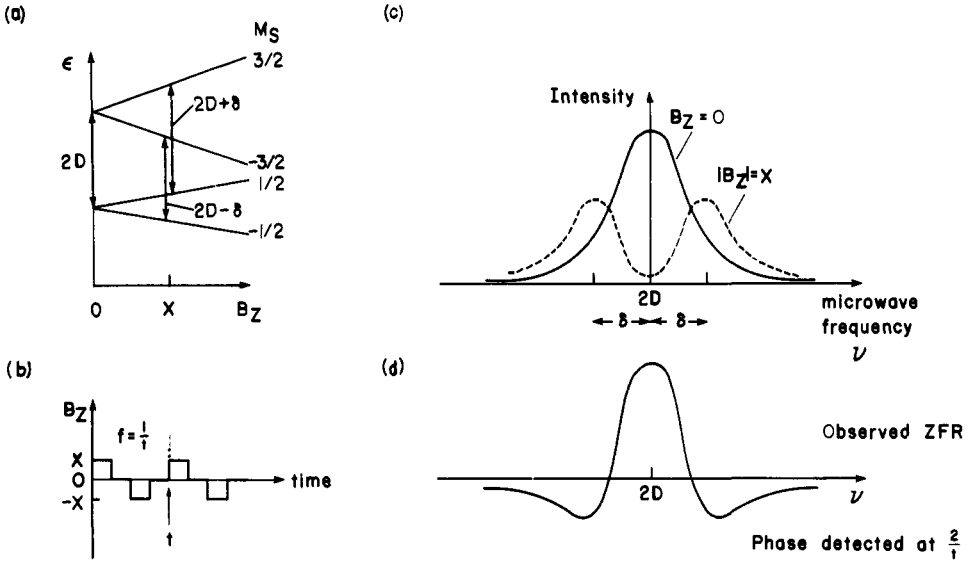

Figure 3. Origin of the ZFR line shape illustrated for an $S = {}^3/_2$ system. Field modulation B_z is directed along the symmetry axis and the microwave field which causes transitions is polarized perpendicular to this direction. (a) Energy level diagram showing transitions at zero field and at a field $B_z = X$; δ is given by $g_z\mu_B X$. (b) Form of the antisymmetric on–off magnetic field modulation, frequency f, amplitude $\pm X$. (c) Absorption intensity as a function of microwave frequency ν, with field $B_z = 0$ and $B_z = \pm X$. (d) Resulting ZFR absorption line shape when phase sensitive detection at twice the modulation frequency is used.

orders of magnitude less than the normal EPR frequency of 100 kHz, particularly since the Fourier synthesis of a square wave contains high harmonics of the fundamental. Some compensation can be provided by a driving waveform with deliberately introduced spikes to compensate for the natural rounding of the square wave. When working with single crystals particularly, due attention should be paid to the relative orientations of microwave and modulating fields and to the polarization of the observed transition. Since ZFR frequencies are often temperature sensitive, all potential sources of sample (or thermometer!) heating should be considered and minimized in spectrometer design. Water-cooled modulation coils minimize heating effects from high modulating currents.

Eddy-current and skin-depth effects require comment. Electromagnetic radiation penetrates into the surfaces of conductors and attenuates by e every skin depth $\delta = (\pi\nu\sigma\mu)^{-1/2}$, where σ is the conductivity and μ the permeability of the material. The design of sample compartments invariably involves a compromise between keeping the microwaves in the transmission line, allowing high-frequency components of modulating fields to penetrate, but at the same time having a mechanically rigid structure. Judiciously placed slots cut into the waveguide for example can minimize eddy-current loops without attenuating the microwave currents.

Finally, a directional coupler inserted just after the isolator allows a small fraction of the incident power to be picked off for frequency measurement, power monitoring, and/or power leveling. With care, it is possible to observe relative transition intensities with useful precision. It should be remembered that the Boltzmann population differences are frequency dependent, increasing linearly with frequency in the high-temperature limit. This contrasts with fixed-frequency EPR where the population differences are relatively field independent.

Some specific examples of nonresonant transmission spectrometers will now be given. Although not strictly a zero-field experiment, Pake, Townsend, and Weissman's 1952 study[6] of paramagnetic resonance structure due to ^{14}N hfs in the peroxylaminedisulfonate radical ion is the probable precursor to the use of nonresonant waveguide in EPR experiments at low or zero fields. X-band waveguide linked a klystron to a detector and contained the sample. At fields of the order of a few gauss, hyperfine structure was well-resolved. A complementary study at low frequency (9–120 MHz) appeared a year later,[7] again sweeping a small field at fixed frequency. Use of nonresonant waveguide transmitting 50–150 GHz radiation was made by Mock in 1960, but again as part of a field-swept spectrometer.[12] In the same paper, a scheme for operation at these frequencies at zero field was described wherein the frequency was swept through resonance with only a modulating magnetic field present. A novel placement of the sample in only half the waveguide allowed the line shape to be recovered as the derivative. Compared with the arrangement in Figure 1, this zero-field spectrometer adds an attenuator and E/H tuner. For the description of these and other microwave elements, Poole's book is an invaluable resource.[25]

At about the same time, Bogle and Symmons became interested in the possibility of using zero-field split levels of transition ions as the basis of maser action.[4] There followed in 1961–1963 four papers reporting the zero-field spectra of a number of high-spin iron complexes[13-15] and of dilute gadolinium sulfate.[26] The 7.8–12.4 and 12.4–18.0 GHz waveguide transmission spectrometers used in this work are described in detail in a paper with Burgess and Sierins.[4] (An extension from 18–26 GHz was also reported and included an echo tunnel for frequency calibration.) In that paper, detailed description of the total spectrometer and modulating system was given along with some useful suggestions for avoiding spurious reflections. The X-band (7.8–12.4 GHz) system shown is a reflection type, but is nonresonant in character. They noted that in a reflection system there is doubt whether all the power has traversed the sample before reflection. Although ab-

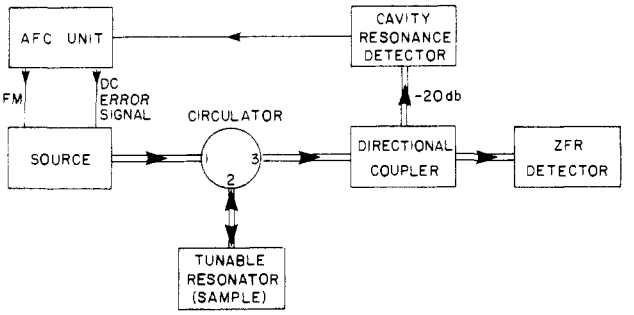

Figure 4. Simplified block diagram of a resonant reflection ZFR spectrometer. Modulation details have been omitted in the interests of clarity but are shown in Figure 1.

sorption may be double that in a transmission system, they preferred the latter. We also have noted that transition intensities in reflection systems are generally not as reliable as in a transmission spectrometer, presumably for the same reason and because standing wave patterns are frequency dependent. They estimated that a minimum of 10^{17} Fe^{3+} ions was required for detection at 80 K. Waveguide transmission spectrometers were also used by Chamberlain and Syms[27] and by Rao and Sastry.[28]

As far as we are aware, there is only one report of the use of coaxial line in a nonresonant mode. Our study[29] of Mn^{2+} in $MgSO_4 \cdot 7H_2O$ and in NH_4Cl shows spectra recorded by replacing some of the coaxial-line dielectric with the sample. The frequency independent Z_0 of coaxial line gives it its ultra-broad-band character and has the advantage that changing sample from one waveguide size to another is unnecessary. The filling factor is wavelength independent, so in a fundamental transmission mode, relative transition intensities can be expected to be more reliable. Where high sensitivity is not a prime requirement and large amounts of material are available (a few grams), such as often occurs in the study of transition ions, the nonresonant spectrometer is entirely adequate.

C. Resonant Spectrometer

The advantage of a spectrometer built around a resonant device or cavity is its sensitivity relative to that of a nonresonant system. This advantage is proportional to Q which can be 20 000 in a cylindrical TE_{011} cavity for example. Over limited frequency ranges, the normally high EPR sensitivities can be duplicated. As in the case of a nonresonant spectrometer, resonant systems can be operated either in reflection or transmission mode. Differences between reflection and transmission resonant systems have been analyzed and shown to be not significant from the sensitivity point of view. However, the advantage of a reflection cavity is that only one coupling mechanism is needed[23] and since this has to couple over a frequency range, having only one simplifies the spectrometer. A block diagram is shown in Figure 4.

Since octave bandwidths are commonly available for most components, this is a desirable and easily achievable design minimum for the frequency range of a spectrometer. Isolators and circulators are available, having bandwidths up to two octaves or more, and resonant devices can in some cases be tuned well over an octave. Even the coupling device can be sufficiently frequency insensitive in some situations, but generally, it causes the most problems, particularly if parts of conventional fixed frequency EPR spectrometers are tried. For example, the Varian cylindrical cavity (V-4533) can be converted into a variable frequency cavity by inserting a noncontacting plate as a movable base inside it to raise the frequency, or a quartz tube to lower it, but the coupling device does not allow optimum coupling over the whole of this range. Urban described a cavity which tuned from 8 to 13 GHz.[30] It was only necessary to drive the plunger or dielectric load smoothly. The spectrometer automatic frequency control (AFC) circuits and/or klystron cavity adjustment then track the klystron with the cavity. Narrow resonances can be explored in this manner without iris adjustment.

One of the more successful devices in our ODMR experience has been a tunable coaxial cavity with magnetic coupling provided by a rotatable loop inserted off-center through an end plate. The loop is an extension of the inner conductor of a coaxial line and terminates on the outer conductor. This was designed to work in its fundamental mode from 1–4 GHz. Over the two octave bands, very little adjustment of the coupling loop is needed. The other end of the cavity is a noncontacting short that is motor-driven by a threaded rod, and an AFC system tracks across each octave source (BWO) without adjustment. It has a Q >1000. Higher modes can be set up at higher frequencies but then coupling is more of a problem. Its disadvantage for conventional detection is a low filling factor at low frequencies (long wavelength and long cavity). In ODMR the filling factor is much less important. Where sample quantity can be increased and the cavity filled at the high frequency end of the range of interest, useful results could be obtained. Bleaney, Scovil, and Trenam used a series of coaxial resonators in their study of gadolinium and neodymium ethyl sulfates.[9] These could be frequency trimmed, but not tuned over a wide range.

We have explored the adaptation of the Lecher line called the slotted tube resonator (STR) as a good compromise between versatility and performance. So far, the STR has been advocated for fixed frequency use.[24] For tunable use, optimum performance cannot so readily be achieved, however one device we have built runs from 2.5 to 15 GHz in a single mode with well over 1 GHz ranges before coupling adjustments become necessary. The structure is open, which lends itself to cryogenic applications, versatile modulation possibilities, optical irradiation, and other constraints.

In order to regain traditional EPR sensitivities, most features of an EPR spectrometer have to be incorporated in the ZFR design (although see the discussion on the helix, section IIE). In addition, the AFC system must be capable of maintaining synchronism over the full frequency range without adjustment (for example, of a klystron cavity size). Such spectrometers are necessarily complex, the price that must be paid for optimum sensitivity. Resonant ZFR spectrometers for which particularly detailed descriptions have been given are those of Urban,[30] Erickson,[31] and Bernstein and Dobbs.[32] Urban mixed 20-kHz modulation into the carcinotron source supply lines and phase detected the resonance of a cylindrical TM_{011} cavity to keep the two in tune. Erickson as well as Bernstein and Dobbs both

used reentrant cavity designs and achieved almost two octave and somewhat more than one octave performance, respectively. These spectrometers operated in the lower microwave frequency range 1–4 GHz and used bidirectional square-wave modulation. Erickson's design is interesting in that the transmission cavity is in a microwave loop with a trombone line stretcher and travelling wave tube amplifier. The AFC error signal is fed through a servoamplifier to the line stretcher to keep the loop's electric length an integral number of half wavelengths of the radiation resonant with the cavity. The three items thus form a microwave oscillator.

D. Submicrowave Frequency Spectrometers

Low frequency in this context means less than 1 GHz. Since resonant cavities below this frequency tend to be large and have filling factor problems, and since sensitivity is further reduced by the dwindling population difference between resonant states, other designs become necessary.

There is little that can be done with a small population difference in a nonresonant line except to use lower temperatures, more sample, and higher power, lower noise sources, etc. Somewhere in the region of 1000–500 MHz, the switch to resonant systems has to be made. Fortunately, the development of superconducting magnet NMR spectrometers has brought NMR frequencies up to the lower limit of this borderline region. From 0 to 1000 MHz is the region of NQR and a pulsed NMR probe operating outside the magnet can be used as an NQR (or ZFR) spectrometer. It is not proposed to discuss NQR spectrometers since their designs can be traced from the literature reporting such experiments. NMR probes are readily tuned capacitively over at least octave bands with a given coil and the same is true in the case of NQR spectrometers.

Experimentally, most work below 1 GHz has been concerned with radical ($S = {}^1/_2$) species with small nuclear hyperfine interactions and resonances in the 10–200 MHz region. Invariably, the spectrometers are based on continuous-wave NMR spectrometers built before commercial NMR spectrometers were commonplace. From 200 MHz to 1 GHz, no resonances in ground-state systems have been reported as far as we are aware. In the ODMR area, the triplet $2E$ transition commonly occurs in this region and the preferred device is the helix.

E. The Helix

Commonly used in optical microwave double resonance because of its open structure, the slow-wave helix is, next to the screwdriver, the most misused tool. For samples with slow to moderate relaxation rates, and a source power of the order of 100 mW, a twisted paper clip or bent pin inserted into the end of a coaxial line suffices to induce phosphorescence intensity changes at microwave resonance. Since this is the case, then the success of the helix may be incidental in many ODMR applications. For fast relaxation rates, this will not be so and careful use of the helix is essential. In particular, the mode of operation must be known and the sample must, in the resonant or reflection modes, be placed at a position in the helix where B_1, the microwave magnetic field, is a maximum.

Physically, the helix is a single layer coil of conducting material. Its usual function is to act as a slowing structure, the wave propagating around the wire rather than along the helix axis. The ratio of the turn length to the pitch gives the slowing factor. It can operate in several ways determined by the relationship between helix dimensions and wavelength of the microwave radiation.[33] These are as an antenna, as a fundamental mode, slow-wave device or as a higher mode, slowing structure. The antenna case is comparatively trivial in the present context and occurs when the circumference of the helix is less than one-tenth of the free space wavelength. This is equivalent then to a straight wire antenna. For circumferences greater than half the wavelength, the wave can propagate in higher modes which do not have cylindrical symmetry. This is a complication best avoided since even in the fundamental (angularly independent) mode, field configurations can be highly inhomogeneous over the sample volume. In the intermediate region where $(\lambda/10) <$ circumference $< (\lambda/2)$, the fundamental mode dominates. It is this regime which is best used in magnetic resonance devices. Such a fundamental mode helix can then be made to operate either as a travelling wave (transmission) device by matching each end to waveguide or coaxial line and detecting the transmitted power or as a reflection device by shorting one end (an open circuit also presents a reflection but shifts the field antinodes one-half guide wavelength). Absorbed power in the latter case is detected after a circulator or hybrid tee. Finally, if in the reflection case the helix length is an integral number of half guide wavelengths, standing waves can be set up and the system will resonate. It follows that the resonant mode is highly frequency dependent and that its impedance is also a sharply varying function of frequency. Problems occur with the matching device. In general, it is not possible to use the same device to match a helix both on and off resonance. Consequently, EPR transitions can be missed if the mode and the corresponding match are not close to those intended. The matching device for a nonresonant helix can be made comparatively frequency independent over a useful range. For matching nonresonant helices to coaxial connections, e.g., N type, we have found that the length of straight wire and the radius of the bends at the ends of the helix offer enough flexibility to achieve adequate matches. For connecting and matching resonant helices to coaxial connectors and cables, small trimmer capacitors of a few picofarads work well and allow some adjustment for different resonances in the same helix.

The resonant helix has been little used. In zero-field work this is not hard to understand since the frequency is restricted to the resonant bandwidth. We have found some use for the device in zero-field ODMR where the transition frequency was known and a higher B_1 was needed to compete with fast spin–lattice relaxation. In some circumstances it can give higher sensitivity than a resonant cavity. Such situations are discussed by Volino, Csakvary, and Servoz-Gavin.[34] High rf fields are also useful in ENDOR experiments. Fourrier-Lamer and Grandjean describe the use of a resonant helix in such an application.[35] Here the helix doubles as a coil for the nuclear magnetic dipole transitions. The helix, travelling wave or nonresonant, is popular

in high-pressure experiments, it being much easier to contain in a pressure cell than to insert a pressure cell into a resonant cavity. Plachy and Schaafsma used a resonant helix in a high-pressure application.[36] In similar situations Nowicki, Hillmer, and Urban used a nonresonant helix.[37] The essential difference in these two high-pressure experiments is that the former is a high-field EPR experiment, the latter a zero-field one. Both papers describe the helix and its coupling to the line in useful detail.

The principles of design for the travelling wave helix have been developed by Webb and co-workers in two papers.[33,38] In particular different matching schemes were discussed and one recipe given which was frequency independent over a range of 1.6 GHz at 9 GHz. It is these papers which are most frequently quoted as the basis for helix design. Pearlman and Webb[38] also showed that travelling wave helices can be designed to produce the high magnetic fields necessary for electron nuclear double resonance work. A good discussion of the theory and design of a helix has been given by Newman and Urban.[39] The practical aspects are given in considerable detail. Bernstein and Dobbs also described a nonresonant helix spectrometer in the reentrant cavity paper[32] and compared performances of the cavity and helix.

III. First Row Transition Ions—$3d^n$

The first frequency-swept ZFR measurements for transition ions came out of an interest in using the zero-field split levels in a maser. This interest pointed to the suitability of high-spin Fe^{3+} systems. As these studies were progressively reported, other advantages of ZFR were apparent, for example in dealing with the complexities of magnetic inequivalence which complicate EPR spectra. Simple diagnostic tests for phase changes emerged, the number of structurally inequivalent ions appearing as a well resolved multiplicity in the ZFR spectrum contrasting with unresolvable EPR spectra.

The simplicity of $S = {}^5/_2$, $I = 0$ ZFR spectra was appealing and the complementary potential of the ZFR technique was applied to further Fe^{3+} systems. It was not until 1981 that ZFR spectra involving fine and hyperfine structure of a transition ion were reported (Mn^{2+}, $S = {}^5/_2$, $I = {}^5/_2$). Whereas spin Hamiltonian parameters were in general agreement from the two techniques for Fe^{3+}, this has not proved to be so for Mn^{2+}, especially in low symmetry environments. As a result it may be expected that ZFR will be more routinely applied in such systems. This observation will apply to all ions having both high electron and nuclear spin.

In addition to those ions mentioned above, ZFR of Cr^{3+} and Ni^{2+} is also discussed. The zero-field spectrum of Cu^{2+} pairs is reported here for the first time. The application of far infrared ZFR techniques to Fe^{3+} ($S = {}^5/_2$ and $S = {}^3/_2$ states) and to Mn^{3+} ($S = 2$) is also included in this section.

A. General Comments on the $S = {}^5/_2$ Spin Hamiltonian

A number of publications on the ZFR spectra of high-spin Fe^{3+} doped into various salts appeared between 1961 and 1970.[4,13-15,27,28,40] Most of these were concerned with the paramagnetic ion in an axially distorted octahedral environment. With symmetry no lower than this, that is, no lower than trigonal or tetragonal, exact expressions and useful approximations can be obtained for the ZFR frequencies. Regrettably there exist several notation conventions for the spin Hamiltonian.[41,42] The first part of this section is devoted to a brief discussion of the expressions used for axially symmetric $S = {}^5/_2$ systems.

For an S state ($L = 0$) ion, the effect of the crystal field on the spin states is described by the spin Hamiltonian

$$\mathcal{H}_S = \sum_{0<n<2S} \sum_{|m|\leq n} B_n^m O_n^m \qquad (1)$$

where S is the total electron spin, O_n^m (strictly $\bar{O}_n^m$[43]) are various operators of the total electron spin (Stevens' operator equivalents[44]) and B_n^m are parameters to be determined. The point symmetry of the surroundings of the ion determines which parameters must be zero. For the cases considered here, the most important effects of symmetry are that all terms with odd n disappear due to time-reversal symmetry[45] and that when the highest rotational symmetry axis is p-fold then the only nonzero terms have $m = lp$ where l is integral or zero. In a few low symmetry cases, negative m values are required. Buckmaster and Shing[46] give a complete discussion of the terms required for different point groups for $S = {}^7/_2$, which is applicable to all $S \leq {}^7/_2$ if it is remembered that $n < 2S$ in eq 1. Their formalism is that of the tensor operators[47] T_{nm} which are related to the Stevens' operator equivalents through O_n^m = constant$[T_{nm} + (-1)^m T_{n-m}]$; imaginary terms correspond to O_n^m with m negative, definitions of which have been given by Newman and Urban[39] and Tennant[48] (the latter uses $\bar{R}_n^m$ for such terms, and $\bar{O}_n^m$ for Stevens' operators with $m \geq 0$). In high-symmetry situations, there are relations which connect some of the B_n^m, a fact which leads to some confusion in notation.

For Fe^{3+} in which the environment is an axially distorted octahedron, the zero-field spin Hamiltonian is

$$\mathcal{H}_S = B_2^0 O_2^0 + B_4^0 O_4^0 + B_4^3 O_4^3 \qquad \text{(trigonal)} \quad (2)$$

$$\mathcal{H}_S = B_2^0 O_2^0 + B_4^0 O_4^0 + B_4^4 O_4^4 \qquad \text{(tetragonal)} \quad (3)$$

The explicit forms of O_n^m relevant to the discussion in this section are

$$O_2^0 = 3S_z^2 - S(S+1)$$

$$O_2^2 = (S_+^2 + S_-^2)/2$$

$$O_4^0 = 35S_z^4 - 30S(S+1)S_z^2 + 25S_z^2 - 6S(S+1) + 3S^2(S+1)^2$$

$$O_4^3 = [S_z(S_+^3 + S_-^3) + (S_+^3 + S_-^3)S_z]/4$$

$$O_4^4 = (S_+^4 + S_-^4)/2$$

The spin operators O_n^m have been tabulated in a number of publications,[39,41,43,49-51] in some cases along with the matrix elements $\langle M_S|O_n^m|M_S'\rangle$; a compilation of all operators and matrix elements for $n \leq 6$ is given by Al'tshuler and Kozyrev.[52] (The caption of Table 2.1 given by Newman and Urban[39] should read $[x,y] = xy + yx$.) An important feature is that non-zero elements occur only when $|M_S - M_S'| = |m|$ for each term $B_n^m O_n^m$. It

should be noted that equations relating the B_n^m with other notation conventions depend on the choice of axes and this must be specified if the experimental parameters are to be correctly compared with the theoretical estimates or results from environments of other symmetries. With few exceptions, most authors relate b_n^m to B_n^m by the following factors (for numerical convenience reasons); $b_n^m = f_n B_n^m$ where $f_2 = 3$, $f_4 = 60$ (and $f_6 = 1260$). An exception is the definition of $b_6^3 = 36B_6^3$ and $b_4^3 = 3B_4^3$ used by Buckmaster and Shing.[46]

For d^5 systems, parameters D, F, and a have been most often used for high-symmetry situations and in the work described in this section, so for consistency we also will describe these systems using this convention. The spin Hamiltonians in this notation are

$$\mathcal{H}_S = DO_2^0/3 + (F - a)O_4^0/180 - 2^{1/2}aO_4^3/9 \quad \text{(trigonal } z \text{ // 3-fold axis)} \quad (4)$$

$$\mathcal{H}_S = DO_2^0/3 + (a + 2F/3)O_4^0/120 + aO_4^4/24 \quad \text{(tetragonal } z \text{ // 4-fold axis)} \quad (5)$$

It should also be pointed out that Abragam and Bleaney[53] in their discussion of d^5 systems use a different operator equivalent formalism and relate this to the usual D, a, F parameters. For tetragonal symmetry their Hamiltonian for the electron spin takes the form $B_2^0O_2^0 + (B_4^0 + B_4)O_4^0 + 5B_4O_4^4$ which should be compared with the form of eq 3. Similarly with trigonal symmetry they use $B_2^0O_2^0 + (B_4^0 - 2B_4/3)O_4^0 - 40(2)^{1/2}B_4O_4^3/3$ which should be compared with the form of eq 2. They use a $B_n^{(m)}$ notation not all of which are the same as the conventional B_n^m coefficients. Unfortunately there exists a repeated error in the literature in the definition of F in terms of operator equivalent coefficients $F = 180B_4^0$ when B_4^0 is used as in eq 1. This relation only holds if the formalism of Abragam and Bleaney is being used (or if B_4^4 and B_4^3 are zero). Here we reserve B_n^m for the simplest possible operator equivalent spin Hamiltonian (eq 1).

For completeness we list the relations between the parameters for the two symmetries. The authors' names in parentheses are given where different numerical factors relating b_n^m to B_n^m have been used.

Trigonal

$$a = -9B_4^3/2^{1/2} = -3b_4^3/2^{1/2} \text{ (Buckmaster and Shing}^{46}\text{)}$$
$$\text{or } -3b_4^3/(20(2)^{1/2}) \text{ (Hutchings}^{41}\text{)}$$

$$F = 9(20B_4^0 - B_4^3/2^{1/2}) = 3(b_4^0 - b_4^3/2^{1/2}) \text{ (Buckmaster and Shing)}$$
$$\text{or } 3(b_4^0 - b_4^3/(20(2)^{1/2})) \text{ (Hutchings)}$$

$$b_4^0 = (F - a)/3$$

Tetragonal

$$a = 24B_4^4 = 2b_4^4/5$$

$$F = 36(5B_4^0 - B_4^4) = 3(5b_4^0 - b_4^4)/5$$

$$b_4^0 = (a + 2F/3)/2$$

Coefficients of the second-order spin terms are not controversial and are defined by

$$D = 3B_2^0 = b_2^0$$

$$E = B_2^2 = b_2^2/3$$

The latter is introduced when the symmetry is less than axial. An orthorhombic crystal field also requires a parameter B_4^2.

It is important to note that a and F are defined differently according to whether a tetragonal or trigonal axis is taken as the z axis. In both axis systems $F = 0$ for cubic symmetry.

To determine the energy levels, the b_n^m parameters are numerically more convenient and in terms of the high field spin states $|M_S\rangle$ the interaction matrix for trigonal symmetry is as follows:

M_S	$\pm 5/2$	$\mp 1/2$	$\pm 3/2$
$\pm 5/2$	$10b_2^0/3 \quad b_4^0$	$\pm b_4^3/(2 \times 10^{1/2})$	
$\mp 1/2$	$\pm b_4^3/(2 \times 10^{1/2})$	$-8b_2^0/3 + 2b_4^0$	
$\pm 3/2$			$-2b_2^0/3 - 3b_4^0$

where the conventions $b_2^0 = 3B_2^0$, $b_4^3 = 60B_4^3$, and $b_4^0 = 60B_4^0$ have been used.

The eigenvalue solutions are as follows:

$$\epsilon_{1,3} = b_2^0/3 + 3b_4^0/2 \pm \tfrac{1}{2}\{(6b_2^0 - b_4^0)^2 + (b_4^3)^2/10\}^{1/2}$$

$$\epsilon_2 = -2b_2^0/3 - 3b_4^0$$

Normally b_4^3 and b_4^0 are much smaller than b_2^0 so the square-root term can be expanded to give approximations to the energies, given below to second order in b_4^3, with the corresponding exact spin states

$$\epsilon_1 \simeq 10b_2^0/3 + b_4^0 + (b_4^3)^2/40(6b_2^0 - b_4^0)$$

$$\cos\alpha\,|\pm 5/2\rangle \mp \sin\alpha\,|\mp 1/2\rangle$$

$$\epsilon_2 = -2b_2^0/3 - 3b_4^0$$

$$|\pm 3/2\rangle$$

$$\epsilon_3 \simeq -8b_2^0/3 + 2b_4^0 - (b_4^3)^2/40(6b_2^0 - b_4^0)$$

$$\sin\alpha\,|\pm 5/2\rangle \pm \cos\alpha\,|\mp 1/2\rangle$$

where

$$\tan 2\alpha = -b_4^3/(10^{1/2}(6b_2^0 - b_4^0))$$

Such approximate expressions are useful in estimating b_4^3 and have been used in this way (with D, F, a nomenclature).[13,14,27,28] For predicting a ZFR spectrum from given values of the parameters the exact expression should be used and these are given using both parameterization sets for trigonal and tetragonal distortions from cubic symmetry in Tables I and II, along with fourth-order transition energy expressions, assuming b_2^0 is much greater than other parameters in the Hamiltonian. Relative transition intensities are also shown in these tables.

Figure 5 gives the energy level diagram for magnetic field parallel to the symmetry axis of an Fe^{3+} ion in a trigonal environment where the axial term is dominant. ZFR transitions, EPR transitions, and special EPR transitions near to repelling levels are shown; the latter are dealt with in the discussion on sapphire (see section IIIC).

The exact expressions in Tables I and II apply to all combinations of D, a, and F; they give the equations for cubic symmetry when the parameters D and F are set

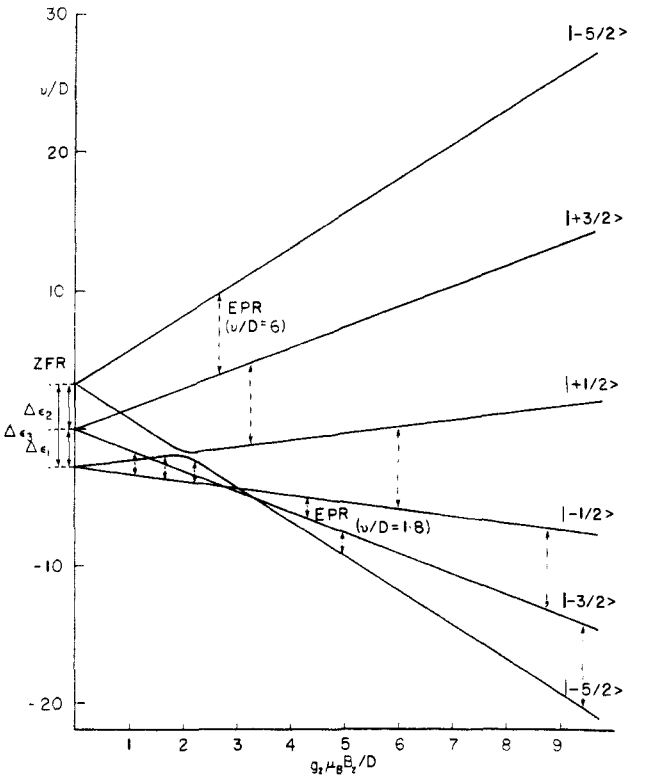

Figure 5. Energy level diagram for $S = {}^5/_2$ as a function of magnetic field parallel to a threefold symmetry axis. Axes are in units of D. The diagram is appropriate for sapphire (Fe^{3+} in α-Al_2O_3). The three ZFR transitions and the five strong field-swept EPR transitions expected for a constant microwave frequency $\nu >> D$ (in this case $\nu \simeq 30$ GHz) are indicated. Also shown are X-band transitions ($\nu \simeq 9.3$ GHz) used to determine the minimum energy gap between the two repelling levels.

to zero. Other sets of approximate solutions can be derived depending on the parameters and would of course be different for $a >> D$, for example. Lower symmetries introduce further off-diagonal terms and analytical expressions are not possible; the complete matrix has then to be diagonalized to obtain the zero-field energies. This forms the basis for our method of predicting ZFR frequencies for $S = {}^5/_2$ systems in low symmetry.[29]

In order to make clear the effects of different terms in the spin Hamiltonian on the ZFR spectrum of dilute Fe^{3+} ($S = {}^5/_2$), plots of ZFR frequencies, with intensities indicated, are shown in Figure 6. This is for a basically cubic environment with a distortion along a fourfold (z) axis. Considering second-order terms only, two transitions at $2D$ and $4D$ are predicted. D is often the principal interaction and so forms the starting point in Figure 6.

Off-diagonal terms such as E ($b_2^2/3$) or a ($2b_4^4/5$) shift the transition energies and also impart intensity into the third ($\Delta\epsilon_1 + \Delta\epsilon_2$) transition frequency. The effect of introducing E is always to bring the two main transitions closer together irrespective of its sign. Analytical expressions for the zero-field energy levels in terms of D and E (in the absence of other terms) for $S = {}^5/_2$ have been given by Bowers and Owen.[54] The effect of the term a should be considered more carefully: with $F = 0$ its effect is to shift the main transitions more closely together or further apart depending on whether a is negative or positive, respectively (Figure 6b). Specifying $F = 0$ implies $b_4^4 = 5a/2$ and $b_4^0 = a/2$ and the first-order effect of the latter dominates the shifts of the main transitions. Considered alone, the off-diagonal parameter b_4^4 increases the separation between the two main transitions, irrespective of its sign, as is shown in Figure 6c and can be seen from the second-order equation in Table II (b). Thus b_2^2 (or $3E$) has the opposite effect of b_4^4 on the main transitions, and both impart intensity

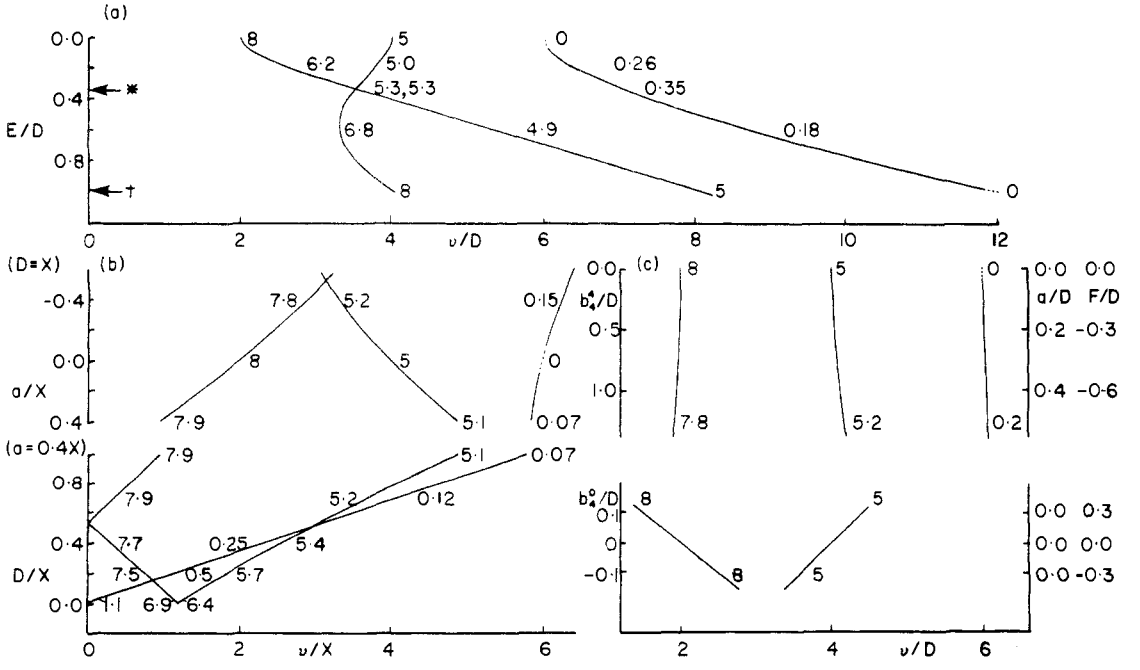

Figure 6. Effects of combination of spin Hamiltonian parameters on ZFR frequencies for $S = {}^5/_2$ system. Parameters not specified are zero. (a) D and E. E and ν given in units of D. When $E = D/3$ (marked *) a rotation of the axis system ($x \rightarrow y'$, $y \rightarrow z'$, $z \rightarrow x'$) gives a new pair of values D' and E' related to the original pair by $D' = -D$, $E' = E$. When $E = D$ (marked †) the values in the new axis system are $D' = -2D$, $E' = 0$. (b) D and a. Ordinates and frequency given in arbitrary units of X. (c) D (b_2^0), b_4^0, and b_4^4. The fourth order parameters a and F define "diagonal" (b_4^0) and "off-diagonal" (b_4^4) parameters in the case of tetragonal symmetry; this illustrates the effects of b_4^0 and b_4^4, given in units of D (b_2^0). Numbers alongside the resonant positions represent relative intensities (not weighted by Boltzmann population factors).

Table I. Zero-Field Energy Levels, Spin States, Transition Energies, and Intensities for High-Spin d^5 Ions in Cubic Field with Trigonal Distortion

(a) b_n^m Notation, z Direction along Trigonal Axis

energy	spin state
$\epsilon_1 = {}^1/_3\, b_2^0 + {}^3/_2\, b_4^0 + {}^1/_2\{(6b_2^0 - b_4^0)^2 + {}^1/_{10}\,(b_4^3)^2\}^{1/2}$	$\cos\alpha\ \lvert\pm{}^5/_2\rangle \mp \sin\alpha\ \lvert\mp{}^1/_2\rangle$
$\epsilon_2 = -{}^2/_3\, b_2^0 - 3b_4^0$	$\lvert\pm{}^3/_2\rangle$
$\epsilon_3 = {}^1/_3\, b_2^0 + {}^3/_2\, b_4^0 - {}^1/_2\{(6b_2^0 - b_4^0)^2 + {}^1/_{10}\,(b_4^3)^2\}^{1/2}$	$\sin\alpha\ \lvert\pm{}^5/_2\rangle \pm \cos\alpha\ \lvert\mp{}^1/_2\rangle$

transition energy	intensity: x or y	intensity: z
$\Delta\epsilon_1 = -b_2^0 - {}^9/_2\, b_4^0 + {}^1/_2\{(6b_2^0 - b_4^0)^2 + {}^1/_{10}\,(b_4^3)^2\}^{1/2}$	${}^5/_2 + {}^3/_2\cos^2\alpha$	0
$\simeq 2b_2^0 - 5b_4^0 + \dfrac{(b_4^3)^2}{40(6b_2^0 - b_4^0)} - \dfrac{(b_4^3)^4}{160(6b_2^0 - b_4^0)^3}$		
$\Delta\epsilon_2 = b_2^0 + {}^9/_2\, b_4^0 + {}^1/_2\{(6b_2^0 - b_4^0)^2 + {}^1/_{10}\,(b_4^3)^2\}^{1/2}$	${}^5/_2 + {}^3/_2\sin^2\alpha$	0
$\simeq 4b_2^0 + 4b_4^0 + \dfrac{(b_4^3)^2}{40(6b_2^0 - b_4^0)} - \dfrac{(b_4^3)^4}{160(6b_2^0 - b_4^0)^3}$		
$\Delta\epsilon_3 = \Delta\epsilon_1 + \Delta\epsilon_2 = \{(6b_2^0 - b_4^0)^2 + {}^1/_{10}\,(b_4^3)^2\}^{1/2}$	${}^9/_8\sin^2 2\alpha$	${}^9/_2\sin^2 2\alpha$
$\simeq 6b_2^0 - b_4^0 + \dfrac{(b_4^3)^2}{20(6b_2^0 - b_4^0)} - \dfrac{(b_4^3)^4}{80(6b_2^0 - b_4^0)^3}$		

where $\alpha = {}^1/_2\tan^{-1}\left\{\dfrac{-b_4^3}{10^{1/2}(6b_2^0 - b_4^0)}\right\}$

(b) D, a, F Notation[a]

energy
$\epsilon_1 = {}^1/_3\, D - {}^1/_2\,(a - F) + {}^1/_6\{(18D + a - F)^2 + 80a^2\}^{1/2}$
$\epsilon_2 = -{}^2/_3\, D + (a - F)$
$\epsilon_3 = {}^1/_3\, D - {}^1/_2\,(a - F) - {}^1/_6\{(18D + a - F)^2 + 80a^2\}^{1/2}$

transition energy
$\Delta\epsilon_1 = -D + {}^3/_2\,(a - F) + {}^1/_6\{(18D + a - F)^2 + 80a^2\}^{1/2}$
$\simeq 2D + {}^5/_3\,(a - F) + \dfrac{20a^2}{3(18D + a - F)} - \dfrac{400a^4}{3(18D + a - F)^3}$
$\Delta\epsilon_2 = D - {}^3/_2\,(a - F) + {}^1/_6\{(18D + a - F)^2 + 80a^2\}^{1/2}$
$\simeq 4D - {}^4/_3\,(a - F) + \dfrac{20a^2}{3(18D + a - F)} - \dfrac{400a^4}{3(18D + a - F)^3}$
$\Delta\epsilon_3 = {}^1/_3\{(18D + a - F)^2 + 80a^2\}^{1/2}$
$\simeq 6D + {}^1/_3\,(a - F) + \dfrac{40a^2}{3(18D + a - F)} - \dfrac{800a^4}{3(18D + a - F)^3}$

[a] Spin states and intensities are as defined with $\alpha = {}^1/_2\tan^{-1}[(80^{1/2}a)/(a - F + 18D)]$.

into the $\Delta\epsilon_3$ transition. The term b_4^0 has a first-order effect on the main transition energies (Figure 6d) but alone does not give rise to intensity in the $\Delta\epsilon_3$ transition. All parameters in a low symmetry situation are not determinable from the ZFR spectrum alone, but as discussed later, consideration of intensities, further interaction with magnetic nuclei, or additional variable frequency EPR measurements allows the determination of complete parameter sets.

A word of warning is necessary about the parameter E. A common convention is to define an axis system such that $E \leq |D/3|$ and $E \geq 0$ (the sign of E simply depends on the choice of x,y axes). The effect of $E \geq |D/3|$ is shown in Figure 6a. A change of axis systems when $E > |D/3|$ (primed axes and parameters refer to the new system) $z' = y$, $y' = x$, $x' = z$ leads to[49] $D' = -D/2 - 3E/2$, $E' = D/2 - E/2$ with $E' \leq |D'/3|$ once again satisfied. It is important to be aware of this in the EPR of isomorphous crystals doped with transition ions where a slight increase in an E ($\simeq D/3$) parameter could be analyzed in terms of a D with the opposite sign as given by expressions such as those above. Apparently anomalous changes of sign of D for Mn^{2+} doped into a series of Tutton salts[55] have recently been shown to be due to different authors unknowingly using different axis systems in order that $E < |D/3|$.

B. ZFR of Fe^{3+} ($S = {}^5/_2$)

Much of the 1960s' work of Bogle and Symmons was applied to testing the validity of the spin Hamiltonian at zero field. Most of this work was done with powders. The first case they examined in detail was Fe^{3+} in polycrystalline methylamine alum.[13] Because the X-band EPR is complicated by a large number of lines, ZFR was used to analyze the spin Hamiltonian and to determine how many species give rise to the EPR spectrum. In an X-band frequency variation experi-

TABLE II. Zero-Field Energy Levels, Spin States, Transition Energies, and Intensities for High-Spin d^5 Ions in Cubic Field with Tetragonal Distortion

(a) b_n^m Notation, z Direction along Tetragonal Axis

energy	spin states
$\epsilon_1 = {}^4/_3 b_2^0 - b_4^0 + \{4(b_2^0 + b_4^0)^2 + {}^1/_5(b_4^4)^2\}^{1/2}$	$\cos\alpha \lvert\pm {}^5/_2\rangle + \sin\alpha \lvert\mp {}^3/_2\rangle$
$\epsilon_2 = {}^4/_3 b_2^0 - b_4^0 - \{4(b_2^0 + b_4^0)^2 + {}^1/_5(b_4^4)^2\}^{1/2}$	$\sin\alpha \lvert\pm {}^5/_2\rangle - \cos\alpha \lvert\mp {}^3/_2\rangle$
$\epsilon_3 = -{}^8/_3 b_2^0 + 2b_4^0$	$\lvert\pm {}^1/_2\rangle$

transition energy	intensity: x or y	intensity: z
$\Delta\epsilon_1 = 4b_2^0 - 3b_4^0 - \{4(b_2^0 + b_4^0)^2 + {}^1/_5(b_4^4)^2\}^{1/2}$	$4\cos^2\alpha$	0
$\simeq 2b_2^0 - 5b_4^0 - \dfrac{(b_4^4)^2}{20(b_2^0 + b_4^0)} + \dfrac{(b_4^4)^4}{1600(b_2^0 + b_4^0)^3}$		
$\Delta\epsilon_2 = 2\{4(b_2^0 + b_4^0)^2 + {}^1/_5(b_4^4)^2\}^{1/2}$	${}^5/_2\cos^2 2\alpha$	$8\sin^2 2\alpha$
$\simeq 4b_2^0 + 4b_4^0 + \dfrac{(b_4^4)^2}{10(b_2^0 + b_4^0)} - \dfrac{(b_4^4)^4}{800(b_2^0 + b_4^0)^3}$		
$\Delta\epsilon_3 = \Delta\epsilon_1 + \Delta\epsilon_2 = 4b_2^0 - 3b_4^0 + \{4(b_2^0 + b_4^0)^2 + {}^1/_5(b_4^4)^2\}^{1/2}$	$4\sin^2\alpha$	
$\simeq 6b_2^0 - b_4^0 + \dfrac{(b_4^4)^2}{20(b_2^0 + b_4^0)} - \dfrac{(b_4^4)^4}{1600(b_2^0 + b_4^0)}$		
where $\alpha = {}^1/_2 \tan^{-1}\left\{\dfrac{b_4^4}{5^{1/2}(2b_4^0 + 2b_2^0)}\right\}$		

(b) D, a, F Notation[a]

energy
$\epsilon_1 = {}^4/_3 D - {}^1/_2(a + {}^2/_3 F) + \{(2D + a + {}^2/_3 F)^2 + {}^5/_4 a^2\}^{1/2}$
$\epsilon_2 = {}^4/_3 D - {}^1/_2(a + {}^2/_3 F) - \{(2D + a + {}^2/_3 F)^2 + {}^5/_4 a^2\}^{1/2}$
$\epsilon_3 = -\dfrac{8}{3}D + a + \dfrac{2}{3}F$

transition energy
$\Delta\epsilon_1 = 4D - {}^3/_2(a + {}^2/_3 F) - \{(2D + a + {}^2/_3 F)^2 + {}^5/_4 a^2\}^{1/2}$
$\simeq 2D - {}^5/_2(a + {}^2/_3 F) - \dfrac{15a^2}{8(60 + 3a + 2F)} - \dfrac{25.27a^4}{128(6D + 3a + 2F)^3}$
$\Delta\epsilon_2 = 2\{(2D + a + {}^2/_3 F)^2 + {}^5/_4 a^2\}^{1/2}$
$\simeq 4D + 2(a + {}^2/_3 F) + \dfrac{15a^2}{4(6D + 3a + 2F)} - \dfrac{25.27a^4}{64(6D + 3a + 2F)^3}$
$\Delta\epsilon_3 = 4D - {}^3/_2(a + {}^3/_2 F) + \{(2D + a + {}^2/_3 F)^2 + {}^5/_4 a^2\}^{1/2}$
$\simeq 6D - {}^1/_2(a + {}^2/_3 F) + \dfrac{15a^2}{8(6D + 3a + 2F)} + \dfrac{25.27a^4}{128(6D + 3a + 2F)^3}$

[a] Spin states and intensities are as defined with $\alpha = {}^1/_2 \tan^{-1}[(5^{1/2}a)/[2(a + {}^2/_3 F) + 4D]]$.

ment Bleaney and Trenam[8] had foreshadowed this experiment by extrapolating the EPR transition back to zero field to obtain approximate transition energies. Bogle and Symmons[13] observed two zero-field resonances at 22.043 ± 0.010 GHz and 12.227 ± 0.005 GHz at 90.2 K and concluded that only one paramagnetic species existed.

The equations for zero-field transition energies for trigonal symmetry (Table I) were used to second order in a to obtain $D = 1893\ (\pm 2) \times 10^{-4}$ cm^{-1}, $(a - F) = 171 \times 10^{-4}$ cm^{-1}. Only the relative signs of D and $(a - F)$ (i.e., b_2^0 and $-3b_4^0$) are obtainable from the ZFR experiment; in this case the positive sign of D was taken from specific heat measurements. In other alums a was fairly constant with values of about 130×10^{-4} cm^{-1} (the positive sign has been determined for Fe^{3+} in rubidium alum[56]) which implies that $F \simeq -40 \times 10^{-4}$ cm^{-1}. F here is much larger than in other alums, a fact which may correlate with a much larger axial parameter D in this system.

The use of the approximate equations to second order is justified in this and other ZFR measurements of Fe^{3+} since higher order terms are negligible for such magnitudes of a and D. It is obvious that three parameters cannot be determined from the two main zero-field resonances and recourse has to be made to other ways of obtaining one of the parameters. For the purposes of checking whether spin Hamiltonian parameters determined from EPR satisfy the ZFR frequencies, there is no such problem since all the parameters from EPR can be put into the exact expression for the energies to predict the ZFR frequencies. (The same holds true for lower symmetries in which four or more parameters appear in the spin Hamiltonian; in this case the ZFR

spectrum is predicted by a single diagonalization of the complete matrix.) Symmons and Bogle tested the exactness of the spin Hamiltonian for Fe^{3+} in sapphire (α-Al_2O_3 with various impurity ions) by analyzing the EPR spectrum and then comparing observed ZFR frequencies with those calculated from the EPR analysis.[14] Using the spin Hamiltonian (eq 4) appropriate for a threefold symmetry axis, they found the second-order equations (Table Ib) sufficiently accurate to predict the frequencies (although, as pointed out above, there is no reason not to use the exact expressions). A maximum discrepancy of 11 MHz was found, this being well within the EPR and ZFR experimental errors. Thus they concluded that the spin Hamiltonian fitted the observations from 0 to 10000 G between 4 and 299 K.

Shortly before the publication of this work by Symmons and Bogle,[14] results of another detailed EPR examination and ZFR measurements on this system were given by Kornienko and Prokhorov.[5] The two main zero-field resonances (at about 11.8 and 18.9 GHz at 290 K) were measured at 290 and 4.2 K and were the same within experimental error as the results of Symmons and Bogle. Kornienko and Prokhorov gave no details of how the ZFR measurements were accomplished. In their field-swept EPR measurements with the magnetic field along the symmetry axis they made use of the mutual repulsion between the (high field designation) $|^1/_2\rangle$ and $|^{-5}/_2\rangle$ electron spin levels to make an accurate measurement of a ($=-3b_4^3/(20 \times 2^{1/2})$). They determined the maximum frequency of the EPR transition between the unperturbed level $|^{-1}/_2\rangle$ and one of the repelling levels ($\sim|^1/_2\rangle$ at low field) and the minimum frequency of the transition between $|^{-3}/_2\rangle$ and the other repelling level ($\sim|^{-5}/_2\rangle$ at low field). (See Figure 5.) Both of these have a first order dependence on $|a|$ and so enable a direct determination of $|a|$. The microwave frequencies necessary to perform this experiment conveniently fell within the "tunable range" of the X-band microwave source and cavity. In principle, this is the same technique as was later developed by Urban who measured the minimum energy gap between repelling levels to determine the off-diagonal element causing the repulsion (see section IVC). This later work employed variable frequency EPR measurements at a number of fixed magnetic fields (parallel to the z axis); this removed some of the problems encountered by Kornienko and Prokhorov[5] of line broadening of the transitions near repelling points when field-swept spectra were measured. This extension of variable frequency techniques to the high field situation is extremely useful in the determination of small off-diagonal elements and is discussed again later (section IVC).

Studies continued by Bogle and Symmons et al. with Fe^{3+} doped into cobalt and aluminum acetylacetonates and in pure ferric acetylacetonate using EPR and ZFR.[15] Space group symmetry of the pure ferric acetylacetonate crystal and of the two host lattices requires a spin Hamiltonian of the form (terms involving O_n^m with odd m being neglected)

$$\mathcal{H}_S = g\mu_B B\cdot S + B_2^0O_2^0 + B_2^2O_2^2 + B_4^0O_4^0 + B_4^2O_4^2 + B_4^4O_4^4$$

The authors unconventionally wrote b_n^m for B_n^m and therefore have probably redefined the O_n^m operators to absorb the numerical factors. The expression for F should be $F = 3b_4^0 - 3b_4^4/5$. Parameters were obtained for $Fe^{3+}/Co(acac)_3$ by conventional EPR analysis at 80 K. These predicted zero-field resonances at 8.640 GHz and 16.422 GHz, compared with the experimental values 8.562 ± 0.005 GHz and 16.417 ± 0.015 GHz at the same temperature. The difference of 80 MHz is well within the EPR measurement error, which we estimated from their tabulated parameters. The authors noted a splitting of the high frequency ZFR line into three components at 4.2 K which indicates that the space group is different at low temperature, allowing three distinguishable sites.

For Fe^{3+} doped in aluminum acetylacetonate and pure ferric acetylacetonate, the ZFR frequencies were listed for different temperatures and approximate values for $|b_2^0|$ were obtained from the total splitting ($\simeq 6b_2^0$). No previous EPR analyses had been made. The EPR spectrum at 80 K and below was too complex to analyze but the ZFR showed three different spectra. It would normally be difficult to pair off the main ZFR frequencies in such a case but because the "forbidden" transitions were reasonably strong the level schemes were immediately apparent. A "forbidden" transition occurs at the sum of the other two frequencies, and is quite strong in this case because of the unusually large value of $b_4^4 = 5a/2 = 802(\pm 100) \times 10^{-4}$ cm^{-1} (b_2^2 and b_4^2 also contribute mixing of different levels which imparts more intensity into the $'|\pm^1/_2\rangle' \leftrightarrow '|\pm^5/_2\rangle'$ transitions). Since the line widths of the $'|\pm^3/_2\rangle' \leftrightarrow '|\pm^1/_2\rangle'$, $'|\pm^5/_2\rangle' \leftrightarrow '|\pm^3/_2\rangle'$, and $'|\pm^5/_2\rangle' \leftrightarrow '|\pm^1/_2\rangle'$ transitions are in approximate ratio 1:2:3 at 90 K, this strongly suggests that the widths are due to local inhomogeneity of b_2^0 (= D) of about 40 MHz. At room temperature the widths are similar which suggests that spin-lattice relaxation has become the dominant broadening mechanism. In the case of ferric acetylacetone the EPR spectra could not be measured because of the large line widths but the ZFR at 80 K and at 4.2 K was observed. Transitions were centered at 15.90 ± 0.15 GHz and 30.97 ± 0.2 GHz at 80 K with full widths of 1.4 and 3.0 GHz, respectively. No splitting was detectable in either of the transitions.

Bogle and Symmons pointed out that the spin Hamiltonian parameters could not be determined precisely from ZFR since there were only two strong transitions but four parameters to be determined. Their estimation of b_2^0 (D) from the total splitting (i.e., the sum of the two main transition frequencies) is obviously very approximate and relies on b_2^0 being by far the most dominant interaction. In principle, extra information is available from the third transition which is only allowed through off-diagonal mixing of the high field $|M_S\rangle$ states. With the development of sensitive resonant variable frequency techniques and control of the power arriving at the sample, very weakly allowed transitions make the ZFR determination of some low symmetry parameters feasible. Accurate measurement of the intensities of transitions is, however, a prerequisite. As an example consider the case of a fourfold symmetry axis. From Table II certain combinations of the strongly allowed transitions remove the higher order terms:

$$\Delta\epsilon_1 + \Delta\epsilon_2/2 = 4b_2^0 - 3b_4^0 \qquad \text{(exact)}$$

which can be useful for estimating b_2^0.

The ratio of intensities of the $\Delta\epsilon_3$ and $\Delta\epsilon_1$ transitions, for example, is $\tan^2\alpha$ (× ratio of Boltzmann factors) where

$$\tan 2\alpha = b_4^4/(5^{1/2}[2b_4^0 + 2b_2^0])$$

Together with the exact expression for $\Delta\epsilon_1$ and $\Delta\epsilon_2$ these form the starting point for an iterative determination of all three parameters b_2^0, b_4^0, and b_4^4. Similar techniques can be used for a threefold symmetry axis. When more parameters occur (twofold axis or lower symmetry) then again the solution is not obtainable with a three level ssystem but it may be possible to determine combinations of parameters.

In another example of Fe^{3+} in a trigonal symmetry environment, Chamberlain and Syms[27] examined the ion contained in $AlCl_3{\cdot}6H_2O$. The iron substitutes for aluminum which is surrounded by an octahedron of water molecules distorted along the [111] direction. The strong zero-field resonances were measured and compared with zero-field frequencies predicted from a conventional EPR analysis at Q band. D and $(a-F)$ were determined from the EPR spectrum with the static field along the axis, and a from the angular variation of the $(+^1/_2, -^1/_2)$ transition in the (001) plane. The values at 77 K (D = 1495.6 ± 0.7, a = 164 ± 2, F = 13 ± 4; units 10^{-4} cm^{-1})) predict zero-field resonances at 9.738 ± 0.005 and 17.347 ± 0.016 GHz, which should be compared with the observed frequencies 9.740 ± 0.002 and 17.36 ± 0.01 GHz. The signs of the parameters depend on the expectation that a is positive and $a > F$. From the zero-field equations (Table I) the second order and higher terms are small so D and $(a-F)$ must have the same sign. There are misprints in eq 1 and 2 of this paper. Again the spin Hamiltonian adequately represented the energy level scheme and the authors pointed out that higher order Zeeman terms linear in B that could be included in the Zeeman effect Hamiltonian must be less than 0.1% of the zero-field splittings.

Cook and Matarrese have measured the zero-field spectrum of Fe^{3+} in synthetic brown quartz (SBQ), the "I" center.[40] Their technique was similar to that used by Chamberlain and Syms in that they swept the field through zero for a number of frequencies around the zero-field resonance frequency. When the microwave frequency was very close to the zero-field splitting two EPR lines were symmetrically disposed about zero field (really the same transition but with opposite polarities of the magnetic field) and these coalesced at zero field when the frequency exactly matched the zero-field splitting. The zero-field frequencies were obtained by fitting the resonant fields versus frequency plots to straight lines and extrapolating to zero separation. This method gave better precision than attempts at varying the frequency to obtain the most intense coalesced line. This field extrapolation method has no advantages over direct frequency-swept zero-field spectrometry (so long as ambient fields are removed or have no significant effect); the apparent advantage in being able to use fitting procedures would lead to no greater precision than taking the mean value of the same number of direct determinations (by variable frequency ZFR) of the zero-field splitting. The experimentally determined zero-field splittings were compared with those predicted from EPR analyses. Yet another spin Hamiltonian notation (based on the Racah irreducible tensors) was used and recommended for general use. The parameters are related to the equivalent operator coefficients, B_n^m, but the advantage of using them is that they readily transform to different axis systems. Using the Stevens' operators, the site symmetry C_2 requires terms $B_n^m O_n^m$ with n = 2, 4, m = 0, −2, 2, −4, 4 (i.e., parameters B_2^{-2}, B_4^{-2}, B_4^{-4} in addition to the ones for orthorhombic symmetry).

The zero-field resonances are not far apart (an effect of the large B_2^2 term) and are as follows (with predicted values from an EPR analysis parenthesized): 7113.2 ± 0.2 (7109.8 ± 5.9) and 8812.5 ± 0.2 (8775.6 ± 6.5) MHz, which the authors regarded as showing that the EPR derived spin Hamiltonian was essentially correct. However, a deviation of 37 MHz when an expected error of 6.5 MHz is quoted would indicate some significant error in the spin Hamiltonian parameters. This shows the usefulness of ZFR in checking the validity of spin Hamiltonians even where many parameters are required by low symmetry.

The same authors also measured the ZFR of Fe^{3+} in natural amethyst and obtained resonances at 24 157.5 ± 0.5 (24150 ± 20), 35 365.0 ± 2.0 (35 390 ± 40) MHz where predicted values from Hutton's EPR analysis,[57] with which they agree within the errors quoted, are parenthesized. However, terms in the spin Hamiltonian involving operator equivalents O_4^0 and O_4^4 would be required for more exact EPR analysis.

Rao and Sastry have studied the ZFR of Fe^{3+} doped into NH_4Cl at room temperature.[28] EPR measurement at 77 K had indicated Fe^{3+} in both tetragonal and orthorhombic sites but with zero-field splittings so large that analysis could not be made at Q band. At room temperature NH_4Cl is in a different phase (transition temperature −32.5 °C) and Rao and Sastry observed three zero-field resonances at 10 274 (± 5) MHz, 10 750 (± 5) MHz and 20 681 (± 10) MHz sweeping the frequency from 8 to 12 and 18 to 26 GHz. They associated the 10 274 and 20 681 MHz transitions with a site of tetragonal symmetry both on the basis of the frequency ratio being close to 2 and on intensity grounds. The 10 750 MHz transition was associated with a site of orthorhombic symmetry (by analogy with the low temperature phase EPR results). Such an assignment can be criticized on the grounds that a frequency ratio of 2 is only expected to hold closely when b_4^0 (or $(a + 2F/3)/2$) is very small and this is not usually the case for Fe^{3+}; in fact their assignment leads to an unusually small value for a. Also the use of intensities to associate lines must be made with the utmost caution and with careful attention to microwave power levelling at the sample. The spin Hamiltonian is correctly quoted for tetragonal symmetry, but an approximate solution for trigonal symmetry was actually used. While this does not affect the magnitude of D it does affect the sign. Because of the different definitions of a and F in the two symmetries, these are also affected. The parameters are here recalculated for both possible pairs of lines in tetragonal symmetry with the usual assumption of $a > 0$ and $a > F$:

Pair 10 274, 20 681 MHz

$$D = 1721 \quad a + 2F/3 = 6.3\ (\times 10^{-4}\ cm^{-1})$$

(Rao and Sastry gave D = −1720, $a - F$ = 9 ($\times 10^{-4}$ cm^{-1})).

Pair 10750, 20681 MHz

$$D = -1744 \quad a + 2F/3 = 39 \ (\times 10^{-4}\ cm^{-1})$$

For a site of orthorhombic symmetry the effect of introducing the parameter E is to cause the two main transitions, originally at approximately $2D$ and $4D$, to approach one another and to impart intensity into the $'|\pm^1/_2\rangle' \leftrightarrow '|\pm^5/_2\rangle'$ transition ($\sim$6D) (see Figure 6). Thus their suggestion that a transition for this symmetry might be above the range of their equipment (> 26 GHz) should only apply to the semiforbidden transition; the second line is probably in the 12–18 GHz region which is also not covered by their microwave sources.

Finally, a novel frequency variation technique in the range 3–100 cm^{-1} (90–3,000 GHz) has been used to measure zero-field transitions of Fe^{III} and Mn^{III} complexes, including some biologically important compounds.[58,59] Many iron complexes of biological importance have large axial crystal fields and conventional EPR is only observed between the $'M_S' = \pm^1/_2$ states and can be described in terms of an effective **g** tensor. Thus D and E parameters are determined only by second order effects on the "normal" EPR resonances, the microwave quantum being much smaller than D. The extension of ZFR and EPR techniques into the far infrared region described by Richards et al.[59] provides a method for direct determination of some of the zero-field parameters. Here we outline the method of analysis; details for each of the many complexes examined can be found in the original publications.

For large values of D, fourth-order terms in the spin Hamiltonian (b_4^m) can be neglected and only the effects of D and E need be considered. At zero field, there are three energy levels (Figure 5) whose separation depends on E; (Figure 6a shows the transition energies between these levels). For $E = 0$ the separations are $2D$ and $4D$. At 4.2 K with D of the order of several cm^{-1} only the ground state is significantly populated; for $E = 0$ and positive D one transition at $\Delta\epsilon_1 = 2D$ would be detectable, but with negative D the energy levels are inverted and one transition at $\Delta\epsilon_2 = 4D$ is predicted. When $E \neq 0$, the transition at the sum of the two ZF splittings $\Delta\epsilon_3$ becomes allowed. Determination of $\Delta\epsilon_1$ (or $\Delta\epsilon_2$), $\Delta\epsilon_3$ and the absence of $\Delta\epsilon_2$ (or $\Delta\epsilon_1$) immediately gives the signs and magnitudes of D and E, which can be confirmed by the appearance of $\Delta\epsilon_2$ (or $\Delta\epsilon_1$) at higher temperatures. Observing the convention $E \leq |D/3|$, if one ZF transition occurs at less than half of $\Delta\epsilon_3$, this transition is $\Delta\epsilon_1$ and D is positive. Additional confirmation of the sign of D is obtained from absorption measurements in a magnetic field at low temperature: when D is positive, the ground-state spin functions, which are approximately $|\pm^1/_2\rangle$, are split by the field and EPR transitions are allowed between them; for D negative the ground state is $|\pm^5/_2\rangle$ and no EPR transitions would be seen at low temperature between the split states. Zero-field resonances between 3 and 36 cm^{-1} were observed for a number of systems including several Fe^{III}, $S = {}^5/_2$ systems. As an example we quote the result for tris(pyrrolidyl dithiocarbamato)iron(III) for which $\Delta\epsilon_2 = 8.4\ cm^{-1}$ and $\Delta\epsilon_3 = 13.2\ cm^{-1}$ were measured leading to $D = -2.14(\pm 0.05)\ cm^{-1}$ and $E/D = -0.10(\pm 0.01)$. ZFR spectra of Fe^{III}, $S = {}^3/_2$, and of Mn^{III}, $S = 2$ were also measured and are briefly discussed in separate sections below.

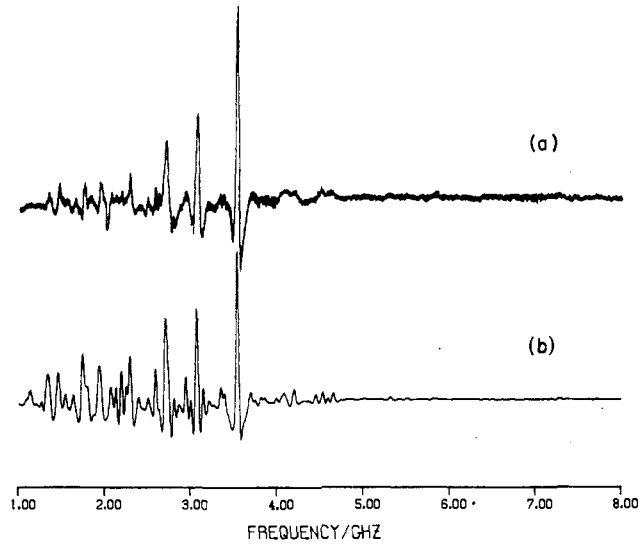

Figure 7. ZFR spectra of Mn^{2+} in $Mg(NH_4)_2(SO_4)_2 \cdot 6H_2O$ (powder $\sim$1.5 mol %). (a) Spectrum observed at 295 K. A coaxial line sample cell in a reflection microwave apparatus and magnetic field modulation (perpendicular to the microwave field) of ±16 G were used. (b) Spectrum predicted from least-squares fit to (a) with $D = -722.5$, $E = 188.7$, $F = -2.0$, $a = 14.4$, $A_x = A_y = -265.8$, $A_z = -264.3$ MHz (all ± 2–3 MHz) and line width 50 MHz. Second derivative Lorentzians were used to simulate the line shapes approximately.

C. ZFR of Mn^{2+} ($S = {}^5/_2$, $I = {}^5/_2$)

The ZFR spectra of $S = {}^5/_2$ systems become very much more complicated when hyperfine interaction with the $I = {}^5/_2$ nucleus occurs, particularly in low symmetry situations. Instead of three, a maximum of 630 transitions between the combined electron and nuclear spin levels is possible. We have shown that it was possible to obtain the main parameters of an orthorhombic spin Hamiltonian from the complex zero-field spectrum of Mn^{2+} doped in $MgSO_4 \cdot 7H_2O$ powder.[29] No analytical solution was possible and the technique used was iterative variation of all the parameters until the predicted spectrum was as close as possible to the observed spectrum. It was first necessary to obtain good starting values of the parameters from a preliminary EPR powder spectrum analysis. The final parameters were significantly different from previous EPR analyses. These were considered to be subject to errors of crystal alignment and magnetic field measurement. Exact analysis would require more terms in the spin Hamiltonian (e.g., b_4^2 is required for orthorhombic symmetry, and if the C_1 point group of the ion in the lattice is taken into account further terms in the Hamiltonian are required). However, analysis in terms of five parameters D, E, a, $A_\parallel$ and $A_\perp$ fitted the zero-field spectrum within the accuracy of the experiment. The previous EPR analysis predicted a ZFR spectrum whose features did not correspond to the experimental measurement.

Similar techniques were used to analyze the ZFR spectra of Mn^{2+} in several Tutton salts (orthorhombic point symmetry) (see Figure 7) and once again improvements in and more accurate values of the parameters were obtained[55] compared with previous EPR work. Most of the features of the ZFR spectra of Mn^{2+} in these salts result from the overlap of many individual

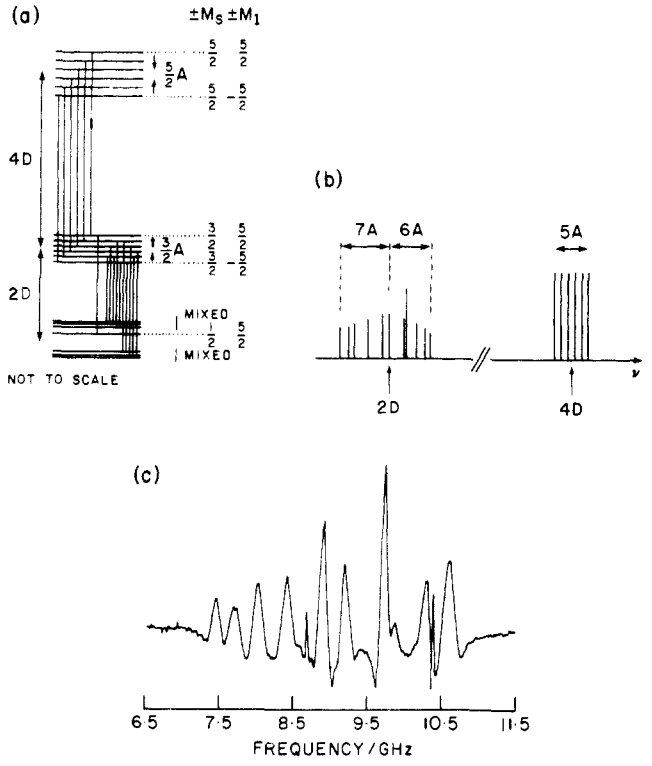

Figure 8. (a) Schematic energy level diagram for $S = {}^5/_2$, $I = {}^5/_2$ with dominant $D >> A$ (isotropic hyperfine interaction). (b) Resulting ZFR transitions (transitions in the region of $\nu = 5A$ are not shown). (c) Observed ZFR spectrum for 0.1 mol % Mn^{2+} doped in NH_4Cl at 295 K which could be simulated with $D = -4508$, $a + {}^2/_3F = 21$, $A_\parallel = -247$, $A_\perp = -254$ MHz. The powdered sample was contained in a coaxial line sample cell and the spectrometer was used in transmission mode. Magnetic field modulation (perpendicular to the microwave field) of ±33 G was used. The spectrum is the '2D' group of lines, slightly different from the pattern in (b) because of anisotropy of A. Sharp features are spurious effects of the reflection spectrometer.

lines. Adequate simulation of the zero-field line shapes was obtained by using second derivative Lorentzians simply because this function happened to produce modulation wings of about the right magnitude. Such simulation does not reproduce the variability of line widths observed in the experimental composite line shapes.

In the case of Mn^{2+} in NH_4Cl[29] a partial ZFR spectrum showed general agreement with that predicted from previous EPR work but it was shown that a slight error existed in either or both of D and a. The dominant interaction in the spin Hamiltonian (which has a fourfold symmetry axis in this case) is D, the next most important interaction being an almost isotropic hyperfine interaction A of about one-twentieth the magnitude of D. The general appearance of the ZFR spectrum can readily be calculated using first-order perturbation theory and is illustrated in Figure 8. Writing the unperturbed spin states in the high field designation $|M_S M_I\rangle$, the perturbation $A(I_z S_z + (S_+ I_- + S_- I_+)/2)$, treated to first order, adds to the diagonal terms only for $M_S = \pm{}^3/_2$ or $\pm{}^5/_2$ and the energies are as follows:

$$M_S = \pm{}^5/_2 \qquad \epsilon = 10D/3 \pm 5M_I A/2$$

$$M_S = \pm{}^3/_2 \qquad \epsilon = -2D/3 \pm 3M_I A/2$$

For $M_S = \pm{}^1/_2$ states the perturbation occurs between degenerate levels and the first-order energies comprise five doubly degenerate and two single levels, mixed states of type $c_1|{}^1/_2, M_I\rangle + c_2|{}^{-1}/_2, M_I + 1\rangle$ occurring. These levels are at $17A/4$, $4.022A$, $13A/4$, $5A/4$ (the two states which have this energy are pure $|{}^1/_2, {}^5/_2\rangle$ and pure $|{}^{-1}/_2, {}^{-5}/_2\rangle$), $-15A/4$, $-4.522A$, and $-19A/4$, relative to $-8D/3$. The lower group of transitions between $M_S = \pm{}^1/_2$ and $M_S = \pm{}^3/_2$ states then occurs in a characteristic 11-line pattern whose frequencies (with intensities parenthesized) are $2D - 7A$ (0.357), $2D - 6.277A$ (0.441), $2D - 5A$ (0.5), $2D - 3.272A$ (0.559), $2D - A$ (0.643), $2D$ (0.643), $2D + 2.272A$ (0.554), $2D + 2.5A$ (1.0), $2D + 4A$ (0.5), $2D + 5.272A$ (0.441), $2D + 6A$ (0.357).

The transitions between $M_S = \pm{}^3/_2$ and $M_S = \pm{}^5/_2$ states have the appearance of an EPR first-order hyperfine pattern. Resonances occur at $4D + M_I A$, that is there are six lines of equal intensity and equal separation A. (See Figure 8.) Further ZFR transitions between the hyperfine components of the $M_S = \pm{}^1/_2$ levels are also predicted at lower frequency.

Such characteristic patterns for $M_S = \pm{}^1/_2$ states when the main interaction is of D (b_2^0) type, with an isotropic hyperfine interaction as a secondary effect, are discussed for the cases of Gd^{3+} ($S = {}^7/_2$, $I = {}^3/_2$, see section IVA) and Cr^{3+} ($S = {}^3/_2$, $I = {}^3/_2$, see section IIID). A feature of these zero-field patterns is that splittings greater than A occur (e.g., up to $2.272A$ for Mn^{2+}) showing that ZFR can be more sensitive to the effects of hyperfine interaction than EPR. The relative signs of A and D are immediately obtained from the spectrum: the lower frequency pattern of eleven hyperfine lines (Figure 8) is reversed if A and D are of opposite sign. In EPR, the relative signs can only be determined from second-order effects.[60]

An important point in the analysis of Mn^{2+} ZFR spectra is that the splitting into many lines by the hyperfine interaction (e.g., as in Mn^{2+}/NH_4Cl) allows the determination of more electron spin parameters than is possible with Fe^{3+}. The following simple illustrations confirm this. Figure 9a,b shows predicted ZF line positions and relative intensities (uncorrected for population differences) for an $S = {}^5/_2$ system with $D = 500$, $E = 50$ (MHz) (a), and $D = 507.1$, $a = -31.9$ (d), whose spectra are, apart from intensity changes, almost identical. Figure 9b,c shows the line positions for an $S = {}^5/_2$, $I = {}^5/_2$ system with $D = 500$, $E = 50$, $A = 10$ MHz (b), and $D = 507.1$, $a = -31.9$, $A = 10$ MHz (c). The presence of the isotropic hyperfine interaction A causes E and a to have different and distinguishable effects on the spectrum.

D. ZFR of Cr^{3+} ($S = {}^3/_2$, $I = {}^3/_2$)

Cole, Kushida, and Heller observed two of the three zero-field, low frequency resonances possible for the 10% magnetic isotopes of Cr^{3+} doped into MgO (cubic symmetry).[61] For $S = {}^3/_2$, $I = {}^3/_2$ the spin states can be combined to give $F = 0, 1, 2, 3$ states at zero field with separations A, $2A$, and $3A$ (obtainable from the Landé interval rule) for an isotropic hyperfine interaction A. The two higher frequencies were observed giving $A = 48$ MHz. Because no splitting of the lines was observed the authors concluded that electron spin–spin coupling (which should be zero in an exactly cubic environment for $S = {}^3/_2$) and quadrupole coupling

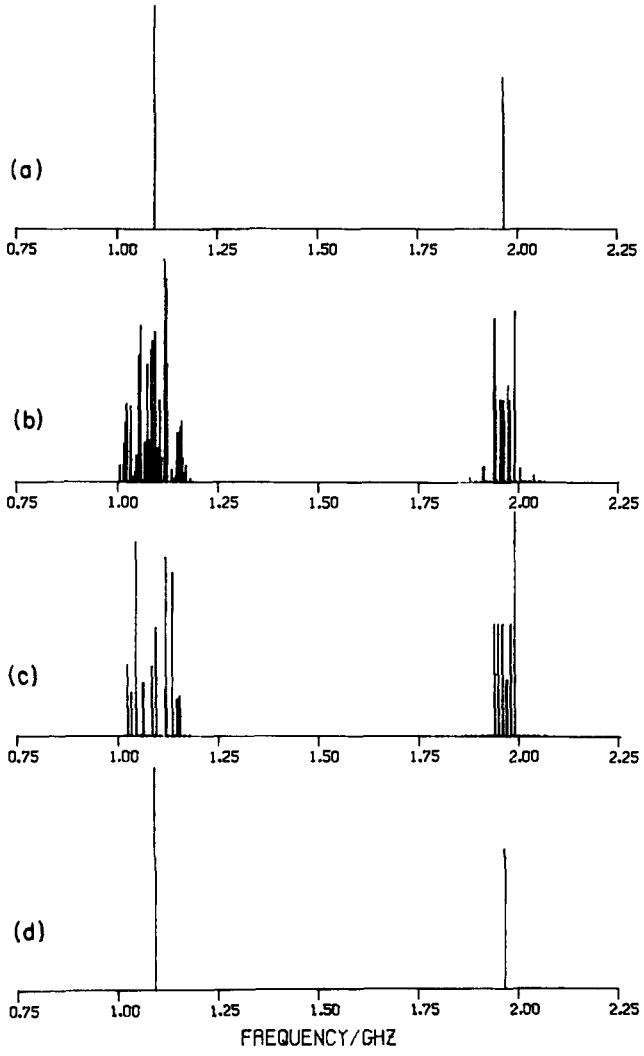

Figure 9. Stick diagrams illustrating ZFR frequencies predicted between 0.75 and 2.25 GHz for various combinations of spin Hamiltonian parameters D, a, E and isotropic hyperfine interaction A_{iso} for an $S = {}^5/_2$ ion (z defined as the fourfold axis before introduction of E). In the absence of hyperfine interaction almost identical ZFR spectra are predicted for D = 500.00, E = 50.00 MHz (spectrum a) and for D = 507.14, a = −31.92 MHz (spectrum d). When an isotropic hyperfine interaction with an $I = {}^5/_2$ nucleus is introduced the previously indistinguishable ZFR spectra take on very different appearances (spectrum b has D = 500.00, E = 50.00, A_{iso} = 10 MHz and spectrum c has D = 507.14, a = −31.92, A_{iso} = 10 MHz).

were less than the line width at half maximum height (4 MHz).

ZFR of Cr^{3+} in α-Al_2O_3 (ruby) was first reported in 1956 by Geusic[10] at a frequency of 11.593 GHz, which was within the error limit of the zero-field splitting predicted from his EPR analysis but about 100 MHz higher than later analyses. In this experiment, the spectrum was observed by sweeping the field; the frequency was adjusted until the two resonances coalesced at zero field. We have observed the single zero-field resonance for the nonmagnetic isotopes of Cr^{3+} in α-Al_2O_3 at 11.493 ± 0.005 GHz (T = 295 K) using our variable frequency spectrometer. This was shown in Figure 2. In the wings of the peak are suggestions of further transitions which could be due to ^{53}Cr resonances. It is noteworthy that whereas the ^{53}Cr ($I = {}^3/_2$) hfs pattern is a quartet in high field EPR, the pattern predicted for zero field for this $\nu = 2D$ resonance is an asymmetric pattern with transitions at $\sim 2D - 3.8A$ (intensity 18), $2D - 2.5A$ (25), $2D - 0.8A$ (32), $2D - 0.2A$ (32), $2D + 1.5A$ (two degenerate transitions, intensities 50 and 25), and $2D + 2.8A$ (18). A similar situation occurs with Gd^{3+} (section IVA) and Mn^{2+} (section IIIC) where this was discussed more fully.

E. ZFR of Fe^{3+} ($S = {}^3/_2$)

In addition to measurements on Fe^{3+}, $S = {}^5/_2$ states (see section IIIB), Brackett, Richards, and Caughey[59] measured high frequency ZFR and EPR transitions using (variable frequency) far infrared spectroscopy in bis(dithiocarbamate)iron(III) compounds. D values ranged from −2.1 to 8.17 cm^{-1} in a series of compounds with different ligands. For an $S = {}^3/_2$ state, there is only one zero-field resonance irrespective of whether E is zero or not, so D and E are not separable by ZFR. For $E << D$, the sign of D is obtainable from the far infrared absorption in the presence of a magnetic field (20–50 kG) since the ground levels split in different ways for D positive and D negative.

F. ZFR of Mn^{3+} ($S = 2$)

The only ZFR measurements on an isolated non-Kramers transition ion were published by Brackett et al.[59] in their studies using far infrared Fourier transform spectroscopy. The spin Hamiltonian necessary to describe an $S = 2$ system is basically the same as that for $S = {}^5/_2$. The energy levels are different. If a dominant D term is considered, then zero-field energy levels lie at $-2D$ ($M_S = 0$), $-D$ ($M_S = \pm 1$), and $2D$ ($M_S = \pm 2$) with the main zero-field resonances at D and $3D$. A magnetic field in the z direction splits the $M_S = \pm 2$ and $M_S = \pm 1$ levels linearly but does not affect $M_S = 0$; an E term splits $M_S = \pm 1$ in first order (analogous to $S = 1$) and $M_S = \pm 2$ in second order. Zero-field resonances were observed in two Mn^{III} porphyrins. In one case ZFR was observed at 7.6 cm^{-1}. Since no higher frequency transition was observed at higher temperatures this corresponds to the $3D$ transition, so D = −2.53 cm^{-1} since the $3D$ transition observed at 4.2 K must be from the ground state. (The other transition at 2.53 cm^{-1} would be detectable at higher temperatures, but was below the lower limit of their spectrometer, 3.5 cm^{-1}). The other Mn^{III} porphyrin with a ZFR spectrum had D = −3.08 cm^{-1}. From the line width of the ZFR absorption an upper limit on E could be estimated, since the ZFR line would split with large enough E.

G. ZFR of Cu^{2+} Dimers ($S = 1$ State)

Early EPR measurements[62] on copper acetate monohydrate showed that the structure comprised relatively isolated pairs of Cu^{2+} ($S = {}^1/_2$) ions strongly exchange coupled to produce a diamagnetic ground state ($S = 0$) and a low lying triplet state ($S = 1$) which is sufficiently populated at temperatures above about 20 K for EPR to be detectable. We have succeeded in observing two of the three possible zero-field resonances from the fine-structure part of the Hamiltonian at 145 K and at room temperature. The zero-field electron spin Hamiltonian for a rhombic environment is $\mathcal{H}_S = D(S_z^2 - S(S+1)/3) + E(S_x^2 - S_y^2)$ (eq 1 for $S = 1$ in D, E notation) and results in three energy levels at $D/3 + E$, $D/3 - E$, and $-2D/3$. Zero-field transitions are predicted at $D + E$, $D - E$, and $2E$ each allowed by a

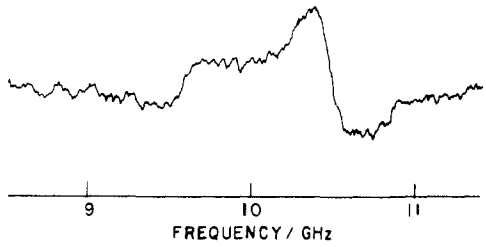

Figure 10. ZFR spectrum of anhydrous copper benzoate powder at 142 K. The sample was contained in a teflon tube which traversed the waveguide cell; the spectrometer was operated in transmission mode and magnetic field modulation (perpendicular to the microwave field) of amplitude ±140 G was used.

different linear polarization of the microwave field. Further details of the theory of ZFR for $S = 1$ can be found in the literature on excited organic triplet states.[63] Our EPR measurements gave $D = 10.082$ (± 0.005) GHz and $E = 0.296$ (± 0.005) GHz at 150 K so the $'D + E'$ and $'D - E'$ transitions were readily accessible. The ZFR spectrum of powdered copper acetate monohydrate showed two very broad resonances ($\Delta W_{1/2} \simeq$ 350 MHz) centered at 9.78 (± 0.04) and 10.46 (± 0.02) GHz at 150 K. Discrepancies between the observed and predicted resonance centers are thought to be due to the influence of the copper nuclear hyperfine interactions ($A_z \simeq 240$ MHz[62] at 90 K, $I = {}^3/_2$ for ^{63}Cu and ^{65}Cu), copper nuclear quadrupole interaction ($P = 23.36$ (± 0.03) for ^{63}Cu, 21.65 (± 0.05) MHz for ^{65}Cu at 52 K[64]) and water proton hyperfine interactions (range of anisotropic hyperfine interactions up to 12 MHz[65]). These interactions have a complicated effect on the ZFR line shape and are partly responsible for the observed width. ZFR peak frequencies would not therefore be expected to correspond exactly to $D + E$ and $D - E$. Detailed line shape simulation including all the above interactions would be necessary to correlate with the observed line shape. ZFR was also observed for the similar $S = 1$ low lying triplet state of anhydrous copper benzoate powder and is shown in Figure 10. In this case resonances at 9.68 GHz and 10.36 GHz at 140 K were somewhat sharper than those in copper acetate and showed deviations from the resonant positions predicted from the D, E terms of the EPR analysis[66] for similar reasons to those given above.

Modulation wings (see section IIB) take on a rather different appearance for non-Kramers states (integer S). Only one strong wing occurs for each of the two high frequency transitions, being on the high frequency side of the $'D + E'$ transition and on the low frequency side of the $'D - E'$ transition. Such effects can readily be understood qualitatively from a consideration of low field EPR transition intensities.

H. ZFR of Ni^{2+} ($S = 1$)

A recent publication by Mirzakhanyan[67] reported ZFR of Ni^{2+} in α-$LiIO_3$ at 93.1 (± 0.1) GHz and in $LiNbO_3$ at 152.1 (± 0.3) GHz at 85 K. EPR measurements up to 5000 G combined with the ZFR measurements showed that the system was well described by an axially symmetric spin Hamiltonian (zero-field term D only). Details of the 20–200 GHz tunable EPR spectrometer or details of ZFR measurement were not given in this paper. It was concluded from these measurements that the Ni^{2+} ion substitutes for Li^+ in both crystals and that any charge compensation vacancy must be on the threefold axis or is not local. ZFR of Gd^{3+} in $LiNbO_3$ is discussed in section IVE.

IV. Lanthanide Ions—4f^n

A. ZFR of Gd^{3+} in Lanthanum Ethyl Sulfate (LES)

Several authors have considered the EPR of Gd^{3+} doped into $La(C_2H_5SO_4)_3 \cdot 9H_2O$ at low and zero magnetic fields as well as at high field with conventional EPR. EPR work on this system illustrates the importance of considering ZFR experiments as an integral part of EPR studies. Historically, EPR measurements came first. The early realization that EPR could be observed at zero magnetic field led to prediction of the expected ZFR frequencies and then their measurement by an extrapolation of low field results. Disagreements between calculated and observed values were noted. This prompted a true ZFR experiment which successfully resolved the earlier discrepancy. However, it was noticed that the uncertainties in the measurements were relatively high. This in turn led to a major and detailed study of this system which resulted in the determination of hyperfine and quadrupole interactions together with fine structure terms for the first time in any system using ZFR techniques. Splittings were resolved which had previously overlapped in high field EPR experiments. The interest stimulated in this system has extended to low-field EPR measurements and to further questions about the electronic interactions underlying the spectroscopy.

The rare-earth ion in the host salt has C_{3h} point symmetry and the effective sixfold rotational symmetry of the crystal field[68] is represented by a zero-field spin Hamiltonian of the form

$$\mathcal{H}_S = B_2^0 O_2^0 + B_4^0 O_4^0 + B_6^0 O_6^0 + B_6^6 O_6^6 \qquad (6)$$

and the conventions $b_2^0 = 3B_2^0$, $b_4^0 = 60B_4^0$, $b_6^m = 1260B_6^m$ are used. The form of the spin Hamiltonian renders ZFR (and EPR when the Zeeman term is added) analysis straightforward since b_6^6 is small.

Bleaney, Scovil, and Trenam analyzed the single crystal EPR of this system and fitted the X-band EPR resonant fields to within 3 G at 90 K and within 7 G at 20 K.[9] They obtained the ZFR frequencies by extrapolating field–frequency plots of EPR transitions at low fields back to zero field. These were compared with calculated zero-field frequencies which in this case were obtainable directly from the X-band EPR line positions with field parallel to the symmetry axis since the b_6^6 parameter displaces the zero-field lines by less than 10^{-6} cm^{-1}. Neglecting the off-diagonal terms the zero-field resonances occur at

$$\begin{aligned}
M_S = \pm{}^1/_2 \leftrightarrow M_S = \pm{}^3/_2 \qquad & \Delta\epsilon_1 = 2b_2^0 - 12b_4^0 + 14b_6^0 \\
M_S = \pm{}^3/_2 \leftrightarrow M_S = \pm{}^5/_2 \qquad & \Delta\epsilon_2 = 4b_2^0 - 10b_4^0 - 14b_6^0 \\
M_S = \pm{}^5/_2 \leftrightarrow M_S = \pm{}^7/_2 \qquad & \Delta\epsilon_3 = 6b_2^0 + 20b_4^0 + 6b_6^0
\end{aligned} \qquad (7)$$

EPR transitions for the magnetic field parallel to the crystal axis are given by

$$\begin{aligned} M_S = +\tfrac{1}{2} &\leftrightarrow M_S = -\tfrac{1}{2} \qquad B = B_0 \\ M_S = \pm\tfrac{1}{2} &\leftrightarrow M_S = \pm\tfrac{3}{2} \\ B = B_0 &\pm (-2b_2^0 + 12b_4^0 - 14b_6^0)/g_z\mu_B \\ M_S = \pm\tfrac{3}{2} &\leftrightarrow M_S = \pm\tfrac{5}{2} \\ B = B_0 &\pm (-4b_2^0 + 10b_4^0 + 14b_6^0)/g_z\mu_B \\ M_S = \pm\tfrac{5}{2} &\leftrightarrow M_S = \pm\tfrac{7}{2} \\ B = B_0 &\pm (-6b_2^0 - 20b_4^0 - 6b_6^0)/g_z\mu_B \end{aligned} \tag{8}$$

where $B_0 = \nu/g_z\mu_B$, ν being the fixed microwave frequency. Thus the transition energies (eq 7) are given by half the difference (in energy units) between the pairs of EPR transitions given in (8).

The observed ZFR frequencies (1.349, 2.557, 3.457 GHz at 90 K and 1.466, 2.497, 3.388 GHz (all ±0.003 at 20 K) agreed within 15 MHz with those calculated from the EPR for the $|\pm^5/_2\rangle \leftrightarrow |\pm^7/_2\rangle$ and $|\pm^3/_2\rangle \leftrightarrow |\pm^5/_2\rangle$ transitions, but a discrepancy of 50 and 100 MHz occurred for the $|\pm^1/_2\rangle \leftrightarrow |\pm^3/_2\rangle$ transition. While the authors give some possible explanations for this discrepancy, these are not given here in view of the subsequent agreement between EPR and ZFR results (vide infra). The most likely explanation is that errors have come in the field-frequency method of obtaining zero-field frequencies; this method relies on accurate crystal alignment and magnetic field measurements and thus lacks the main advantages of direct frequency-swept ZFR measurement. Errors in the EPR analysis were also indicated by discrepancies between the predicted and measured resonant fields.

Dagg, Kemp, and Symmons[69] measured the zero-field resonances in this system between 4.5 and 285 K using the frequency-swept technique developed by Bogle and Symmons and co-workers.[4] Their measurements at 90 K (1.395 ± 0.014, 2.550 ± 0.010, 3.455 ± 0.012 GHz) and at lower temperatures indicated that the frequency determination for the transition by Bleaney et al.[9] was in error. Exact fitting of EPR transitions, including $\Delta M_S = \pm 3, \pm 5$ lines, yielded all the parameters of the spin Hamiltonian (e.g., at 288 K, $g_{iso} = 1.9920 \pm 0.0002$; $b_2^0 = 195.24 \pm 0.06$, $b_4^0 = -3.866 \pm 0.005$, $b_6^0 = 0.46 \pm 0.08$, $b_6^6 = -4.1 \pm 0.2$; units 10^{-4} cm^{-1}). Calculated ZFR frequencies agreed with the measurements within experimental error at 90 K and 4.2 K, although the EPR determinations were less precise at these two temperatures, b_6^6 being undetermined. EPR measurements were made at 10 temperatures and showed a maximum in the zero-field splitting at about 130 K due to the maximum in b_2^0 which is the dominant term. The absolute value of b_4^0 has a maximum at about the same temperature. As indicated by Bernstein and Dobbs[70] the zero-field measurements on this sytem by Dagg, Kemp, and Symmons were subject to high experimental uncertainty (up to 25 MHz in measured line positions).

Bernstein and Dobbs, in a most detailed publication,[70] carefully examined and analyzed the ZFR of this system and also obtained measures of the hyperfine and quadrupole interaction for the first time for $Gd^{3+}/La(C_2H_5SO_4)_3{\cdot}9H_2O$ using isotopically enriched ^{155}Gd, ^{157}Gd, and ^{160}Gd. Accurate measurements were obtained by using the more sensitive helix and cavity spectrometers. At 77 K they obtained zero-field splittings of 1371.9 (±3.9), 2503 (±3.6), and 3383.0 (±2.1) MHz in isotopically enriched (99.99% ^{160}Gd) samples. These splittings were the same within the error limits as 1366.2 (±3.9), 2502.7 (±4.2), and 3381.4 (±2.8) MHz calculated from the EPR analysis of Dagg et al.[69] The error limits quoted for the ZFR measurements were defined as three times the standard deviations as determined from measurements using various modulation field strengths, both types of spectrometer and ^{160}Gd as well as natural Gd. Similar agreement was found at 4.2 K. Bernstein and Dobbs pointed possible that the error limits in the ZFR resonant positions are mainly determined by the line width (~ 25 MHz); if not hampered by line broadening, measurements of frequency would be possible to an accuracy of 1 ppm whereas magnetic fields in conventional EPR can only be measured readily to 100 ppm. This shows that ZFR is inherently more precise than EPR.

The parameter b_6^6 is small and almost temperature independent so the other parameters could be determined from the three zero-field frequencies by taking $b_6^6 = 4.25 \times 10^{-4}$ cm^{-1} obtained by Dagg et al.[69] from EPR. Bernstein and Dobbs show that such a value shifts the $|\pm^5/_2\rangle$ (this was misprinted as $|\pm^1/_2\rangle$) or $|\pm^7/_2\rangle$ energy levels by about 0.5 MHz which is about the standard deviation of the transition frequencies. It follows that quite accurate values of b_2^0, b_4^0, and b_6^0 can be calculated from eq 7 which ignore b_6^6 and the authors used this procedure for the remainder of the analyses. Expressions for eigenvalues, transition energies, and probabilities similar to those given in section IIIA can be derived. Values of the three parameters for $^{160}Gd/La(C_2H_5SO_4)_3{\cdot}9H_2O$ at 77 K and 4 K (with b_6^6 fixed at 4.25×10^{-4} cm^{-1}) are in reasonable agreement with the determination using EPR by Dagg et al. although a slight discrepancy exists at 77 K in b_2^0 and b_4^0 values. Unlike Bernstein and Dobbs who use 3σ, Dagg et al. do not indicate the origin of error limits and one cannot always presume that the 3σ definition is used. A splitting of 26.1 MHz in the lowest ZFR frequency, obtained by extrapolation from above 10 G by Gerkin and Thorsell,[71] was not confirmed.

Bernstein and Dobbs[70] then measured and analyzed the zero-field spectra of Gd^{3+} in deuterated lanthanum ethyl sulfate and the hydrated and deuterated salts of samarium and erbium. In the lanthanum case the same temperature dependence of b_{2n}^0 (although only b_2^0 had a change significant within the error limits) from measurements at 4 and 77 K was found for the hydrate and deuterate. (In Table III of ref 70 the first b_4^0 should read b_2^0). From the lanthanide ion variation experiment the same variation of b_2^0 with 4f electron radius was found for the hydrates and deuterates. In all the measurements b_2^0 was 4% larger for the deuterate than the hydrate, findings which were interpreted in terms of a change in position of the hydrogen bonded deuteron because of the mass effect on the vibrational potential.

This study continued with ZFR measurements on isotopically enriched (>99%) ^{155}Gd and ^{157}Gd samples ($I = {}^3/_2$). Extra splittings seen in these samples were interpreted in terms of isotropic hyperfine interaction A and nuclear quadrupole interaction P which give

additional terms in the spin Hamiltonian $AS_zI_z + A(S_+I_- + S_-I_+)/2 + P[I_z^2 - I(I+1)/3]$. These parameters were obtained by a least-squares fit to the observed splittings using numerical diagonalization of the complete 32 × 32 matrix which arises from $S = {}^7/_2$, $I = {}^3/_2$ states. For the purpose of obtaining estimates of A and P with which to initiate the fitting procedure, first-order expressions for the energy levels and transition frequencies were obtained. For states with $M_S > {}^1/_2$ the high field states $|M_SM_I\rangle$ are valid to this level of approximation and the two strongly allowed resonances between these levels are both split evenly into four lines separated by A (as in high field EPR). The $M_S = \pm{}^1/_2$ states are mixed by the off-diagonal hyperfine term and split into three doubly degenerate and two single energy levels. Transitions to the $M_S = \pm{}^3/_2$ levels are then shifted by $7A/2$, $A-P-R$, $A-P+R$, $+3A/2$, $-2A+P-R$, $-2A+P+R$, and $-9A/2$ relative to the zero-order transition energy, where $R = [49A^2/4 - AP + P^2]^{1/2}$. Characteristic asymmetric patterns for transitions involving the $M_S = \pm{}^1/_2$ states, and EPR-like splittings for higher M_S states, always occur for $A \ll b_2^0$ and these effects have been described for $S = {}^5/_2$, $I = {}^5/_2$ in section IIIC and $S = {}^3/_2$, $I = {}^3/_2$ in section IIID for the case of hyperfine interaction alone. In this case with $S = {}^7/_2$, $I = {}^3/_2$ the transitions from $M_S = \pm{}^1/_2$ would be shifted by $-11A/2$, $-9A/2$, $-5A/2$, $3A/2$, $7A/2$, $9A/2$ in the absence of quadrupolar interaction P with relative intensities 6:7:8:22:7:6. The first, third, part of the fourth, and sixth of these are shifted in the presence of an axial quadrupole interaction but the remaining lines are unaffected. Because of the asymmetry of the pattern the signs of A and P relative to b_2^0 can be determined. The sign of b_2^0 had been determined as positive from low temperature EPR intensity measurements by Bleaney et al.[9] so the signs of all diagonal terms (b_n^0, A, and P) were now determined. The $|\pm{}^3/_2\rangle \leftrightarrow |\pm{}^5/_2\rangle$ and $|\pm{}^5/_2\rangle \leftrightarrow |\pm{}^7/_2\rangle$ transitions showed incompletely resolved hyperfine structure but the $|\pm{}^1/_2\rangle \leftrightarrow |\pm{}^3/_2\rangle$ showed four clearly resolved peaks, three other lines being overlapped near the center. This clearly demonstrates the value of ZFR in resolving otherwise overlapped hyperfine structure in EPR. A further advantage is that the quadrupole interaction has a first-order effect, as do the signs of P and A relative to b_2^0. Parameters obtained, for example at 77 K, were $A = 18.26$ ($\sigma = 0.37$), $P = -52.86$ ($\sigma = 1.26$) MHz for ^{157}Gd and $A = 14.59$ ($\sigma = 0.37$), $P = -48.01$ ($\sigma = 1.26$) MHz for ^{155}Gd. It was not clear from the text whether the $|\pm{}^3/_2\rangle \leftrightarrow |\pm{}^5/_2\rangle$ or $|\pm{}^5/_2\rangle \leftrightarrow |\pm{}^7/_2\rangle$ lines were used in the fit. There is no reason why peak positions of overlapped lines cannot be used in a least-squares fit to experiment provided that adequate line shape simulation is used, and this is the procedure we used to analyze the severely overlapped lines in Mn^{2+} spectra. Bernstein and Dobbs showed that the line shape can be qualitatively but not exactly simulated if different effective line widths are used for the field-on and field-off parts of the modulation cycle, slightly different shapes occurring with different orientation of modulation field with respect to the crystal axis. Integration over the entire powder sample volume would be necessary to obtain the exact line shape. The authors painstakingly indicated the origin of all standard deviation measurements, a practice which is essential for useful EPR/ZFR comparisons. It is somewhat surprising that some evidence for hyperfine structure was not observed with natural Gd (abundance of magnetic isotopes 15% each).

The ratio of hyperfine constants for the two isotopes was in reasonable agreement with other measurements. Such determinations are useful in determining the hyperfine anomaly Δ, defined by $^{155}A/^{157}A = [g_n^{(155)}/g_n^{(157)}](1 + \Delta)$, but a large experimental error in the g_n ratio results in Δ values of low accuracy. An improved value of the g_n ratio would be necessary to improve the accuracy of Δ, which can distinguish core-polarization or relativistic effects giving rise to hyperfine interaction for half-filled shells. The ratio of quadrupole constants for the two isotopes was in agreement with ENDOR and EPR data for Gd^{3+} in bismuth magnesium double nitrate (BMDN) and in YPO_4 and with atomic beam measurements of the ratio of nuclear quadrupole moments; the authors showed that the absolute values for P were in reasonable agreement with current theories.

Bernstein and Dobbs also illustrated the $M_S = \pm{}^3/_2 \leftrightarrow M_S = \pm{}^5/_2$ ZFR transitions for $^{157}Gd^{3+}$ in $Bi_2Mg_3(NO_3)_{12}\cdot 24H_2O$ (BMDN) where the narrow line width (10 MHz) affords clear resolution of the four hyperfine lines. The line width in LES ($\sim$ 25 MHz) was ascribed to a combination of dipolar coupling with neighboring protons (BMDN only has 6 compared with 18 in LES) and statistical variations in the crystal field due to lattice strains. However, it appears that there was no measurable local inhomogeneity in b_2^0 since this would result in a 1:2:3 line width effect on the three main transitions.

Bernstein and Dobbs' contribution is the most detailed analysis of a metal ion by ZFR in the literature and demonstrates the power of the technique in the agreement between ZFR observed frequencies and those calculated from precise EPR analysis and also in the determination of hyperfine and quadrupole constants for the first time by ZFR in a lanthanide ion.

A discussion of the ZFR of Gd^{3+}/LES would not be complete without some mention of the low-field, variable frequency EPR measurements on Gd^{3+} in this and other salts. Bleaney, Scovil, and Trenam used this method in an attempt to measure the ZFR transition frequencies by extrapolation as described above,[9] but their discrepancy with high-field EPR results was probably due to experimental error and the effects discussed in this section are not related. Two groups have made a claim for a zero-field splitting of the $M_S = +{}^1/_2$ and $-{}^1/_2$ states or nonlinearity in the energy levels for magnetic field along the crystal symmetry axis, or both effects.

It should first be made clear that for a spin Hamiltonian of the form (eq 6), with the addition of a Zeeman term $g\mu_BB_zS_z$ for a magnetic field B_z directed along the crystal axis z, the energy levels of the $M_S = \pm{}^1/_2$ and $\pm{}^3/_2$ states are exactly linear in B_z and all the $\pm M_S$ states for given M_S are degenerate at zero field. For most fields the $M_S = \pm{}^5/_2$ and $\pm{}^7/_2$ states are almost exactly linear but the small B_6^6 term causes mixing of $\pm{}^5/_2$ with $\mp{}^7/_2$ states; the effect of this is only of importance where the interacting levels would otherwise have crossed, which occurs when B_z is equal to one-sixth of the zero-field separation of the $\pm{}^7/_2$ and $\pm{}^5/_2$ levels expressed in magnetic field units. (See the discussion

of Gd^{3+} in section IVC.) Any splitting of the $|\pm^1/_2\rangle$ levels at zero field, or nonlinearity of these or other levels with a low magnetic field in the z direction implies a breakdown of the spin Hamiltonian.

Gerkin and Thorsell made variable frequency EPR measurements on Gd^{3+} doped in LES, SmES, and also BMDN with fields between 10 and 40 G.[71] With the crystal mounted with the z axis parallel to the field the transition energies should extrapolate linearly back to the ZFR transition energies. It was found that the $|+^3/_2\rangle \leftrightarrow |+^1/_2\rangle$ and $|-^3/_2\rangle \leftrightarrow |-^1/_2\rangle$ transitions extrapolated back to different zero-field splittings for all three salts. The authors assumed that at very low fields the levels became nonlinear so as to coincide at zero field in accordance with Kramers' theorem. Also observed were $\Delta M_S = 2$ transitions between $|\pm^3/_2\rangle$ and $|\mp^1/_2\rangle$ states but the extrapolation of these at $\theta = 0°$ was not shown; this would be important in determining relative splittings of the $|\pm^3/_2\rangle$, $|\pm^1/_2\rangle$ states at zero field. It is wrongly stated that at low magnetic fields the high-field states $|\pm M_S\rangle$ are no longer accurate, linear combinations resulting in allowed $\Delta M_S = 2$ transitions. For $B//z$, as discussed above, the $|\pm^1/_2\rangle$ and $|\pm^3/_2\rangle$ states are exact descriptions ($\Delta M_S = 2$ transitions should be strictly forbidden), and $|\pm^5/_2\rangle$ and $|\pm^7/_2\rangle$ states are almost exact descriptions. In view of the later paper by Gerkin, Rogers, and Tourek[72] in which angular misorientations of the crystal in the earlier paper are said to have occurred, this work does not provide an accurate description of the low-field energy levels of Gd^{3+} in these salts.

Subsequently Shing and Buckmaster again found a zero-field splitting of the $|\pm^1/_2\rangle$ states at zero field by linear extrapolation of measurements between 15 and 60 G on Gd^{3+} in LES.[73] In these more accurate measurements, in which the alignment of field with crystal axis is stated to be within 0.5°, the $\Delta M_S = 2$ transitions were also detected between $|\pm^3/_2\rangle$ and $|\mp^1/_2\rangle$ states and extrapolation of these indicated the same discrepancy as the allowed transitions. Examination of transitions between states with higher $|M_S|$ ($\geq^3/_2$) values indicated that there were no differences between $|M_S\rangle \leftrightarrow |M_S{+}1\rangle$ and $|{-}M_S\rangle \leftrightarrow |{-}M_S{-}1\rangle$ transition frequencies within the measurement error. It should be noted that equal splittings of $\pm M_S$ and $\pm(M_S{+}1)$ states at zero field would produce such a result; $\Delta M_S = 2$ transitions would be necessary to detect such splittings (see Figure 5 of ref 71). The authors assumed that the linear field dependence of levels found above 15 G extended back to zero field and concluded that the $|\pm^1/_2\rangle$ levels are split at zero field, with the $|\pm^3/_2\rangle$, $|\pm^5/_2\rangle$, $|\pm^7/_2\rangle$ levels probably not split. A temperature dependence of this anomalous splitting (16 MHz at 290 K, 10 MHz at 77 K for 0.5 mol % Gd^{3+}) and also a dependence on concentration of Gd were found. They noted that such a splitting can be phenomenologically described by an extra term in the spin Hamiltonian of the form $\Delta_x S_x + \Delta_y S_y$, which, if time reversal symmetry is strictly obeyed, is only possible if it originates from a mechanism magnetic in nature (although vide infra), such as spin–spin interaction. Such a term also gives intensity to the $\Delta M_S = 2$ EPR transitions between $|\pm^1/_2\rangle$ and $|\mp^3/_2\rangle$ states. Referring to the direct ZFR measurements of Bernstein and Dobbs (presumably from Figure 1 of ref 70) Shing and Buckmaster noted that the width of the $|\pm^1/_2\rangle \leftrightarrow |\pm^3/_2\rangle$ transition for ^{160}Gd was significantly greater than that of the $|\pm^3/_2\rangle \leftrightarrow |\pm^5/_2\rangle$ or $|\pm^5/_2\rangle \leftrightarrow |\pm^7/_2\rangle$ and took this as independent confirmation of the splitting of the $\pm^1/_2$ states. However, it should be noted that in the ZFR of magnetic isotopes of Gd (Figure 3 of ref 70) the individual transition widths in the $|\pm^1/_2\rangle \leftrightarrow |\pm^3/_2\rangle$ transitions are of comparable widths to those of the higher M_S transitions. The ZFR lines for ^{160}Gd are much broader than those for ^{157}Gd. This is probably due to the modulation field being much larger in the ^{160}Gd case: any deviation from square wave modulation would broaden the absorption line. Thus it is doubtful whether the extra broadening of the low frequency ZFR transition at high modulation levels can be taken as direct evidence for splitting of $|\pm^1/_2\rangle$ states.

In a series of papers by Smith, Buckmaster, and Chatterjee[74-76] various mechanisms for the apparent zero-field splitting of $|\pm^1/_2\rangle$ levels and concomitant anomalous g values of EPR transitions at low field are investigated. The use of magnetic field modulation to detect EPR signals at low field can lead to line shape distortion and incorrect resonant field positions. This effect would lead to an apparent $|\pm^1/_2\rangle \leftrightarrow |\pm^3/_2\rangle$ zero-field splitting but an order of magnitude smaller than observed. Higher order terms in the Zeeman effect are not sufficient to explain the weak field g values. For C_{3h} symmetry, crystal field terms O_n^m can occur in principle for n = 2,3,4,5,6. In the spin Hamiltonian for Gd^{3+} in C_{3h} symmetry, equivalent operator terms O_n^m have zero coefficients for the odd n values if the spin state arises from one electronic configuration only. However, if the ground state contains admixtures of different 4f and 5p configurations then nonzero matrix elements for n = 3 and 5 may occur which satisfy time reversal invariance. Calculations showed that such terms involving O_3^3, O_5^3, which split only the $|\pm^3/_2\rangle$ levels, affect the low field g values and predict splitting of the $|\pm^1/_2\rangle \leftrightarrow |\pm^3/_2\rangle$ transitions opposite to that which is observed. An equal splitting of the $|\pm^3/_2\rangle \leftrightarrow |\pm^5/_2\rangle$ transition is also predicted but not observed. None of these effects satisfactorily explains the observations.

Gerkin and Rogers extended the low-field EPR measurements on Gd^{3+}/LES, using isotopically enriched (95.2%) ^{160}Gd, by making measurements down to 2 G.[77] They found nonlinearity with field for all EPR transitions especially below 10 G. For EPR transitions between the $|M_S| = {}^1/_2$ and $^3/_2$ states they found the $\Delta M_S = 1$ transitions almost coinciding at 2 G (although extrapolation down to zero field would cause the transition energies to cross and differ again) whereas the $\Delta M_S = 2$ transitions diverged markedly near zero field. The authors concluded that the $\Delta M_S = 1$ transitions were identical at zero field, but did not have a satisfactory explanation for the $\Delta M_S = 2$ transitions. Reference to their earlier work[71] shows that such a situation would arise if the $|\pm^1/_2\rangle$ levels and $|\pm^3/_2\rangle$ levels were equally split.

Low-field measurements such as these require the utmost care, particularly with regard to field/crystal orientation and field homogeneity. Fine orientation of the magnetic field with respect to the crystal axis was attempted in this work[77] by having two orthogonal fields whose ratio could be adjusted thereby controlling the direction of the field. Alignment of field with crystal

axis was obtained from EPR magnetic field strength extrema. However, the authors indicate that some inconsistencies were found in aligning the field with the crystal axis, the direction having to be varied according to the EPR transition and field strength. Such effects indicate that again exact alignment of B with z may not have been achieved. Any component of B_x or B_y would cause a shift in energy levels of the type found by the various authors since the form of the extra term is analogous to the phenomenological term of Shing and Buckmaster.[73]

While much evidence has been presented for anomalous behavior of the energy levels for Gd^{3+} in LES near zero field, it has not been conclusively demonstrated that these effects are not caused by extraneous factors. In addition, none of the investigators of the low-field energy levels of Gd^{3+} in this salt has considered the effect of unresolved hyperfine splittings from the magnetic isotopes present. Gerkin and Rogers[77] used isotopically enriched ^{160}Gd for their measurements but this still contained 5% magnetic isotopes. The other low field measurements by Gerkin and Thorsell[71] and Shing and Buckmaster[73] used natural Gd which has 30% magnetic isotopes. The $|\pm^1/_2\rangle \leftrightarrow |\pm^3/_2\rangle$ ZFR transition for magnetic isotopes is an asymmetric pattern as shown by Bernstein and Dobbs;[70] this is also true at fields of sufficiently low magnitude for the electron spin states to be still significantly mixed by the hyperfine interaction. The EPR transitions showing the greatest signs of anomalous behavior at low fields were those involving these levels. Thus it is possible that hyperfine effects in the spectra for magnetic isotopes influences the measured resonance centers of low field EPR transitions in a nonlinear fashion. Such influences must be considered before conclusions about anomalous behavior are drawn. A decisive experiment would probably involve direct ZFR of Gd^{3+} in a salt where much narrower lines occur (such as in BMDN). The use of ZFR, with ambient fields exactly cancelled, to detect small splittings is much more desirable than attempting precise orientation of very small magnetic fields.

B. ZFR of Gd^{3+} in Lanthanide Sulfates, $Ln_2(SO_4)_3 \cdot 8H_2O$

In addition to their ZFR work on Fe^{3+}, Bogle and Symmons[26] also examined Gd^{3+} doped into $Ln_2(SO_4)_3 \cdot 8H_2O$ where Ln is Sm, Y, or Nd. Their main interest was in the form of the spin Hamiltonian and the zero-field energy level scheme, particularly with respect to the possibility of the dilute salts being used in a zero-field maser. Earlier EPR measurements for $Gd/Sm_2(SO_4)_3 \cdot 8H_2O$ had been analyzed in terms of the phenomenological spin Hamiltonian:[78]

$$\mathcal{H}_S = g\mu_B B \cdot S + b_2^0 O_2^0/3 + b_2^2 O_2^2/3 + b_4^0 O_4^0/60 \quad (9)$$

At room temperature $b_2^0 = 1.898$ GHz, $b_2^2 = 1.139$ GHz, $b_4^0 = -0.039$ GHz for this dilute salt. Comparison was then made between observed zero-field resonances and predicted frequencies from the above spin Hamiltonian, and at 290 K satisfactory agreement (within 50 MHz) for the three main ZFR transitions (10 208 ± 10, 7320 ± 30, 7790 ± 30 MHz) was found with the zero-field frequencies predicted on the basis of EPR measurements (accuracy ~100 MHz). It was also shown that, because of the large off-diagonal term involving b_2^2, second-order perturbation analysis was inadequate and that empirical fourth-order terms improved the accuracy. Exact diagonalization was used in comparing EPR with ZFR results. $'\Delta M_S = 2, 3'$ ZFR transitions were also noted; these are given considerable intensity by the b_2^2 term.

The ZFR spectra were also measured as a function of temperature in the three salts. For the Sm salt, the energy level scheme was deduced by consideration of the three main ZFR transitions combined with the three weaker transitions which occur at all possible sum frequencies of the main transitions. Using perturbation expressions, Bogle and Symmons deduced that b_2^0 increased by about 10% on cooling from room temperature to 80 K, and b_2^2 decreased by about 50%. Similar behavior was found in the other two salts. For Gd^{3+} in the Sm salt, splittings of the $'|\pm^3/_2\rangle \leftrightarrow |\pm^5/_2\rangle'$, $'|\pm^5/_2\rangle \leftrightarrow |\pm^7/_2\rangle'$ and $'|\pm^1/_2\rangle \leftrightarrow |\pm^5/_2\rangle'$ transitions were noted at 4.2 K. This effect was attributed to the magnetic Sm ions of the host which are more slowly relaxing at the lower temperatures and thus give rise to local fields rather than a rapidly fluctuating, average field.

The EPR of Gd^{3+} in these types of salts has been reanalyzed more recently.[79-81] Additional terms in the spin Hamiltonian involving O_4^2, O_4^4, O_6^0, O_6^2, O_6^4, O_6^6 were then added to (9). These are some of the extra terms required for the monoclinic symmetry[82] of the host lattice. The resulting coefficients of these terms were small, but of similar magnitude to b_4^0. Malhotra and Bist[81] compared their ZFR frequencies calculated by exact diagonalization of the spin Hamiltonian with the ZFR frequencies observed by Bogle and Symmons[26] for the Sm and Nd salts (interpolated for $T = 273$ K). Quite large discrepancies of up to 150 MHz were found. They believed the better agreement between the calculated and observed frequencies of Bogle and Symmons at 290 K to be fortuitous, since the latter included only terms b_2^0, b_2^2, and b_4^0 in the spin Hamiltonian used to analyze the EPR. However, the other reasons given in support of their claim for fortuitous agreement cannot be substantiated. These were that the use of polycrystalline samples and the presence of forbidden transitions broaden the zero-field resonances and that square wave-modulation (0–80 G) gives rise to a line shape which is not the true zero-field line shape[80] and shifts the resonance positions.[81] Square-wave magnetic field modulation does not shift or broaden zero-field resonances in a frequency swept spectrometer, it simply adds negative "modulation wings" to either side of the transitions. The use of polycrystalline samples and the presence of extra weakly allowed EPR transitions at low field certainly broadens these modulation wings; but if adequate modulation field strength is used and the modulation waveform is reasonably square, this has no effect on the central part of the ZFR line shape (see section IIB and Figure 3).

Misra and Mikolajczak[83] claimed a more accurate EPR analysis for Ln = Pr, Sm, Eu, Y, Nd, Yb involving several directions in the zx plane and complete least-squares analysis (Malhotra and Bist analyzed only the z and x directions) at "room temperature" and analyses were also given for the first four of these lanthanide hosts at 77 K and 4.2 K. Predictions of zero-field splittings which could be compared with Bogle and

Symmons' direct measurements were not given numerically. However, they did give zero-field energy level schemes (wrongly labelled as zero-field splittings); from these it appears that there are again differences with Bogle and Symmons' measurements. Misra and Miolajczak also noted a splitting of the three highest field EPR lines near the z direction for temperatures below 15 K and agree with the proposed explanation of Bogle and Symmons.[26]

This case needs reexamining to see if differences between EPR-derived ZF splittings and direct measurements really exist. Observations have to be made at the same, controlled temperature. A possible source of error in the spin Hamiltonian is the presence of magnetic ions in the host salts.

C. ZFR of Gd^{3+} in Zircon Structure Compounds

A series of publications by Urban and co-workers was concerned with the spin Hamiltonian parameters for Gd^{3+} as a dilute impurity in zircon structured compounds of the type ABO_4 [A = Y, Lu, Sc; B = P, V, As; Gd: A $\simeq$ 1:500].[37,84-89] A combination of zero-field resonance, and variable frequency EPR at a number of fixed magnetic fields, was used and an elegant method developed for determining all five zero-field parameters.[85] This work sought principally to elucidate the mechanisms of interaction of S-state ions with the crystal field. To this end, temperature and pressure variations of the crystal field were also studied. A variable frequency EPR spectrometer was used for both zero-field and high-field resonance detection, the two techniques differing only with respect to magnetic field modulation, square-wave to detect the zero-field resonances and sine-wave when a constant field was applied.

Most of the important results are summarized in the last two papers of the series.[37,89] The structure of these compounds has been well-characterized,[90] the most important feature for analysis of the spectra being the D_{2d} point symmetry of the trivalent ion. The appropriate spin Hamiltonian to describe the ground state zero-field splitting of Gd^{3+} therefore reflects the fourfold inversion axis and takes the form

$$\mathcal{H}_S = b_2^0O_2^0/3 + b_4^0O_4^0/60 + b_6^0O_6^0/1260 + b_4^4O_4^4/60 + b_6^4O_6^4/1260 \quad (10)$$

General expressions were given[85] for the energy levels in the presence of a magnetic field along the symmetry axis (which required an extra term $g\mu_BBS_z$ in (10)). [Δ_o and Δ should be interchanged in Figures 2 and 3 of ref 85.] The best presentation of the formulas which were used to obtain all the operator equivalent coefficients directly was given in the third paper in the series.[86] We present these later, but first give a description of their origin. In terms of spin states $|M_S\rangle$ where $M_S = {}^7/_2, {}^5/_2, \ldots, -{}^7/_2$ the only off-diagonal elements in the matrix of (10) involve the fourfold operators O_4^4 and O_6^4 and they connect spin states which differ in M_S by 4. The matrix then factorizes into four 2 × 2 matrices from which the energy levels are readily obtained. In the case of an applied magnetic field along the symmetry (z) axis the same type of factorization occurs because the $g\mu_BBS_z$ term only affects diagonal terms. An energy level diagram for magnetic field in the z direction is shown in Figure 11 together with relevant transitions which are

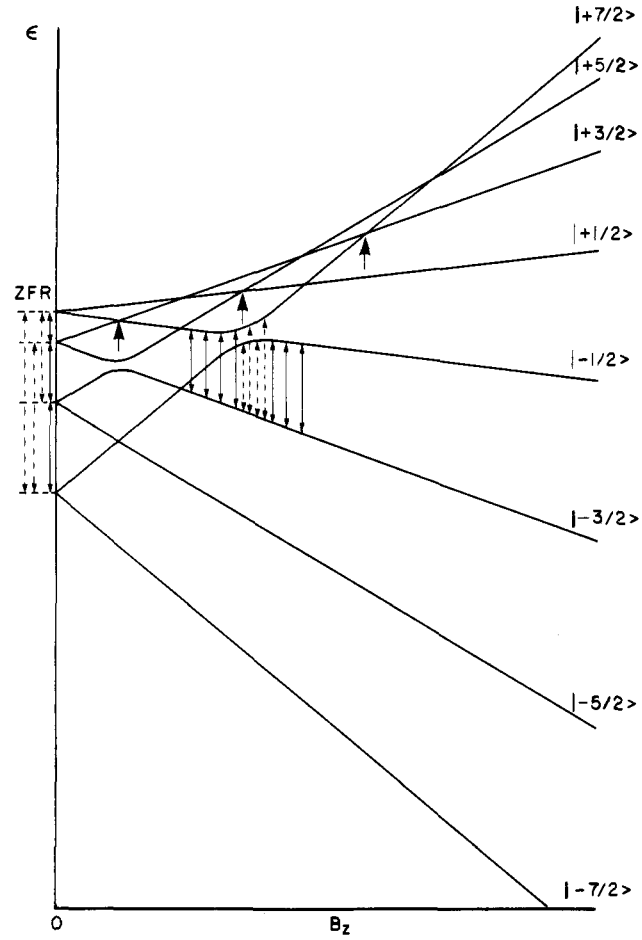

Figure 11. Schematic energy level diagram for an $S = {}^7/_2$ ion in tetragonal symmetry, with the magnetic field directed along the symmetry axis. The dominant parameter in the spin Hamiltonian is b_2^0; repulsion between levels differing in (high-field) spin M_S by 4 are caused by terms b_4^4 and b_6^4. Zero-field transitions, used to determine the b_n^0, and some of the transitions used to determine the b_n^4 by variable frequency EPR are shown. Weak transitions are indicated by dashed lines. Further level repulsion would occur, for example, at the crossings indicated by arrows if an orthorhombic distortion occurred around the ion (extra parameters b_n^2).

discussed in this section. Energy level solutions in the case of zero applied field are as follows:

$$\epsilon_{1,2} = b_2^0 + 8b_4^0 - 2b_6^0 + \{[6b_2^0 - b_4^0 + 3b_6^0]^2 + 35[b_4^4/5 + b_6^4/7]^2\}^{1/2}$$

$$\epsilon_{3,4} = -b_2^0 - 8b_4^0 + 2b_6^0 + \{[2b_2^0 - 5b_4^0 - 7b_6^0]^2 + [3^{1/2}b_4^4 - 3^{-1/2}b_6^4]^2\}^{1/2}$$

$$\epsilon_{5,6} = -b_2^0 - 8b_4^0 + 2b_6^0 - \{[2b_2^0 - 5b_4^0 - 7b_6^0]^2 + [3^{1/2}b_4^4 - 3^{-1/2}b_6^4]^2\}^{1/2}$$

$$\epsilon_{7,8} = b_2^0 + 8b_4^0 - 2b_6^0 - \{[6b_2^0 - b_4^0 + 3b_6^0]^2 + 35[b_4^4/5 + b_6^4/7]^2\}^{1/2}$$

The corresponding wave functions consist mainly of $|\pm{}^7/_2\rangle$, $|\pm{}^5/_2\rangle$, $|\pm{}^3/_2\rangle$, and $|\pm{}^1/_2\rangle$, respectively if the off-diagonal elements are much smaller than those on the diagonals. Strongly allowed ZFR transitions occur at $\nu_1 = |\epsilon_{5,6}-\epsilon_{7,8}|$, $\nu_2 = |\epsilon_{3,4}-\epsilon_{5,6}|$, and $\nu_3 = |\epsilon_{1,2}-\epsilon_{3,4}|$ and if the dominant term is (as is usual) b_2^0 (= D in the notation often used for d^5 systems) these resonances occur respectively near $2b_2^0$, $4b_2^0$, and $6b_2^0$ (exactly if other terms are zero). In analyzing the resonance results the following combinations of ZFR frequencies are useful:

$$\nu_3 - \nu_1 = 4(b_2^0 + 8b_4^0 - 2b_6^0)$$

$$\nu_1 + \nu_2 + \nu_3 = 2\{[6b_2^0 - b_4^0 + 3b_6^0]^2 + 35[b_4^4/5 + b_6^4/7]^2\}^{1/2} \quad (11)$$

$$\nu_2 = 2\{[2b_2^0 - 5b_4^0 - 7b_6^0]^2 + [3^{1/2}b_4^4 - 3^{-1/2}b_6^4]^2\}^{1/2}$$

Three zero-field resonances are not sufficient to determine all five parameters uniquely. Urban developed a method for directly determining the off-diagonal elements which is made possible only by variable frequency, high-field EPR. This method was previously used by Kornienko and Prokhorov[5] to evaluate the off-diagonal term in the spin Hamiltonian of Fe^{3+} in α-Al_2O_3; they used variable-field EPR at a number of fixed frequencies at X-band which by chance corresponded to the correct energy gaps for determining the off-diagonal term. This was discussed in section IIIB.

In this case when a magnetic field is directed along the fourfold symmetry axis, energy levels in the high-field designations $|\pm^7/_2\rangle$, $|\pm^5/_2\rangle$ are mixed with $|\mp^1/_2\rangle$, $|\mp^3/_2\rangle$ respectively, via the fourfold parameters of (10). The off-diagonal element causes a mutual repulsion of energy levels with, for example, the mostly $|^7/_2\rangle$ level at high field being repelled from the mostly $|^{-1}/_2\rangle$ level and becoming mostly $|^{-1}/_2\rangle$ at low field (see Figure 11). (The spin levels which repel one another are those which would otherwise have crossed and this depends on the sign of b_2^0; in this case b_2^0 was negative and repulsion occurs for $|^7/_2\rangle$, $|^{-1}/_2\rangle$ levels, not for $|^{-7}/_2\rangle$, $|^1/_2\rangle$). The maximum effect of an off-diagonal element occurs at the field where the levels would otherwise have crossed if the off-diagonal element were zero. If we consider one of the 2×2 matrices where X and Z are

$$\begin{bmatrix} X & Y \\ Y & Z \end{bmatrix}$$

field dependent, Y is field independent, and solve the secular determinant for the energies we obtain

$$\epsilon = [(Z + X) \pm \{(Z - X)^2 + 4Y^2\}^{1/2}]/2$$

The gap between the repelling levels at constant field is

$$\Delta\epsilon = \{(Z - X)^2 + 4Y^2\}^{1/2}$$

and the minimum gap is obtained from the condition

$$d\Delta\epsilon/dB = 2(Z - X)[(Z - X)^2 + 4Y^2]^{-1/2}(dZ/dB - dX/dB) = 0$$

Since Z and X have different field dependences this occurs when $Z = X$ and the minimum gap $\Delta\epsilon_{min} = |2Y|$. Thus the absolute value of the off-diagonal element is determined by a measurement of this minimum gap. Experimentally this can be done by using an appropriate EPR transition and measuring its resonant frequency at a series of fixed magnetic fields near to the cross-over condition $Z = X$. For example, the off-diagonal element connecting $|^7/_2\rangle$ and $|^{-1}/_2\rangle$ was determined from the minimum frequency difference between the branches of the $|^{-3}/_2\rangle$ to $|^{-1}/_2\rangle$ EPR transition when the spin function with predominantly $|^{-1}/_2\rangle$ character changes from one level to another.

The relevant off-diagonal elements in this case are[85] as follows:

$$\Delta_0/2 = 35^{1/2}|b_4^4/5 + b_6^4/7| \quad \text{connects } \langle \pm^7/_2| \text{ with } |\mp^1/_2\rangle$$

$$\Delta_1/2 = |3^{1/2}b_4^4 - 3^{-1/2}b_6^4| \quad \text{connects } \langle \pm^5/_2| \text{ with } |\mp^3/_2\rangle \quad (12)$$

and are determined directly as half of the residual gaps between appropriate interacting levels.

From eq 11 and 12 it can be seen that all five parameters can be obtained from measurements of the three zero-field resonances and two residual gaps:

$$b_4^4 = (35)^{1/2}[\Delta_0 + \Delta_1(15/7)^{1/2}]/44$$

$$b_0^4 = (315)^{1/2}[\Delta_0 + \Delta_1(7/15)^{1/2}]/44$$

$$b_2^0 = -\{3[(\nu_1 + \nu_2 + \nu_3)^2 - \Delta_0^2]^{1/2}/2 + [\nu_2^2 - \Delta_1^2]^{1/2}/2 + (\nu_3 - \nu_1)/4\}/21$$

$$b_4^0 = -\{[(\nu_1 + \nu_2 + \nu_3)^2 - \Delta_0^2]^{1/2}/2 + 5[\nu_2^2 - \Delta_1^2]^{1/2}/2 + 4(\nu_3 - \nu_1)\}/154$$

$$b_6^0 = -\{3[(\nu_1 + \nu_2 + \nu_3)^2 - \Delta_0^2]^{1/2}/2 - 7[\nu_2^2 - \Delta_1^2]^{1/2}/2 - (\nu_3 - \nu_1)\}/66 \quad (13)$$

In these equations the signs were chosen to agree with those from EPR determinations. In principle the sign of b_2^0 (and therefore of b_4^0, b_6^0) can be determined from observation of low temperature ZFR intensities. The only signs not determined by this method are those of the fourfold parameters, and there is in addition to the sign ambiguity another set of parameters which fits the equations. This is discussed in an analogous situation for Gd^{3+} in CdS (section IVD).

We feel that this technique of measuring minimum gaps between repelling levels to determine off-diagonal elements directly is a very useful additional "trick" for EPR spectroscopists. It generally requires a variable frequency EPR setup. In the case just discussed all the parameters of the spin Hamiltonian can be accurately determined using ZFR and variable frequency EPR. The only disadvantages in the high-field technique are: (a) in common with conventional single crystal EPR experiments, measurements are subject to any errors in the crystal orientation and (b) ambiguities occur when more than one parameter occurs in the off-diagonal element. Errors in magnetic field strength measurements do not contribute to parameter errors since the important measurement is frequency; the field at which the minimum energy gap occurs does not have to be measured. Direct measurement of transitions between the two repelling levels has not yet been attempted. Whereas the $\Delta M_S = \pm 1$ transition (rf field perpendicular to static field) between a nonrepelled level and one of the repelled levels becomes less allowed as the field for maximum repulsion is approached (and subsequently becomes very weak or "forbidden"), a $\Delta M_S = 0$ transition (rf field parallel to the static field) between the two repelling levels is allowed and has greatest intensity at the field at which the minimum energy gap (and minimum transition frequency) is attained. This would appear to be the optimum method for determining off-diagonal elements. While some of the predicted z polarized transitions occur at frequencies so far unexplored by variable frequency EPR (280 and 400 MHz in the present case), others occur in re-

gions which have been studied (Gd^{3+} in CdS, discussed in the next section, would have three such transitions, two at 171 and 151 MHz; for Fe^{3+} in α-Al_2O_3 (see section IIIB) the transition would occur at about 2.08 GHz).

We also propose a general theorem concerning the number of zero-field splittings and repelling energy levels for $B//z$. The number of level repulsions is the same as the number of parameters b_n^m for a given m which cause the repulsions. The number of zero-field splittings is the same as the number of parameters b_n^0. This holds for half integral S, even n and $m \geq 0$ and shows that in principle all parameters in such cases are determinable from measurements of the zero-field splittings and all minimum energy gaps between repelling energy levels (apart from ambiguities of the type discussed above).

The spin Hamiltonian parameters obtained for Gd^{3+} in YVO_4 were in good agreement with the EPR analysis of Rosenthal,[91] although the latter measurements were more precise. However, Urban pointed out that the lower precision arose entirely from the frequency measurement (wavemeter) errors. Improvements to the apparatus by the addition of a frequency counter reduced the parameter errors by almost an order of magnitude.[86] To give an idea of the relative magnitudes of parameters and errors obtained from the more accurate frequency measurement, we quote the results for Gd^{3+} in $ScVO_4$ at 300 K; units are MHz (10^{-4} cm^{-1}). $b_2^0 = -1121.3 \pm 0.5$ (-374.0 ± 0.2), $b_4^0 = -7.6 \pm 0.2$ (-2.54 ± 0.05), $b_6^0 = 2.5 \pm 0.3$ (0.83 ± 0.1), $b_4^4 = 149 \pm 1$ (49.3 ± 0.3)8 $b_6^4 = -0.9 \pm 0.4$ (-0.30 ± 0.15). [A factor of 3.0000 rather than 2.9979×10^{10} cm s^{-1} seems to have been used for the velocity of light[86] and we have adjusted the results accordingly.]

The final set of results gave the parameters as functions of temperature and pressure for Gd^{3+} in nine zircon type matrices. It was found that Δ_0 and Δ_1 were not significantly affected by temperature changes. From (13) it is easy to derive expressions for the temperature coefficients of the axial parameters in terms of the temperature coefficients of the three ZF resonances and analogous expressions for pressure variation. X-ray measurements were also made of the unit cell dimensions as a function of temperature.

By far the most significant temperature and pressure dependence is observed for b_2^0 and the final discussion[37,89] is concerned with the observed correlation of b_2^0 with the unit cell edge ratio c/a. The high precision of both the b_2^0 and c/a measurements establishes a definite monotonic, but nonlinear, relation between them. However, it has so far proved impossible to provide the vital microscopic correlation of b_2^0 with the guest ion's surrounding distorted oxygen tetrahedra (four nearest neighbors and four next nearest neighbors). An empirical but very useful method for interpreting the spin Hamiltonian parameters of S state ions is the superposition theory. In this theory, discussed in more detail in section IVD, any parameter b_n^m is described as a sum of contributions from each ligand (an intrinsic $\bar{b}_n$ value determined from experiment being defined for each ion ligand combination dependent on their separation) weighted by the appropriate spherical harmonic $Y_n^m(\theta,\phi)$, θ and ϕ being coordination angles. Thus in principle it should be possible to calculate any b_n^m given the intrinsic parameters and ligand positions. In the case of the zircon structure compounds, the trivalent atom is surrounded by two distorted tetrahedra of oxygen atoms. Because of the nature of the spherical harmonic term Y_2^0, an exact tetrahedron gives no contribution to b_2^0. It is observed that $b_2^0 \rightarrow 0$ as $c/a \rightarrow 0.92$ and the rationale for this is that the two distorted tetrahedra for $c/a = 0.92$ would give equal but opposite contributions to b_2^0.

D. ZFR of Gd^{3+} in CdS

Urban, Siegel, and Hillmer's study of Gd^{3+} in CdS[92] made use of their variable frequency facilities to analyze more fully the EPR spectra of this system. With a frequency variation capability extending from 1 to 18 GHz, they were able to map large parts of the Zeeman diagram, particularly near the noncrossing regions, and to observe one resonance at zero field. They were able to identify one of the substitutional sites of Gd^{3+} in this host. Three different Gd^{3+} species in CdS, all showing axial symmetry, had previously been found, two of which were doped by diffusion and the third by adding Gd^{3+} to the melt. It was the aim of this paper to determine and interpret the site symmetry of the third species. The combined techniques of ZFR and variable frequency EPR were similar to those described in the previous section. When variable frequency EPR was used, mutual repulsions were found between the $|^{-1}/_2\rangle$ and $|^{-7}/_2\rangle$ levels and between the $|^{1}/_2\rangle$ and $|^{-5}/_2\rangle$ levels and the residual gaps were determined as before. This confirmed a C_3 axis and the appropriate spin Hamiltonian is

$$\mathcal{H}_S = b_2^0O_2^0/3 + b_4^0O_4^0/60 + b_6^0O_6^0/1260 + b_4^3O_4^3/3 + b_6^3O_6^3/36 + b_6^6O_6^6/1260 + g\mu_B BS_z$$

for magnetic field along the symmetry axis. This uses Buckmaster and Shing's coefficients.[46] In this case only one zero-field transition $\nu_1 = 11\,121 \pm 3$ MHz was detectable, the other two being above the range of their spectrometer. A structure was seen in the wings of this transition and claimed to be due to hyperfine interaction or local distortion. In the light of the later ZFR analysis of Gd^{3+} in lanthanum ethyl sulfate by Bernstein and Dobbs[70] (discussed in Section IVA) using almost pure 155 and 157 isotopes ($I = {}^3/_2$), the structure seen by Urban et al. could well be due to hyperfine and quadrupole interactions of the same order of magnitude as obtained by Bernstein and Dobbs. The structure appears as small unresolved satellites; this would occur for the overlapping hyperfine structure for the two magnetic isotopes (natural abundance 15% each). The separation of the satellites is qualitatively what would be expected for hyperfine interactions of similar magnitude to those observed in lanthanum ethyl sulfate.

The two threefold operators cause repulsions between $|^{-7}/_2\rangle$ and $|^{-1}/_2\rangle$ levels and between $|^{-5}/_2\rangle$ and $|^{+1}/_2\rangle$ levels for positive b_2^0; for negative b_2^0 the signs of the spin functions are reversed. The sixfold operator causes repulsion between the $|^{-7}/_2\rangle$ and $|^{+5}/_2\rangle$ levels. The authors were able to measure the residual gaps caused by the threefold operators and which were labelled $\Delta_1^{(3)}$ ($|^{-1}/_2\rangle$, $|^{-7}/_2\rangle$ and $\Delta_2^{(3)}$ ($|^{1}/_2\rangle$, $|^{-5}/_2\rangle$); measurement of the third gap $\Delta^{(6)}$ involves EPR transitions of a frequency too great for their spectrometer. At magnetic fields far removed from values where such level repulsions occur they found a good linear Zeeman effect of magnetic field

on the energy levels and so were able to extrapolate back to zero field to estimate the other two zero-field transition energies.

The 8 × 8 secular determinant splits into two 3 × 3 determinants with two unmixed states ($|+^3/_2\rangle$ and $|-^3/_2\rangle$). An approximation was employed to solve for the three parameters (b_4^3, b_6^3, b_6^6). Often at a noncrossing region the only important off-diagonal element is the one causing the particular repulsion; the other off-diagonal elements in such cases can be neglected to a good degree of approximation. We note that the authors' determinant (eq 2) is inappropriate for the type of mixing of levels indicated in their Figure 1. This does not affect the evaluation of off-diagonal elements, it merely makes the determinant appropriate for negative b_2^0. The elements in this determinant $\langle^1/_2|\mathcal{H}|^{-5}/_2\rangle = \langle^{-5}/_2|\mathcal{H}|^1/_2\rangle$ should read $-5^{1/2}(4b_4^3 - 7b_6^3)$, not $-2(35)^{1/2}(b_4^3 + b_6^3)$ as given. With the above approximation all the off-diagonal elements can be determined from measurements of the residual gaps and we summarize the evaluation below (the spin states are those for positive b_2^0):

mixing levels

$$\Delta_1^{(3)} = 2|-2(35)^{1/2}(b_4^3 + b_6^3)| \qquad |^{-7}/_2\rangle\ |^{-1}/_2\rangle$$

$$\Delta_2^{(3)} = 2|-5^{1/2}(4b_4^3 - 7b_6^3)| \qquad |^{+1}/_2\rangle\ |^{-5}/_2\rangle$$

$$\Delta^{(6)} = 2|2b_6^6/7^{1/2}| \qquad |^{-7}/_2\rangle\ |^{+5}/_2\rangle$$

Approximate values of b_4^3, b_6^3, b_6^6 can be obtained from the gaps. It was not stated how the final values of all the parameters were calculated (b_6^6 was not evaluated). The method of choice would be to obtain approximate values and then iteratively vary all the parameters until the observations were fitted. The sign of b_2^0 was taken from EPR.

It should be pointed out that the equations given for b_4^3, b_6^3:

$$b_4^3 = 7^{1/2}\Delta_1^{(3)}/44(5)^{1/2} + \Delta_2^{(3)}/22(5)^{1/2}$$

$$b_6^3 = \Delta_1^{(3)}/11(35)^{1/2} - \Delta_2^{(3)}/22(5)^{1/2}$$

resulted in four sets of values for b_4^3, b_6^3 (two distinct sets and two with opposite signs) since only the absolute values of the off-diagonals were obtained. A similar ambiguity occurs in the equations for b_4^4 and b_6^4 for Gd^{3+} in YVO_4 discussed in the previous section. Resolution of such ambiguities would be difficult, even using exact diagonalizations, because of the very small values of all parameters other than b_2^0; off-axis EPR measurements would be required.[39]

The superposition theory was used to distinguish three possible sites for Gd^{3+}. In this method b_2^0 is related to the relevant coordination angles θ_i and distances R_i of N ligands through

$$b_2^0 = \sum_{i=1}^{N} \bar{b}_2(R_i) Y_2^0(\theta_i)$$

where $\bar{b}_2(R_i)$ is an intrinsic parameter for a given ion and ligand and has a supposed R dependence $\bar{b}_2(R) = -A(R_o/R)^7 + B(R_o/R)^{10}$; Y is a spherical harmonic.

In CdS the Gd^{3+} ion is surrounded by a tetrahedron of four sulfur ligands (at R_o) with a fifth S ligand at $R = 1.63R_o$ forming a double tetrahedron. Assuming substitutional Gd^{3+} would be displaced 0.2 to 0.3 Å toward the fifth ligand and with a value $\bar{b}_2(R_o) = 1300 \times 10^{-4}$ cm^{-1}, a b_2^0 of 500–800 × 10^{-4} cm^{-1} might be expected. Similarly an interstitial site (octahedral coordination of S) plus an expected shift in the c direction for Gd^{3+} results in b_2^0 between 300 and 800 × 10^{-4} cm^{-1}.

For Gd^{3+} at the substitutional site, but with one of the nearest neighbors missing, b_2^0 is calculated to be between 1800 and 2000 × 10^{-4} cm^{-1} and this is identified as the site in this case (actual $b_2^0 = 1850 \times 10^{-4}$ cm^{-1}). This was supported by chemical evidence which showed a sulfur deficiency for the melt grown sample.

As in the case of first-row transition-metal ions, combinations of zero-field transition frequencies such as $\nu_1 + \nu_2$, $\nu_2 + \nu_3$, $\nu_1 + \nu_2 + \nu_3$ become allowed when there are off-diagonal elements connecting the zero-field spin states. It may be possible to use these in favorable cases to help in the assignment of nonaxial parameters. Accurate measurement of intensity and polarized RF absorption would be required for such an analysis.

Some of the work described in sections IVC and IVD is also summarized in a review on S state ions by Newman and Urban.[39]

E. ZFR of Gd^{3+} in $LiNbO_3$

In spite of the large differences in formal ion charge, Gd^{3+} can be doped into $LiNbO_3$ at concentrations close to the nominal doping level using Czochralski methods. Parallel EPR and ZFR studies were carried out by Dischler et al. in collaboration with Urban.[93] EPR (X- and Q-band) experiments identified at least seven independent patterns for the field parallel to the crystal c axis. This is probably due in part to magnetic inequivalence. The two dominant patterns at this orientation were analyzed and the results used to predict the ZFR frequencies. Only the $'|\pm^1/_2\rangle \leftrightarrow |\pm^3/_2\rangle'$ and $'|\pm^3/_2\rangle \leftrightarrow |\pm^5/_2\rangle'$ transitions (near 7 and 14.5 GHz) were within the range of their ZFR equipment, but agreement was good, confirming the EPR assignments. The ZFR spectra are particularly simple consisting of a doublet at each frequency, the technique distinguishing only physically inequivalent sites (in this case two). The comment that peculiar lineshapes are produced by the square-wave field modulation technique is somewhat surprising since such effects had not been observed in the previous ZFR experiments of Urban et al. on Gd^{3+}. We feel that the distortion of the ZFR lineshapes may well be due to weaker ZFR lines overlapping with the main transitions, that is some of the other five or more inequivalent species detected by EPR with the static field along the c axis may in fact be due to physically inequivalent sites. For species I, the Gd^{3+} ion was thought to substitute for Li^+ or Nb^{5+} (which have threefold symmetry) since the EPR could be analyzed in terms of trigonal symmetry (which requires b_2^0, b_4^0, b_6^0, b_4^3, b_6^3, b_6^6), although b_6^3 and b_6^6 were not determined. For species II, a small but significant b_2^2 was needed to fit the results. This was interpreted in terms of Gd^{3+} in a similar substitutional position to that of I but with a nearby charge compensator lowering the symmetry.

This work illustrates the value of ZFR in complex systems. Predicting correct ZFR frequencies provides valuable confirmation of assignments in such cases of site multiplicity. Given the similar values for b_2^0 for the two sites (0.1185 (3) and 0.1260 (20) cm^{-1}), superposition

theory would not be useful in distinguishing them.

The ZFR spectra show interesting linewidth effects. The authors commented that these give a "qualitative measure of the statistical scattering of the zero-field splittings". However, the two linewidths for species I are similar, contrasting with a factor of 2 between those for species II. Measurements at low temperature would be needed before the particular zero-field splittings responsible for the linewidth variations could be identified. A more extended analysis of this type was given by Symmons and Bogle[15] for $Fe(acac)_3$ (see section IIIB).

F. ZFR of Nd^{3+} in Lanthanum Compounds

In some situations where there is a local-field contribution to the paramagnetic resonance line width (from magnetic nuclei for example), the ZFR line width can be appreciably narrower than the high-field EPR line width. This is because in such situations, the Zeeman effect occurs in second order. This phenomenon can give one or two orders of magnitude narrower lines at zero or low magnetic fields. The ZFR work on Nd^{3+} has made use of this fact.

ZFR has been observed and analyzed for dilute Nd^{3+} in lanthanum ethyl sulfate nonahydrate[9,31] and in lanthanum trichloride.[31] In both these salts Nd^{3+} substitutes for La^{3+} in a site of C_{3h} point symmetry. The Nd^{3+} ($4f^3$) ion has a $^4I_{9/2}$ ground level. This is split according to the symmetry of the crystalline electric field into five Kramers doublets, the lowest of which consists mainly of $|J,M_J\rangle$ where $J = {}^9/_2$, $M_J = \pm{}^7/_2$ plus a small amount with $J = {}^9/_2$, $M_J = \mp{}^5/_2$. Higher order treatment admixes small amounts of states with $J = {}^{11}/_2$, ${}^{13}/_2$, and ${}^{15}/_2$ and $M_J = \pm{}^7/_2$ or $\mp{}^5/_2$. At the low temperatures necessary to slow spin–lattice relaxation, only the ground doublet is populated. This can then be described by an effective spin Hamiltonian of the form:

$$\mathcal{H}_S = \mu_B\{g_\parallel B_z S_z + g_\perp(B_x S_x + B_y S_y)\} + A_\parallel S_z I_z + A_\perp\{S_+ I_- + S_- I_+\}/2 + P\{I_z^2 - I(I+1)/3\} \quad \text{(effective spin } S = {}^1/_2\text{)}$$

where P represents the axial nuclear quadrupole interaction. Hyperfine and quadrupole terms are required for the magnetic isotopes ^{143}Nd and ^{145}Nd which have natural abundances of 12% and 8%, respectively. Both have $I = {}^7/_2$. In the absence of a magnetic field the spin Hamiltonian matrix formed from the high field $|M_S M_I\rangle$ spin functions for general nuclear spin I breaks down into $2I$ 2×2 matrices plus two single (diagonal term) values. The $(S_+I_- + S_-I_+)$ term mixes states such as $|M_S M_I\rangle$ with $|M_S{-}1\ M_I{+}1\rangle$, i.e., states where the total spin angular momentum along the z axis, $k = M_S + M_I$, is constant. The solution to the secular determinant can then be written generally as

$$\epsilon = -A_\parallel/4 + P\{k^2 + 1/4 - I(I+1)/3\} \pm [\{k(A_\parallel - 2P)\}^2 + A_\perp^2\{I(I+1) + 1/4 - k^2\}^2]^{1/2}/2 \quad (14)$$

where k takes all possible values of $M_S + M_I$ (in this case 4, 3, ... −4) with the proviso that for $k = (S + I)$ only, the sign of k is taken in front of the square root term. This restriction arises simply because the energy levels for the two single values (nonmixed states) are consistent with eq 14 for one sign only; eq 14 is really a general equation only for the mixed states (all the 2 × 2 matrices). Care has to be taken with the signs in this equation when it is applied generally; Erickson writes eq 14 differently and has to observe different sign conventions because the absolute signs of k and $(A_\parallel - 2P)$ are lost. The symbol k is the same as M_F used elsewhere.

Allowed EPR transitions occur at zero field between levels containing spin function components with the same M_I, and with M_S differing by 0 or 1. $\Delta M_S = 0$ transitions (allowed for microwave field parallel to z) correspond to $\Delta k = 0$ transitions and occur at

$$\Delta\epsilon = [\{k(A_\parallel - 2P)\}^2 + A_\perp^2(16 - k^2)]^{1/2} \text{ (for } I = {}^7/_2\text{)}$$

With a nonzero quadrupole interaction all but one of the $\Delta M_S = 1$ (corresponding to $\Delta k = 1$) transitions occur in pairs of weak and strong intensity separated by $2P(2k + 1)$ where k is the lower value of $|k|$. A single transition occurs between $k = \pm 4$ and $k = \pm 3$ levels.

Bleaney, Scovil, and Trenam[9] measured $\Delta k = 0$ zero-field transition frequencies by using the same technique they used for $Gd^{3+}/La(EtSO_4)_3{\cdot}9H_2O$, that is extrapolation back to zero field of field/frequency plots of EPR transitions between the appropriate Zeeman levels. For the $k = 0 \leftrightarrow k = 0$ transition, a nonlinear Zeeman effect occurs near zero field and the ZFR frequency was calculated using the exact equation with known value of $g_\parallel$. Some of the $\Delta k = 1$ ZFR transitions, which are predicted to have a first-order Zeeman effect, were obtained in the same way but the direct quadrupole information was lost in the overlapping line pairs. They found that the ^{143}Nd ZFR transition $k = 0 \leftrightarrow k = 0$, which occurs at $4A_\perp$, gave a value for $A_\perp$ agreeing almost exactly with the high-field EPR determination. ZFR transitions were then compared with zero-field frequencies predicted from $A_\parallel$ and $A_\perp$ determined from high-field EPR at the same temperature (presumably 20 K). The quadrupole terms for the two isotopes could then be introduced to produce a best fit calculated spectrum. The fit was not perfect with discrepancies up to 11 MHz (estimated measurement errors were <3 MHz). Since the resonant positions involve P only negligibly the authors compared the ratio of corresponding ZF transition frequencies for the two isotopes with the ratio of $A_\parallel(143)/A_\parallel(145)$ and found a significant error of seven times the estimated ratio error. Calculation of $A_\parallel$, $A_\perp$, and P from zero-field transitions alone also gave inconsistent results since it was found that $A_\parallel(143)/A_\parallel(145) \neq A_\perp(143)/A_\perp(145)$.

Erickson followed a fairly similar procedure,[31] but made measurements at 4 K. He was able to detect the small quadrupole splitting of the $\Delta k = 1$ transitions and noted that the same value of P/A is determined from the relative intensities of the two peaks in the pair. Values for $A_\parallel$, $A_\perp$, and P were obtained by a least-squares fitting method. The RMS deviations of measured and calculated spectra for Nd^{3+}/LES were greater than expected (3 times greater than with $Nd^{3+}/LaCl_3$ discussed below). The isotopic hyperfine ratio for $A_\parallel$ disagreed with that of $A_\perp$ and nuclear magnetic moment ratio[94] ($A_\parallel(143)/A_\parallel(145) = 1.617 \pm 0.003$, $A_\perp(143)/A_\perp(145) = 1.6089 \pm 0.0003$, $\mu_N(143)/\mu_N(145) = 1.60883 \pm 0.00004$). The quadrupole isotopic ratio agreed in magnitude but differed in sign from ENDOR and atomic beam determinations. Unfortunately this

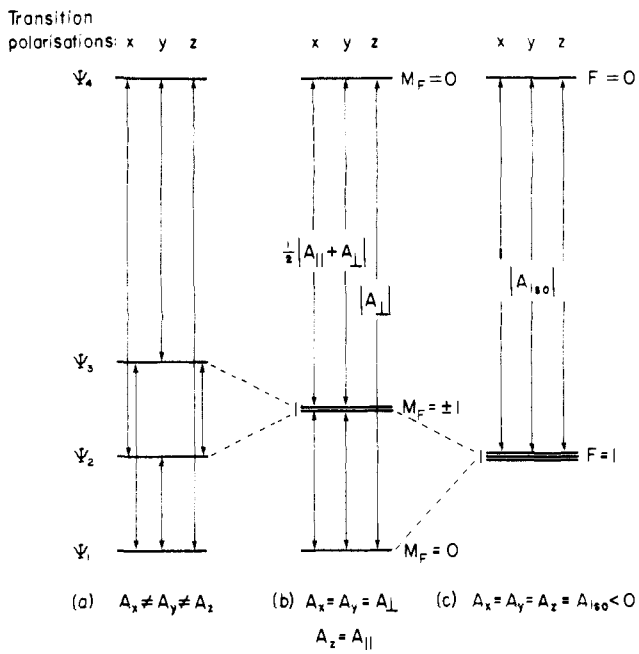

Figure 12. Energy level diagrams and ZFR transitions for an $S = {}^1/_2$, $I = {}^1/_2$ system with (a) orthorhombic, (b) axial, and (c) isotropic hyperfine interactions. The orientation of the magnetic vector of linearly polarized radiation necessary to observe particular transitions is shown at the top of each diagram.

indication of sign difference in P for the two isotopes mentioned in the text is not seen in Table V of Erickson's paper; it can be presumed that P should read −1.76 MHz for ^{143}Nd by comparison with the work of Bleaney, Scovil, and Trenam.[9] No satisfactory explanation for the hyperfine and quadrupole anomalous results was found by either group. Bleaney et al.[9] discounted mixing in of higher Kramers doublets because it was argued that this would have negligible effect, and Erickson[31] did not consider such refinement justified because of incomplete spectral data and coupling corrections.

In the case of $Nd^{3+}/LaCl_3$ Erickson showed that RMS deviations between calculated and experimental ZFR spectra were in accord with expectation and pointed out that this better agreement may be due to the determined zero value of P (within experimental error). The isotopic hyperfine ratios also agreed with the nuclear moment ratio given by Halford.[94]

The $k = 0 \leftrightarrow k = 0$ transition is a good example of a ZFR transition subject to second-order Zeeman effects only, as shown by the expression for the transition frequency for a small field along the z direction:

$$\Delta\epsilon = [\{G^2\} + A_\perp^2\{I(I+1) + 1/4\}]^{1/2}$$

which can be written $\Delta\epsilon_0 + G/(2\Delta\epsilon_0)$ for $G << \Delta\epsilon_0$ where $G = g_\parallel \mu_B B_z$ and $\Delta\epsilon_0$ is the ZF frequency $|A_\perp\{I(I+1) + 1/4\}|$. The splitting only becomes a first order effect when $G >> A_\perp$. For this reason the line width of the zero-field transition is much less than for other transitions. As Erickson pointed out the ratio of the two transition frequencies for $k = 0 \leftrightarrow k = 0$ for the two isotopes provides a simple and accurate determination of the nuclear moment ratios.

V. ZFR of Organic Radicals

A number of organic radicals have been studied by ZFR and hyperfine parameters as good or better than those from EPR have been obtained in some cases. In this section the simple theory for —ĊH— type radicals (i.e., one electron interacting with one proton) is presented. Several radicals having such a proton hyperfine coupling and additional weaker nuclear couplings can be described by this type of spectrum to first order. A discussion of results for the simple radicals is then followed by a discussion of more complex radicals, and the necessary theory is presented where appropriate.

A. ZFR for $S = {}^1/_2$, $I = {}^1/_2$ System

McConnell et al.[11] and Cole et al.[61] have presented the theory for the ZFR of an electron spin interacting with one proton through a completely anisotropic hyperfine interaction. Representing the hyperfine tensor by its principal values A_x, A_y, A_z the relevant spin Hamiltonian in the hyperfine principal axis system is

$$\mathcal{H}_S = A_x S_x I_x + A_y S_y I_y + A_z S_z I_z$$

The spin Hamiltonian interaction matrix for an $|M_S M_I\rangle$ basis set forms two 2 × 2 matrices which give the following energies and spin states:

$$\epsilon_1 = (-A_z + A_x + A_y)/4$$
$$\psi_1 = (|{}^1/_2,-{}^1/_2\rangle + |-{}^1/_2,{}^1/_2\rangle)/2^{1/2}$$
$$\epsilon_2 = (A_z - A_x + A_y)/4$$
$$\psi_2 = (|{}^1/_2,{}^1/_2\rangle - |-{}^1/_2,-{}^1/_2\rangle)/2^{1/2}$$
$$\epsilon_3 = (A_z + A_x - A_y)/4$$
$$\psi_3 = (|{}^1/_2,{}^1/_2\rangle + |-{}^1/_2,-{}^1/_2\rangle)/2^{1/2}$$
$$\epsilon_4 = (-A_z - A_x - A_y)/4$$
$$\psi_4 = (|{}^1/_2,-{}^1/_2\rangle - |-{}^1/_2,{}^1/_2\rangle)/2^{1/2}$$

given in order of increasing energy for the usual values of the hyperfine tensor for —ĊH— radicals, x being the direction of the p orbital symmetry axis, and z being the C–H direction. The energy levels and allowed electron spin transitions between them and their radiation polarizations are shown in Figure 12. It is easy to show that all six transitions between the four levels are allowed with the same intensity if all polarizations of the microwave field are considered. Also shown in Figure 12 are the allowed transitions and polarizations for axial and isotropic hyperfine interactions. For an axial hyperfine interaction the quantum number $M_F = M_S + M_I$ is well-defined, and for isotropic hyperfine the total angular momentum $F = I + S$ (and its projection on one axis) are well-defined.

A property of the $S = {}^1/_2$, $I = {}^1/_2$ system with A_x, A_y, A_z all different is that the energy levels are all nondegenerate at zero field and this leads to no first-order interaction with magnetic fields. This can be seen by the expectation value of the magnetic moment operator $\hat{\mu} = g\mu_B B \cdot S$ (for isotropic g) for all spin states ψ_1 to ψ_4 i.e., $\langle\psi_a|\hat{\mu}|\psi_a\rangle = 0$ for all $a = 1$ to 4. As shown in appendix II of ref 61 small magnetic fields give only second order contributions to shifts in the resonant frequencies of the order $(g\mu_B B)^2/(A_i \pm A_j)$. Thus a typical line width at high field of 9 MHz, if due to local field variation only, leads to a zero-field line width of only 1.3 MHz for a typical $A_i - A_j$ of 60 MHz. Thus zero-field resonances are intrinsically narrower than EPR transitions in this case. Cole et al.[61] pointed out that

the second-order shift depends on the magnitude and direction of the local field so in a polycrystalline sample an asymmetric line shape is expected and observed. Such line narrowings occur whenever the zero-field transition involves two levels which are nondegenerate. For the $S = {}^1/_2$, $I = {}^1/_2$ case with axial hyperfine interction, this narrowing effect would only occur with the z-polarized transition between the two $M_F = 0$ states; other zero-field transitions involve degenerate $M_F = \pm 1$ states which are subject to first-order Zeeman effect. An analogous situation is discussed in the section on Nd^{3+} ($S = {}^1/_2$, $I = {}^7/_2$) where an axial hyperfine interaction leads to one "narrowed" ZFR transition between $M_F = 0$ states (there referred to as $k = 0$). This is a general result for $S = {}^1/_2$, $I = n/2$ systems, the transition leading to very accurate measures of the perpendicular component of the hyperfine interaction.

For —ĊH— radicals the ZFR spectrum is predicted to consist of the following transition energies and linear polarizations:

$\lvert A_x - A_y\rvert/2$	$\lvert A_x + A_y\rvert/2$	z polarized
$\lvert A_y - A_z\rvert/2$	$\lvert A_y + A_z\rvert/2$	x polarized
$\lvert A_x - A_z\rvert/2$	$\lvert A_x + A_z\rvert/2$	y polarized

With a polycrystalline sample all six transitions can be observed simultaneously. Only three transitions would be necessary to determine the three principal values of the hyperfine tensor, other transitions can be used as a check or in a least-squares fitting procedure. In these radicals, normally the $\lvert A_x - A_y\rvert/2$ and $\lvert A_x - A_z\rvert/2$ transitions have the two lowest frequencies and often overlap.

McConnell et al.[11] were the first to observe zero-field resonances in an organic radical, by varying the field through zero at a number of fixed frequencies. In single crystals of X-irradiated malonic acid they were able to observe the two lowest frequencies with the correct polarizations. Using direct frequency-swept ZFR techniques, Cole et al.[61] measured between four and six resonances for —ĊH— radicals in irradiated polycrystalline samples of $CH_2(COOH)_2$, $CH_2(COOH)(COOK)$, and $CH_2(COOK)_2$ at room temperature. Excellent agreement with high field EPR analyses[95-97] was found for the first two radicals. For the dipotassium salt previous EPR measurements had not been fully analyzed because of the presence of more than one species and magnetic inequivalence within the unit cell. Such inequivalences have no effect on the ZFR of powders, and the authors were able to assign the main lines of the spectrum to a radical of the —ĊH— type since the principal values were very similar to those of malonic acid and potassium hydrogen malonate.

Birkle and Schoffa analyzed the ZFR spectra of the —ĊH— radicals produced on irradiating malonic acid, barbituric acid, and cyclohexane-1,1-diacetic acid.[98] The only discrepancy with previous EPR work was in the A_z value for the barbituric acid radical (ZFR: −25.4 MHz; EPR: −31.4 MHz[99]).

It should be pointed out that the relative or absolute signs of the hyperfine tensor components are not determinable from ZFR alone in $S = {}^1/_2$, $I = {}^1/_2$ systems and the assignments for —ĊH— radicals were based on earlier arguments used in analyzing EPR results. In principle, intensity measurements at very low temperatures can give sign information because of changes in population distribution. For such small values of A such an effect would not be detectable but it might be applied to other radicals (inorganic) with large hyperfine couplings.

B. Hyperfine Interactions with Several Protons

When interaction with more than one proton occurs, the calculation of ZFR spectra becomes more complicated since analytical expressions are no longer possible. To treat the problem one has to consider all the hyperfine interactions and diagonalize the spin matrix for all states of interacting spins. In their seminal paper, Cole et al.[61] considered the problem of hyperfine interaction with three protons. The basis functions are spin products $|M_S M_I(1) M_I(2) M_I(3)\rangle$ and for the case of three different diagonal axis systems for the tensors all the interactions have to be referred to some fixed crystal direction X, Y, Z. The zero-field spin Hamiltonian is then

$$\mathcal{H}_S = \sum_i \sum_j \sum_k A_{jk}{}^i S_j I_k{}^i$$

where $i = 1, 2, 3$; $j, k = X, Y, Z$.

The $A_{jk}{}^i$ are the elements of the hyperfine interaction tensor for the ith nucleus expressed in the X, Y, Z system. If these are known then it would be possible to obtain the energy levels and predict the ZFR spectrum. For this case of 3 inequivalent protons, 16 energy levels and 120 transitions are predicted. This illustrates a disadvantage of ZFR: as the number of interacting nuclei increases, the spectrum rapidly becomes very complex. For n inequivalent protons there are 2^{n+1} levels and $2^{2n+1} - 2^n$ transitions. One spectral simplification which could be used in such cases would be the use of liquid solutions, where possible, to average out the anisotropic interactions. The interaction matrix would then have fewer off-diagonal elements compared with the anisotropic case and there would be fewer ZFR transitions.

For the two cases considered by Cole et al.,[61] irradiated glutaconic acid and succinic acid powders, useful simplifications were developed in order to reduce the computational load. The π radical produced in the former case has two equivalent protons H(1) and H(3).

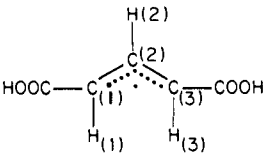

Moreover, the three tensors are diagonal in the same axis system within a few degrees. To this degree of approximation the spin matrix divides into two 8 × 8 submatrices and the authors were able to calculate a ZFR spectrum from high-field data which qualitatively agreed with experiment. Many of the transitions overlap so any exact determination of parameters by least-squares fitting of calculated to experimental spectrum would require a computational procedure which would have to take into account line shape.

For the succinic acid radical HOOC—CH_2—ĊH—COOH, all three tensors are different and have different diagonalizing axis systems. However, the anisotropic parts of the hyperfine tensors for the β protons were

only 10% of the isotropic part so the authors used the reasonable approximation of isotropic hyperfine interaction for these two protons. Again the matrix reduced to 8 × 8 submatrices which the authors could handle in terms of predicting ZF transition energies from high-field derived hyperfine tensors. The eigenvalues were close to those obtained from diagonalization of the complete spin Hamiltonian and thus justified this procedure. Qualitative agreement with the observed ZFR spectrum was again obtained.

A useful paper by Lefebvre and Maruani described a program for calculating ZFR frequencies and intensities for several $I = {}^1/_2$ nuclei interacting with one electron.[100] This allowed for unequal hyperfine principal values and different diagonal axis systems. ZFR spectra were recalculated for the glutaconic and succinic acid radicals. The main finding was that although there is a large number of transitions, only a much smaller number had significant intensity. It was suggested that since errors of a few MHz are usual in EPR analyses, it should be possible to obtain more accurate values by using a ZFR fitting procedure.

This program was later used to interpret the ZFR of other radicals with more than one proton coupling. The significance of these findings is summarized here. Values for the α proton hyperfine tensor were changed slightly by Birkle et al.[98] from those given in EPR analyses[101,102] for the radical $CH_3\dot{C}HCOOH$ (produced by X-irradiation of α-alanine). This gave an improved fit to the observed ZFR spectrum between 12 and 80 MHz. Later Birkle et al.[103] extended the frequency range of their spectrometer and showed that the 100–200 MHz transitions were also fitted by their improved α proton hyperfine tensors. The interpretation by EPR of the spectrum of irradiated fumaric acid in terms of radicals HOOC—RCH—$\dot{C}$H—COOH and HOOC—CH_2—$\dot{C}$H—COOH (the latter being the succinic acid radical) by Cook et al.[104] was confirmed by combination of the two predicted ZFR spectra.[98]

Geiger et al. used Gaussian line shapes to simulate the ZFR spectra of the radical HOOC—CH_2—O—$\dot{C}$H—COOH in irradiated diglycolic acid.[105] In this species the main interaction is with the α proton but there are very small interactions with the methylene protons. The ZFR spectrum looks very much like that of an $S = {}^1/_2$, $I = {}^1/_2$ system, the CH_2 proton couplings causing line shape effects only, in first order, and small shifts in second order. The best value for the CH_2 proton couplings (assumed isotropic and equal) was determined from line shape considerations and the authors then derived α couplings with a claimed accuracy of 0.15 MHz. However, line width and intensity differences indicate that complete simulation of the line shape may be required (including effects of the modulation field) and the accuracy of the results may be optimistic.

A similar procedure was applied to the radicals from thiodiglycolic acid and glycolic acids (the latter having a β proton coupling).[103,106] For the latter the line positions were reasonably well predicted from high field data. In the former case, fitted CH_2 and α proton couplings gave a predicted ZFR spectrum not in full agreement with the observed spectrum. The ZFR spectrum of the malonamide radical $NH_2COCHCONH_2$ was analyzed in terms of a single α proton interaction and values were obtained similar to those for other such radicals. From the broadened lines, however, it was assumed that there was also a small coupling with the amino protons.

The ZFR spectra of irradiated potassium sodium tartrate and malic acid were interpreted in terms of two radicals in both salts.[103]

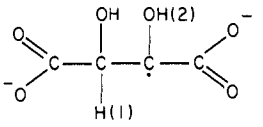

I

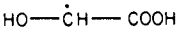

II

The radical I had previously been characterized by EPR[107] as one of several radicals in the irradiated tartrate, and hyperfine tensors from the EPR analysis were used in the ZFR simulation (two β protons). II is the same radical as observed in irradiated glycolic acid.[106] The authors[103] were not certain that this was the only interpretation of the spectrum. I was predicted to have lines at 88 and 110 MHz: only the 110 MHz transition was observed as a broader line than usual—this being due to normal EPR linewidths applying for degenerate states which occur at zero field when the interaction is with two protons. Birkle et al. also observed ZFR of the succinic acid radical with their extended frequency range 10–200 MHz. The group of lines between 160 and 190 MHz predicted by Lefebvre and Maruani[100] was confirmed, and some previously observed extra lines were confirmed as being due to a second species since they disappeared after 6 days leaving a ZFR spectrum very much as predicted from the high-field data.

Treating the adipic acid radical HOOC—$\dot{C}$H—$(CH_2)_3$—COOH in terms of an anisotropic α proton coupling and two isotropic, but different β couplings, Birkle et al.[103] obtained slightly different α proton tensor principal values than from previous EPR analysis.[108] However, the fit was not perfect, intensities were poorly predicted and some predicted lines were not present. The authors pointed out that this discrepancy was probably due to the use of isotropic β couplings and ignoring possible γ couplings. Similar problems of overlapping zero-field transitions due to coupling with several inequivalent nuclei occur in the triplet state of naphthalene and analogous full matrix diagonalization procedures are required to predict the ZFR spectrum; this has been described by Hutchison et al.[109]

There is scope for development in such ZFR work. In complex cases, preliminary EPR analysis is necessary, and to simulate the ZFR spectrum great care has to be taken to include all significant hyperfine interactions, their anisotropy and principal axis directions. Also the exact line shape may have to be better simulated.

Heller[110] has pointed out that in general the relative signs of two hyperfine interactions are determinable from ZFR measurements, but use of this has not been made so far.

C. ZFR of Radicals with $I = {}^1/_2$ and $I = 1$ Nuclei

Mangiaracina was the first to examine ZFR of systems with an N group adjacent to the radical center in a series of irradiated glycine peptides.[111] All the spectra

were closely related and interpreted in terms of radicals containing the grouping —CONHĊHCO$_2$H. The ZFR spectra consisted of features characteristic of a —ĊH— radical (6 lines between 10 and 70 MHz), but the lines were much broader than usual. Some of the lines show signs of splitting, and Mangiaracina interpreted the ZFR spectra in terms of two slightly different radicals, the difference being in orientation in the crystal or in which methylene proton is lost on irradiation. This contrasts with previous EPR interpretations as one radical, e.g., for acetylglycine.[112] The spectra shown in this paper[111] only indicate a possible splitting of the fifth line (~50 MHz) and the evidence for two radicals is far from convincing. However, there is some evidence for the presence of two radicals from EPR work where some extra splittings were found in deuterated glycylglycine and acetylglycine at 77 K. Hyperfine tensors were deduced by using the equation for $S = {}^1/_2$, $I = {}^1/_2$, for both the main species and the secondary species where it was thought to be present. Acetylglycine enriched in ^{15}N was also examined; little difference in the ZFR could be detected and it was assumed that the N hyperfine coupling must be negligible.

Birkle et al. examined the ZFR of electron irradiated amino acid derivatives, including acetylglycine and glycylglycine.[113] They found no evidence in the form of line splitting for more than one radical species. In analyzing the zero-field resonances they also considered the hyperfine interaction with ^{14}N using values from high-field EPR measurements on glycylglycine and carbamylglycine of 5.5, 8.5, 11 MHz for the principal values.[114,115] Direction cosines were specified for each set of tensor principal values, and a gaussian line shape was added to each transition position. They also discussed the effect of a small nitrogen hyperfine interaction using perturbation arguments and showed that there is no first-order effect for the same reasons that there is no first-order Zeeman effect on the energy levels of the $S = {}^1/_2$, $I = {}^1/_2$ system with completely anisotropic hyperfine interaction. Exact calculation showed that each transition in the $S = {}^1/_2$, $I = {}^1/_2$ system was replaced by nine resonances closely spaced over about 5 MHz in the $S = {}^1/_2$, $I = {}^1/_2$, $I = 1$ system including the EPR determined nitrogen hyperfine tensor.[114,115] These overlapped to give one broadened line whose maximum (which occurs very near to the average of the component frequencies) was characteristically shifted from each of the six original positions for the electron–proton system. Thus, it is important to include the effect of the nitrogen hyperfine interaction in order to be able to extract the correct proton interaction, which the authors did by iterative fitting of the calculated to the experimental spectrum. It was argued that the final principal values for the proton tensor were more precise than those from previous EPR measurements since the anisotropic parts were much more in accord with expectation for —ĊH— radicals and the isotropic parts varied much less from radical to radical. Analyses were given for glycylglycine, carbamylglycine, glycocyamine, and acetylglycine radicals. They also considered the radical produced on irradiating creatinine by taking account of two nitrogen couplings. The EPR derived α proton hyperfine tensor had to be changed to fit the ZFR spectra, although their analysis was not complete.

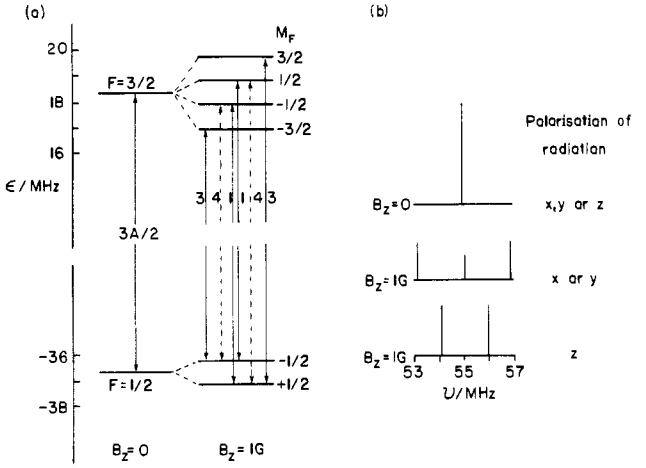

Figure 13. Energy level diagram (a) and predicted transition frequencies, intensities, and polarizations (b) for $S = {}^1/_2$, $I = 1$ system with isotropic hyperfine interaction $A = 36.65$ MHz at zero field and for a magnetic field (defining the z direction) of 1 G. This diagram applies to the peroxylaminedisulfonate anion radical in aqueous solution. In (a) levels connected by continuous lines are transitions allowed with the radiation field polarized in the xy-plane; those connected by dashed lines are allowed with polarization in the z-direction. Numbers alongside lines indicate relative intensities. Additional π type EPR transitions ($\Delta M_F = \pm 1$) at low frequencies are allowed within the constant F manifolds but are not marked.

For these systems the data for the α proton hyperfine principal values is not particularly sensitive to the direction of the N hyperfine tensor principal axes nor to the anisotropic part of the N hyperfine tensor, so simpler simulations using just the isotropic N hyperfine interaction are adequate.

VI. Peroxylaminedisulfonate Anion Radical

The conventional EPR spectrum of the radical $(SO_3)_2\dot{N}O^{2-}$ in aqueous solution[6] shows an isotropic hyperfine interaction of the unpaired electron with the nitrogen nucleus (99.6% ^{14}N, $I = 1$). Townsend, Weissman, and Pake[6,7] were the first to obtain the zero-field splitting for this radical. They measured field swept EPR spectra at a variety of frequencies between 9 and 120 MHz with resonant fields all below 60 G. They were able to fit the resonant frequency/field plots using the Breit–Rabi formulas,[116,117] which yielded a value of the single adjustable parameter $\Delta\nu = 54.7$ MHz, the zero-field splitting. Of the 15 combinations of energy level pairs, electron spin transitions are allowed between 10 of them at low field if all polarizations of the radiation field relative to the applied field B are considered. This can be seen by applying selection rules $\Delta M_S = \pm 1, 0$ or $\Delta M_F = \pm 1, 0$ to the low-field spin functions. Of these, two are allowed for z-polarized radiation ($\Delta M = 0$ type, or σ, transitions) and eight are allowed for xy-polarized radiation ($\Delta M = \pm 1$ type, or π, transitions). Two pairs of the eight π transitions are degenerate transitions (within the very good approximation that the nuclear Zeeman splitting has negligible effect) and so a total of six π type transitions occur at low field as shown by Townsend et al.[7] Three of these approach the zero-field splitting as $B_z \rightarrow 0$ and the other three approach zero frequency. The three π transitions and two σ transitions which approach the zero-field splitting are indicated in Figure 13a.

Cole, Kushida, and Heller[61] succeeded in directly observing the ZFR spectrum of this radical in aqueous solution with a frequency-swept spectrometer. This appears to be the only ZFR measurement which has been made on a liquid sample. As mentioned in the introduction, the problems with lossy aqueous solutions at conventional EPR frequencies are much reduced when ZFR resonances occur in the submicrowave region. It was found that the earth's magnetic field (~0.5 G) caused a splitting of the resonances which could be detected because the resonant lines were very narrow ($\Delta W_{1/2} \simeq 0.5$ MHz). The diagram given by Cole et al.[61] illustrating the effect of a small static magnetic field on the energy levels and on transitions in the region of the ZFR resonance has incorrect M_F labels in the $F = {}^1/_2$ group and the wrong polarizations of transitions. We show a correct illustration of the energy levels, transitions and their polarizations in Figure 13.

The spectrum shown by Cole et al. in the weak ambient field appears to have been produced with the rf field approximately perpendicular to a field of about 1 G (earth's field and stray laboratory fields), since three transitions are observed at frequencies approximately equal to those expected from an exact calculation with $B = 1$ G. Equal net contributions from σ and π transitions would occur if the linearly polarized microwave field were inclined at 45° to the modulating field and would result in a five line spectrum with intensity ratios 3:4:2:4:3. The zero-field resonance at 54.97 ± 0.03 MHz was observed by cancelling out the ambient field using the fringing field of a permanent magnet. Exact zero field in such a case is found simply by changing the field until the narrowest single resonance line is observed. For $S = {}^1/_2$ and a general nuclear spin I, zero-field resonance occurs at $(I + {}^1/_2)A$ where A is an isotropic hyperfine interaction; from the ZFR a value $A = 36.65$ ± 0.02 MHz was obtained, in good agreement with the EPR determination.[6,7] This measurement is indicative of the high precision which can be achieved using ZFR in some circumstances.

Pake et al.[7] noted some extra features in the low- and high-field EPR spectra which were unexplained. The weak features in the high-field spectra are probably those later ascribed[118] to hyperfine interaction with naturally occurring ^{15}N and ^{33}S; indeed species with one ^{17}O bonded to ^{32}S have also been detected in natural abundance.[119] However, the extra features shown in the 9.2 MHz EPR spectrum[6] do not correspond to predicted low abundance isotope effects and would be worth investigating.

Figure 13 shows the value in generally considering the very low-field frequency-swept EPR spectrum since it has immediate implications about the effect of ZFR detection by magnetic field modulation. For this case of $S = {}^1/_2$, $I = 1$ the optimum ZFR signal strength would obtain with the modulation magnetic field (which could probably be as low as 2 G) parallel to the microwave field (i.e., both in the z direction) since the resonances are shifted well away from the zero-field resonance during the field-on part of the square-wave modulation. This contrasts with the situation with magnetic field modulation perpendicular to the microwave field where a significantly intense transition remains very close to the ZF resonance position during the on part of the modulation; the modulation detected ZFR signal would be reduced in such a situation. Thus careful consideration of the effects of all polarizations of the modulation field on the form of the ZFR signal can remove the necessity of using high modulation amplitudes, and thus reduce problems caused by amplifying distorted modulation waveforms.

VII. Concluding Remarks

At the time when electron paramagnetic resonance in bulk matter was discovered, microwave sources were largely fixed frequency devices. Since it was the electron Zeeman effect which was then of principal interest, this was no great handicap and an electromagnet provided the essential variable, B. Electron fine structure and nuclear hyperfine structure then appeared in the spectrum in a manner suggested by their names, that is, as perturbations on the Zeeman spectrum. Greater interest then attached to these superimposed interactions which can give rise to a magnetic dipole allowed spectrum in the absence of a magnetic field for a wide variety of materials, from simple organic radicals to compounds of the rare earth ions.

In spite of this, the comparative difficulty of sweeping microwave frequencies over wide ranges and the essentially fixed frequency nature of microwave resonant devices meant that field-swept EPR spectrometers were almost always employed; the fine and hyperfine structure interactions always had to be deconvoluted from the Zeeman effect. In many cases this is straightforward enough. However, as our work on Mn^{2+} has shown, significant errors can arise. These errors have many sources and include the inherent spectral complexity when structural or magnetic inequivalence is present, field measurement errors, inaccurate crystal alignment, assumptions about the alignment of guest ions with respect to host axes, and assumptions of parallelism of the Zeeman tensor with the tensors representing other interactions.

Considerable developments in microwave technology have occurred in the last decade and this remains a growth area. However a new EPR spectrometer still bears detailed similarities to instruments 20 or more years old. Variable frequency sources are now comparatively inexpensive and commonplace. Variable frequency spectrometer design and construction has been given in a number of the papers we have reviewed and EPR sensitivities can be attained if necessary. The time therefore seems ripe to exploit the valuable complementary role that ZFR has in the study of electron paramagnetism.

Zero-field studies confer several benefits. Either because the analysis is simpler and free from field measurement, crystal orientation and Hamiltonian (tensor axes) errors, or because in some cases ZFR linewidths are one or two orders of magnitude narrower than their EPR counterparts, an order of magnitude greater confidence can be placed on ZFR determined parameters, thus allowing finer effects to be probed. These range from hyperfine anomalies to simply better resolution of superimposed resonances. Higher accuracy comes not only from these effects but also from the facts that quadrupole effects turn up in first rather than second order at zero field and that ZF splittings from nuclear hyperfine structure can exceed, by a significant factor, those observed in high field EPR. Sign

information of hyperfine and quadrupole parameters relative to those of fine structure terms also appears in first order at zero field compared with its appearance as a second order effect at high fields. In ZFR there is no competition for the quantization of the angular momentum, so amorphous powders, glasses and polycrystalline materials are well-suited to study by this technique. There is thus scope for investigation of mineralogical and biological materials which do not always occur in the single crystal form preferred for EPR spectroscopy. Overlapping spectra, common in such studies, from paramagnetic ions in several physically distinct sites or from a number of different ions can be much more readily resolved at zero field because of a reduced number of lines and because magnetic inequivalences are not an additional complication. The multiplicity of lines resulting from such effects at high field can be a considerable problem in EPR. On the analytical side, there is the advantage of having to diagonalize the Hamiltonian matrix only once rather than at every field of interest. Finally, the power of variable frequency EPR should not be overlooked, particularly for the evaluation of the many small perturbations that arise from higher order terms in the Hamiltonian. Combining variation in field and frequency allows very full mapping of the Zeeman diagram rather than at selected frequencies, typically one in X-band and another in Q-band.

While advocating the complementary merits of ZFR, cases exist where its power is limited. For example, in organic radicals with several interacting nuclei, the multiplicity of transitions and the problems of different component line shapes may make the technique of limited value in this area. There are cases where the very simplicity of the ZFR spectrum can hide parameters in principle. For example, Cr^{3+} in a nonaxial environment ($E \neq 0$) may not be revealed as such in the straight frequency spectrum, which consists of only one transition. Even in these cases ZFR is useful for checking the validity of an EPR determined spin Hamiltonian.

For the future, it seems that advancing microwave technology and the development of NMR spectrometers at frequencies approaching the microwave region might provide the impetus for more routine use of ZFR procedures. There is still scope for experimental development, particularly of tunable microwave resonators, and areas of applicability of the technique are virtually as wide as in traditional EPR. With equipment sophistication ranging from the normal accessories of a commercial EPR spectrometer to the custom-built resonant ZFR spectrometer covering several frequency bands, this technique is likely to have considerable impact.

Note Added in Proof. Recently two papers have been published describing the loop-gap or split-ring resonator.[120,121] These appear to be promising as tuneable microwave resonators.

VIII. References

(1) Al'tshuler, S.; Zavoiskii, E.; Kozyrev, V. *Zh. Eksp. Teor. Fiz.* **1944**, *14*, 407.
(2) Zavoiskii, E. *J. Phys. (Moscow)* **1944**, *8*, 377.
(3) Zavoiskii, E. *J. Phys. (Moscow)* **1945**, *9*, 245.
(4) Bogle, G. S.; Symmons, H. F.; Burgess, V. R.; Sierins, J. V. *Proc. Phys. Soc., London* **1961**, *77*, 561.
(5) Kornienko, L. S.; Prokhorov, A. M. *Sov. Phys.—JETP (Engl. Transl.)* **1961**, *13*, 1120.
(6) Pake, G. E.; Townsend, J.; Weissman, S. I. *Phys. Rev.* **1952**, *85*, 682.
(7) Townsend, J.; Weissman, S. I.; Pake, G. E. *Phys. Rev.* **1953**, *89*, 606.
(8) Bleaney, B.; Trenam, R. S. *Proc. R. Soc. London, Ser. A* **1954**, *223*, 1.
(9) Bleaney, B.; Scovil, H. E. D.; Trenam, R. S. *Proc. R. Soc. London, Ser. A* **1954**, *223*, 15.
(10) Geusic, J. E. *Phys. Rev.* **1956**, *102*, 1252.
(11) McConnell, H. M.; Thompson, D. D.; Fessenden, R. W. *Proc. Natl. Acad. Sci. U.S.A.* **1959**, *45*, 1600.
(12) Mock, J. B. *Rev. Sci. Instrum.* **1960**, *31*, 551.
(13) Bogle, G. S.; Symmons, H. F. *Proc. Phys. Soc., London* **1961**, *78*, 812.
(14) Symmons, H. F.; Bogle, G. S. *Proc. Phys. Soc., London* **1962**, *79*, 468.
(15) Symmons, H. F.; Bogle, G. S. *Proc. Phys. Soc., London* **1963**, *82*, 412.
(16) Burland, D. M. *Chem. Phys. Lett.* **1980**, *70*, 508.
(17) Griesser, H. J.; Bramley, R. *Chem. Phys. Lett.* **1982**, *88*, 27.
(18) El-Sayed, M. A. *MTP Int. Rev. Sci.: Phys. Chem., Ser. One* **1972**, *3*, 119.
(19) Kwiram, A. L. *MTP Int. Rev. Sci.: Phys. Chem., Ser. One* **1972**, *4*, 271.
(20) El-Sayed, M. A. *Annu. Rev. Phys. Chem.* **1975**, *26*, 235.
(21) Clarke, R. H., Ed., "Triplet State ODMR Spectroscopy"; Wiley: New York, 1982.
(22) Feher, G. *Bell Syst. Tech. J.* **1957**, *36*, 449.
(23) Wilmshurst, T. H.; Gambling, W. A.; Ingram, D. J. E. *J. Electron. Control* **1962**, *13*, 339.
(24) Mehring, M.; Freysoldt, F. *J. Phys. E.* **1980**, *13*, 894.
(25) Poole, C. P., Jr., "Electron Spin Resonance"; Interscience: New York, 1967.
(26) Bogle, G. S.; Symmons, H. F. *Proc. Phys. Soc., London* **1962**, *79*, 775.
(27) Chamberlain, J. R.; Syms, C. H. A., *Proc. Phys. Soc., London* **1964**, *84*, 867.
(28) Rao, K. V. S.; Sastry, K. V. L. N. *Chem. Phys. Lett.* **1970**, *6*, 485.
(29) Bramley, R.; Strach, S. J. *Chem. Phys. Lett.* **1981**, *79*, 183.
(30) Urban, W. *Z. Angew. Phys.* **1966**, *20*, 215.
(31) Erickson, L. E. *Phys. Rev.* **1966**, *143*, 295.
(32) Bernstein, E. R.; Dobbs, G. M. *Rev. Sci. Instrum.* **1973**, *44*, 1314.
(33) Webb, R. H. *Rev. Sci. Instrum.* **1962**, *33*, 732.
(34) Volino, F.; Csakvary, F.; Servoz-Gavin, P. *Rev. Sci. Instrum.* **1968**, *39*, 1660.
(35) Fourrier-Lamer, A.; Grandjean, D. *Rev. Sci. Instrum.* **1972**, *43*, 1318.
(36) Plachy, W. Z.; Schaafsma, T. J. *Rev. Sci. Instrum.* **1969**, *40*, 1590.
(37) Nowicki, P.; Hillmer, W.; Urban, W. *Phys. Status Solidi B* **1971**, *47*, 549.
(38) Pearlman, M. R.; Webb, R. H. *Rev. Sci. Instrum.* **1967**, *38*, 1264.
(39) Newman, D. J.; Urban, W. *Adv. Phys.* **1975**, *24*, 793.
(40) Cook, A. R.; Matarrese, L. M. *J. Chem. Phys.* **1969**, *50*, 2361.
(41) Hutchings, M. T. *Solid State Phys.* **1964**, *16*, 227.
(42) Abragam, A.; Bleaney, B. "Electron Paramagnetic Resonance of Transition Ions"; Clarendon Press: Oxford, 1970; p 628.
(43) Buckmaster, H. A. *Can. J. Phys.* **1962**, *40*, 1670.
(44) Stevens, K. W. H. *Proc. Phys. Soc., London* **1952**, *65*, 209.
(45) Reference 42, p 140.
(46) Buckmaster, H. A.; Shing, Y. H. *Phys. Status Solidi A* **1972**, *12*, 325.
(47) Buckmaster, H. A.; Chatterjee, R.; Shing, Y. H. *Phys. Status Solidi A* **1972**, *13*, 9.
(48) Tennant, W. C. *Mol. Phys.* **1976**, *31*, 1505.
(49) Jones, D. A.; Baker, J. M.; Pope, D. F. D. *Proc. Phys. Soc., London* **1959**, *74*, 249.
(50) Reference 42, p 863.
(51) Orbach, R. *Proc. R. Soc. London, Ser. A* **1961**, *264*, 458.
(52) Al'tshuler, S. A.; Kozyyrev, B. M. "Electron Paramagnetic Resonance in Compounds of Transition Elements", 2nd ed.; Wiley: New York, 1974; p 512.
(53) Reference 42, p 437.
(54) Bowers, K. D.; Owen, J. *Rep. Prog. Phys.* **1955**, *18*, 304.
(55) Bramley, R.; Strach, S. J., to be published.
(56) Geschwind, S. *Phys. Rev. Lett.* **1959**, *3*, 207.
(57) Hutton, D. R. *Phys. Lett.* **1964**, *12*, 310.
(58) Richards, P. L.; Caughey, W. S.; Eberspaecher, H.; Feher, G.; Malley, M. *J. Chem. Phys.* **1967**, *47*, 1187.

(59) Brackett, G. C.; Richards, P. L.; Caughey, W. S. *J. Chem. Phys.* **1971**, *54*, 4383.
(60) Bleaney, B.; Ingram, D. J. E. *Proc. R. Soc. London, Ser. A* **1951**, *205*, 336.
(61) Cole, T.; Kushida, T.; Heller, H. C. *J. Chem. Phys.* **1963**, *38*, 2915.
(62) Bleaney, B.; Bowers, K. D. *Philos. Mag.* **1952**, *43*, 372.
(63) McGlynn, S. P.; Azumi, T.; Kinoshita, M. "Molecular Spectroscopy of the Triplet State"; Prentice Hall: Englewood Cliffs, 1969.
(64) Kawamori, A. *J. Magn. Reson.* **1978**, *31*, 423.
(65) Atherton, N. M.; Horsewill, A. J. *Mol. Phys.* **1981**, *42*, 985.
(66) Herring, F. G.; Thompson, R. C.; Schwerdtfeger, C. F. *Can. J. Chem.* **1969**, *47*, 555.
(67) Mirzakhanyan, A. A. *Sov. Phys.–Solid State (Engl. Transl.)* **1981**, *23*, 1434.
(68) Reference 42, p 287.
(69) Dagg, I. R.; Kemp, R. C.; Symmons, H. F. *J. Phys. C.* **1969**, *2*, 1098.
(70) Bernstein, E. R.; Dobbs, G. M. *Phys. Rev. B*, **1975**, *11*, 4623.
(71) Gerkin, R. E.; Thorsell, D. L. *J. Chem. Phys.* **1972**, *57*, 188.
(72) Gerkin, R. E.; Rogers, W. J.; Tourek, W. J. *J. Chem. Phys.* **1977**, *66*, 4166.
(73) Shing, Y. H.; Buckmaster, H. A. *J. Magn. Reson.* **1976**, *21*, 295.
(74) Smith, M. R.; Buckmaster, H. A.; Chatterjee, R. *J. Magn. Reson.* **1977**, *25*, 485.
(75) Smith, M. R.; Chatterjee, R.; Buckmaster, H. A. *J. Magn. Reson.* **1977**, *25*, 495.
(76) Smith, M. R.; Chatterjee, R.; Buckmaster, H. A. *J. Magn. Reson.* **1977**, *25*, 499.
(77) Gerkin, R. E.; Rogers, W. J. *Chem. Phys. Lett.* **1976**, *43*, 592.
(78) Bogle, G. S.; Heine, V. *Proc. Phys. Soc., London, Sect. A* **1954**, *67*, 734.
(79) Malhotra, V. M.; Bist, H. D.; Upreti, G. C. *J. Magn. Reson.* **1976**, *21*, 173.
(80) Malhotra, V. M.; Bist, H. D.; Upreti, G. C. *Chem. Phys. Lett.* **1977**, *48*, 334.
(81) Malhotra, V. M.; Bist, H. D. *Solid State Commun.* **1978**, *27*, 393.
(82) Sherry, E. G. *J. Solid State Chem.* **1976**, *19*, 271.
(83) Misra, S. K.; Mikolajczak, P. *J. Phys. Chem. Solids* **1979**, *40*, 477.
(84) Kahle, H. G.; Koch, V.; Plamper, J.; Urban, W. *J. Chem. Phys.* **1968**, *49*, 2702.
(85) Urban, W. *J. Chem. Phys.* **1968**, *49*, 2703.
(86) Urban, W. *Phys. Status Solidi* **1970**, *37*, 181.
(87) Kahle, H. G.; Schopper, H. C.; Urban, W.; Wuchner, W. *Phys. Status Solidi* **1970**, *38*, 815.
(88) Hillmer, W.; Urban, W. *Phys. Status Solidi* **1970**, *39*, 527.
(89) Urban, W. *Phys. Status Solidi B* **1971**, *46*, 579.
(90) Schwarz, H. *Z. Anorg. Allg. Chem.* **1963**, *323*, 44.
(91) Rosenthal, J. *Phys. Rev.* **1967**, *164*, 363.
(92) Urban, W.; Siegel, E.; Hillmer, W. *Phys. Status Solidi B* **1974**, *62*, 73.
(93) Dischler, B.; Herrington, J. R.; Rauber, A.; Schneider, J.; Urban, W. *Solid State Commun.* **1973**, *12*, 737.
(94) Halford, D. *Phys. Rev.* **1962**, *127*, 1940.
(95) McConnell, H. M.; Heller, C.; Cole, T.; Fessenden, R. W. *J. Am. Chem. Soc.* **1960**, *82*, 766.
(96) Cole, T.; Heller, C. *J. Chem. Phys.* **1961**, *34*, 1085.
(97) Lin, W. C.; McDowell, C. A. *Mol. Phys.* **1961**, *4*, 343.
(98) Birkle, M.; Schoffa, G. *J. Chem. Phys.* **1968**, *49*, 3191.
(99) Bernhard, W.; Snipes, W. *J. Chem. Phys.* **1966**, *44*, 2817.
(100) Lefebvre, R.; Maruani, J. *J. Chem. Phys.* **1965**, *42*, 1496.
(101) Morton, J. R.; Horsfield, A. *J. Chem. Phys.* **1961**, *35*, 1142.
(102) Miyagawa, I.; Itoh, K. *J. Chem. Phys.* **1962**, *36*, 2157.
(103) Birkle, M.; Geiger, A.; Schoffa, G. *Z. Naturforsch., A* **1969**, *24*, 1093.
(104) Cook, R. J.; Rowlands, J. R.; Whiffen, D. H. *J. Chem. Soc.* **1963**, 3520.
(105) Geiger, A.; Birkle, M.; Oliver, G.; Lefebvre, R. *Mol. Phys.* **1969**, *17*, 101.
(106) Birkle, M.; Schoffa, G. *Z. Naturforsch., A* **1968**, *23*, 918.
(107) Moulton, G. C.; Moulton, W. G. *J. Chem. Phys.* **1961**, *35*, 208.
(108) Morton, J. R.; Horsfield, A. *Mol. Phys.* **1961**, *4*, 219.
(109) Hutchison, C. A., Jr.; Nicholas, J. V.; Scott, G. W. *J. Chem. Phys.* **1970**, *53*, 1906.
(110) Heller, H. C. *J. Chem. Phys.* **1965**, *42*, 2611.
(111) Mangiaracina, R. S. *Radiat. Res.* **1965**, *26*, 343.
(112) Miyagawa, I.; Kurita, Y.; Gordy, W. *J. Chem. Phys.* **1960**, *33*, 1599.
(113) Birkle, M.; Schoffa, G.; Lefebvre, R.; Oliver, G. *J. Magn. Reson.* **1969**, *1*, 666.
(114) Katayama, M.; Gordy, W. *J. Chem. Phys.* **1961**, *35*, 117.
(115) Narasimha Rao, D. V. G. L.; Katayama, M. *J. Chem. Phys.* **1962**, *37*, 382.
(116) Breit, G.; Rabi, I. I. *Phys. Rev.* **1931**, *38*, 2082.
(117) Nafe, J. E.; Nelson, E. B. *Phys. Rev.* **1948**, *73*, 718.
(118) Windle, J. J.; Wiersema, A. K. *J. Chem. Phys.* **1963**, *39*, 1139.
(119) Howell, J. B.; McCain, D. C. *J. Phys. Chem.* **1969**, *73*, 4405.
(120) Hardy, W. N.; Whitehead, L. A. *Rev. Sci. Instrum.* **1981**, *52*, 213.
(121) Froncisz, W.; Hyde, J. S. *J. Magn. Reson.* **1982**, *47*, 515.